STRUCTURAL CHARACTERIZATION OF MONOLAYER-PROTECTED METAL

NANOPARTICLES BY ION MOBILITY-MASS SPECTROMETRY

By

Kellen Harkness

Dissertation

Submitted to the Faculty of the

Graduate School of Vanderbilt University

in partial fulfillment of the requirements

for the degree of

DOCTOR OF PHILOSOPHY

in

Chemistry

May, 2011

Nashville, Tennessee

Approved:

Professor David E. Cliffel

Professor John A. McLean

Professor Sandra J. Rosenthal

Professor David L. Hachey

To Alanna, my best friend, true counterpart, and eternal companion.

ACKNOWLEDGEMENTS

Thanks are due to the never-ending chain of people who have, in one way or another, made the physical and mental space in which I live pleasant and green. To each of these people, I wish speedy and abundant reward.

To my grandparents, who gave invaluable virtues and traditions to their progeny, and to my parents, who enriched and enlivened those virtues and traditions while never giving up their integrity, I am eternally indebted. To my friends and the faculty at Harding University, who were always willing to give of themselves without hesitation.

To Profs. Cliffel and McLean, who were precisely the advisors I needed. I learned a great deal from the conversations we had, even those which weren't intentionally didactic. From them I learned that my grammar left much to be desired; I will never forget the lessons I learned – and there were many – since each one I received dealt a fresh blow to my pride. To Profs. Rosenthal and Hachey, who gave their time and effort to my formation as a scientist.

To the three Brians: Huffman, Hixson, and Turner, who made the laboratory a collegial and friendly work environment, and to Dr. Larissa Fenn, Michal Kliman, and Andrzej Balinski, all of whom have given freely of their time and considerable expertise.

To the many others who are not named here: teachers, friends, acquaintances, the many have helped me even if they didn't intend it, and to those who have given me more than I could ever hope to repay.

Above all, I give honor, respect, and undying gratitude to my lovely wife, who has been a source of health and strength in body and mind from the moment I met her.

TABLE OF CONTENTS

Page

LIST OF FIGURES

LIST OF TABLES

CHAPTER I

INTRODUCTION

Monolayer-protected gold nanoparticles: history and characterization

Since their inception in 1994,[1] monolayer-protected gold nanoparticles (AuNPs) have become a ubiquitous nanomaterial, with wide-ranging applications from molecular electronics[2] and catalysis[3] to detection[4] and biomimetics.[5] Their technological precursor, unprotected colloidal metals, have been known for much of recorded history, having been used for various medicinal remedies and to provide color in ceramics and stained glass. In the 19th century, Michael Faraday observed the diversity of colors in colloidal gold and theorized that the spectral diversity was due to size variation, but this was only a small part of the diversity of nanosized gold colloids.[6,7] These unprotected colloids were later functionalized with phosphines, amines, and thiols. In 1984, Nuzzo and coworkers developed self-assembled monolayers (SAMs) of thiols on two-dimensional gold surfaces.[8] Ten years later, Brust and coworkers developed a facile and versatile route to the formation of AuNPs protected by a novel three-dimensional SAM.[1] The unique gold-sulfur bond led to a new class of nanomaterials which were simultaneously versatile, exhibiting some properties of metals[9] while presenting a completely organic surface.

While unprotected, colloidal gold nanoparticles have a core diameter typically between 2-150 nm,[10] monolayer-protected AuNPs are generally <10 nm in diameter.[11] The smallest nanoparticles (<2 nm core diameter) generally have molecular or

quantum properties, such as tunable band gaps, quantized charging, and discrete optical absorbance bands.[12] Larger nanoparticles (>3 nm) exhibit properties of bulk gold, such as a surface plasmon band with a size-dependent λ_{max} near 520 nm.[13] The protecting ligands contribute to the electronic properties of the nanoparticle in addition to determining chemical functionality and solubility. Since the only requirement for a ligand is a free thiol, anything from biologically available glutathione[14] and cysteine-bearing peptides[15] to exotic aromatic "molecular wire" molecules[16] can be used. These molecules can also be mixed in the monolayer to provide a fine-tuned solubility and functionality.

Variations in its two components – metallic core and organic surface – provide both a vast chemical space to explore, and a convenient beginning point for the classification of different monolayer-protected metallic nanoparticles. A standard vocabulary for these classifications is still emerging, but the following is a synthesis of the terms used in the peer-reviewed literature.

The "monolayer" in question should be understood to be a monolayer of gold-thiolate complexes,[17,18] in which the gold and sulfur atoms coordinate to the metallic core. These complexes are somewhat analogous to surfactants, with a highly polarized organometallic headgroup which either binds to the metallic surface or self-aggregates through aurophilic interactions[19] and becomes insoluble. The organic tail can be selected to allow solvation in nearly any conceivable solvent, since the terminus can exhibit any functional group from a negatively charged sulfonate to a positively charged quaternary amine, from a hydrophobic alkane to an amphiphilic glycol.

The nanoparticle has also been referred to as a cluster or crystal, alternatively a nanocluster or nanocrystal. The most popular of these terms is the monolayer-protected cluster (MPC). The use of the term "cluster" specifies a small and well-defined structure, and as such is applicable to the smallest nanoparticles (<2 nm core diameter). It is in this size range that certain molecular formulae are preferred, allowing for syntheses with molecular monodispersity as well as crystallization.[20] The largest of the "magic sizes" whose structure has been predicted, $Au_{146}SR_{60}$, appears to exhibit some diversity in structure which has led to confusion in its molecular formula assignment.[21,22] It is highly likely that any larger nanoparticle will exhibit a greater diversity in structure, primarily in the number, stoichiometry, and orientation of its protecting gold-thiolate complexes. Such nanoparticles which have not yet been observed to have any specific, highly abundant molecular composition are thus better defined as nanoparticles, rather than clusters.

A very recent but exciting development is the exploration of supramolecular structures in the protecting gold monolayer. Credit for the idea goes to de Gennes, who in his 1992 Nobel lecture first coined the term "Janus" to describe complete microphase separation to form two "faces" on the same sphere.[23] While the concept of the Janus particle has been clearly developed on the microscale,[24] proof of complete microphase separation has been elusive. Stellacci and coworkers recently proposed the existence of patches and even stripes in monolayers on metallic nanoparticles.[25] These uniquely organized nanomaterials offer a route to greater mimetic behavior, becoming analogous to biomolecules with binding pockets and hydrophobic and hydrophilic faces. This enhanced mimetic behavior has been proposed to enhance the

controlled entry of AuNPs into cells[26] and binding to proteins.[27]

With such a great amount of chemical space to explore and so many powerful applications, the characterization of these monolayer-protected metallic nanoparticles has become very important. A route to observing the molecular identity of each nanoparticle synthesized and modified – its size, the composition of its monolayer, and any potential supramolecular structure – has not been realized. By using an array of analytical techniques, a rough estimate of the average size and composition can be obtained. Ultraviolet-visible (UV-Vis) spectroscopy can be used to roughly estimate the size of nanoparticles which are >3 nm in diameter, or to estimate the purity of very small MPCs which exhibit discrete optical transitions.[14] Transmission electron microscopy (TEM) allows imaging of the gold core,[1] owing to the high electron density of gold compared to the organic ligands. This leads to a very clear measure of average size and monodispersity. Commonly, nuclear magnetic resonance (NMR)[28] is used to measure purity, and to characterize and quantify the protecting ligands. Elemental or thermogravimetric analysis (TGA)[28] can be used to determine the composition of the nanoparticles, and may lead to insight on purity. This information can be used in conjunction with TEM to give an average molecular formula for the nanoparticles.[28]

Mass spectrometry (MS) is unique in that it has been proven capable of simultaneously measuring core size, characterizing the protecting ligands, and yielding a molecular formula (Figure 1). The remainder of this chapter is a discussion of the history of the use of MS for the characterization of AuNPs. Its advantages and limitations as well as trends for the future will also be discussed.
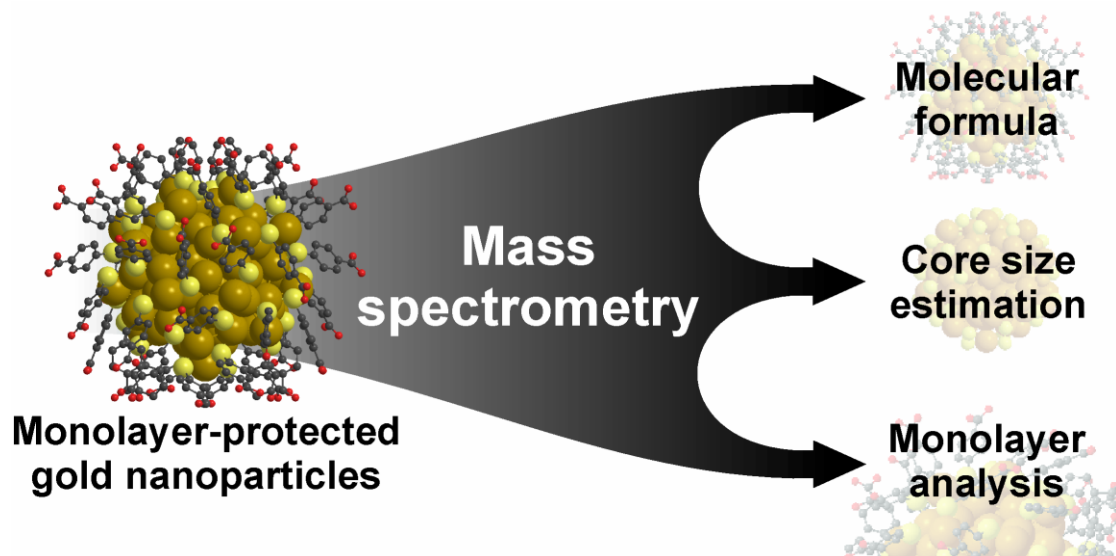
Figure 1. Characterization objectives for the MS analysis of monolayer-protected AuNPs. The generation of ionized intact AuNPs, gold-sulfide clusters, and gold-thiolate complexes allow the measurement of molecular formula, core size, and monolayer properties, respectively.

Early MS analyses: core size estimation and "magic-sized" MPCs

The earliest use of mass spectrometry for the characterization of thiolate-protected AuNPs are found in work from the late 1990s. These reports quickly revealed the problem inherent in mass analysis of AuNPs: ionization typically leads to nanoparticle fragmentation (Figure 2). For electrospray ionization (ESI), the protecting gold-thiolate ions are commonly desorbed.[29] Matrix-assisted laser desorption/ionization (MALDI) and laser desorption/ionization (LDI) without matrix assistance generates few nanoparticle ions until the laser fluence is sufficiently high for photolytic cleavage of the thiolate C-S bond.
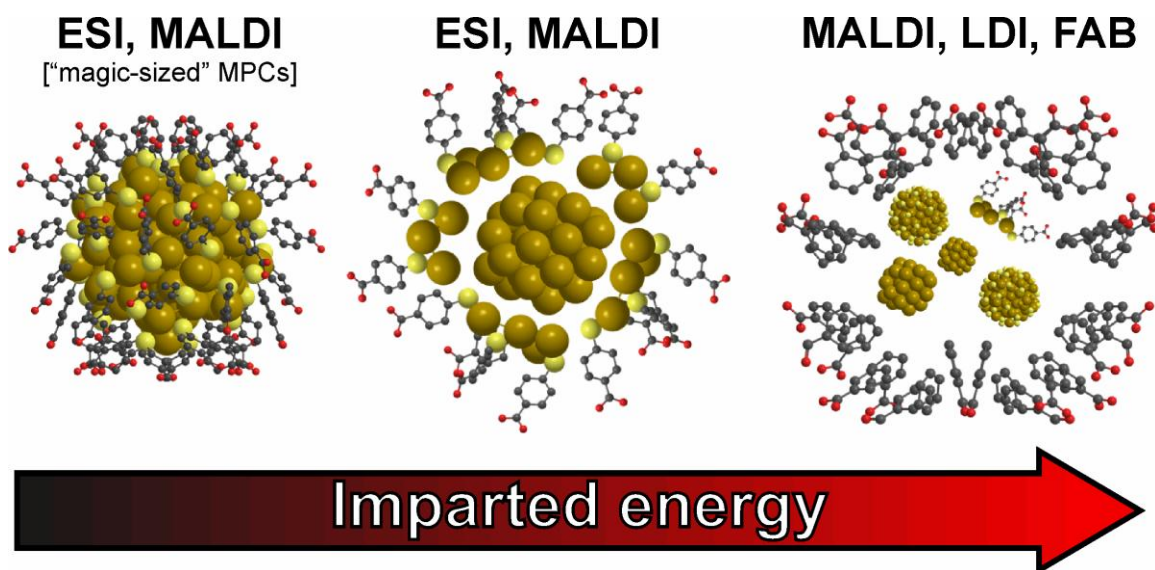
Figure 2. The product fragments of AuNPs at different levels of ionization "softness."For magic-sized MPCs, very soft ionization techniques can generate intact MPC ions. Otherwise, gold-thiolate ions are formed. Ionization with higher amounts of energy generates some gold-thiolate ions with gold-sulfur clusters and ligands cleaved at the C-S bond.

The ions that are observed are generally clusters of gold and sulfur, with a complete loss of the protecting ligands.[30] However, since ions roughly correspond to the mass of the core alone, the size of the core could be inferred from its mass. Using a simple calculation based on the properties of bulk gold, an approximate core diameter could be obtained as described by Schaaff *et al.*:[31]

$$D_{eq} = \left(\frac{6N_{Au}}{\pi \bar{n}_{Au}^{fcc}} \right)^{1/3} \quad (1)$$

From the mass spectrum, the number of gold atoms (N_{Au}) can be estimated. An approximate core diameter (D_{eq}) can then be calculated using two assumptions: first, that the gold adopts a face-centered cubic (fcc) packing structure (with a number density of *ca.* 59 atoms·nm^{-3}) and second, that the nanoparticle is spherical in shape.

The later discovery of gold-thiolate "staple" structures and non-fcc packing[18,21,32] in MPCs introduces some error in the estimated number density term. However, the respective error from denser packing and more distant capping gold atoms drives the number density in different directions, minimizing the net error. To illustrate, the calculated and measured diameters of the MPCs whose structures are known can be compared.[18,32] For $Au_{25}(SCH_2CH_2Ph)_{18}$, if only the dense icosahedral Au_{13} core is considered, the calculated diameter of 7.5 Å is much greater than the measured diameter of 5.6 Å. However, if the staple gold atoms are included, the calculated diameter of 9.3 Å is much closer to the measured diameter of 9.8 Å. For $Au_{102}(p\text{-}MBA)_{44}$ the error is remarkably small: 1.5 nm calculated compared to a roughly 1.55 nm measured diameter.

Equation 1 was first utilized when members of the Whetten lab discovered[33,34] that a portion of synthesized nanoparticles contained a series of discretely sized cores less than 2 nm in diameter. The mere existence of synthetically favored core sizes made this new discovery intriguing. Mass spectrometry was used (Figure 3) to estimate the core diameters of these newly discovered MPCs. The favored or "magic" sizes that were reported included what were later identified as the $Au_{38}(SR)_{24}$, $Au_{102}(SR)_{44}$, and $Au_{144/146}(SR)_{60/59}$ clusters, which continue to be common in studies of MPCs and their properties.

Schaaff later described the FWHM of MPC mass spectra as superior to the resolution of TEM with regards to gold core size measurement.[35] Mass spectrometry is additionally capable of obtaining size population information for mixtures of MPCs which have a size range less amenable to TEM measurements. Ideally, the core size of

larger nanoparticles could be measured using mass spectrometry. However, commonly used detectors exhibit lower sensitivity with increasing mass; since the mass of an AuNP increases exponentially with diameter size, larger ions will be unobservable. The use of kinetic energy-dependent detectors could potentially circumvent this problem, but these detectors are presently not widely used. In addition, the greater dispersity in the molecular formulae of larger AuNPs would partition the signals, requiring high sensitivity and mass resolution for assignments. Nevertheless, mass spectrometry is a very useful tool in the development of applications for MPCs exhibiting desired quantum effects, especially in light of recent synthetic work exclusively creating sizes under 2 nm.[36,37]
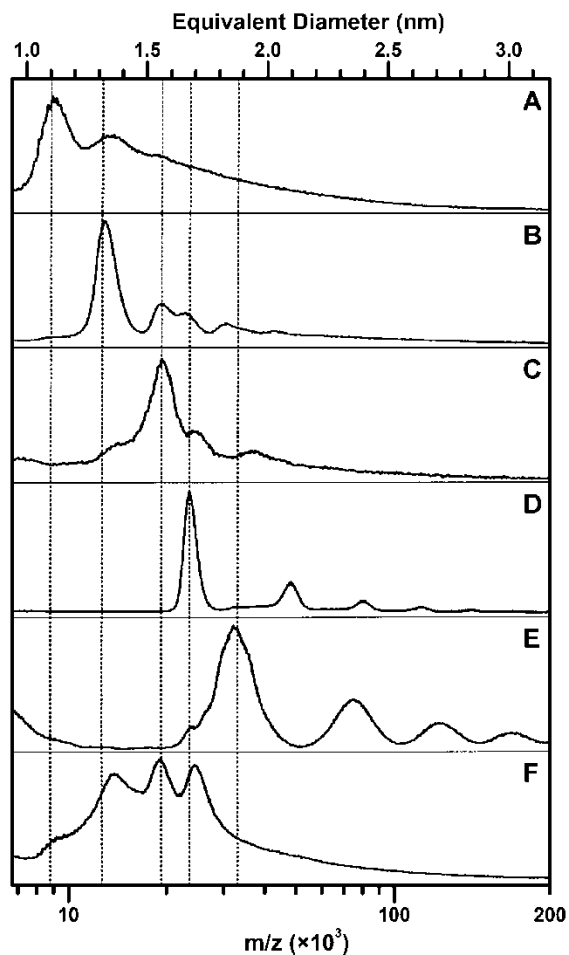
Figure 3. Early LDI mass spectra of various magic-sized MPCs. Spectra A-E each correspond to a particular magic size, having been fractionated from a mixture of synthesized nanoparticles. Spectrum F is a representative unfractionated mixture of nanoparticles with dodecanethiolate ligands. Later spectra using improved methodologies suggest that fractions A-D correspond to $Au_{38}(SC_{12}H_{25})_{24}$,[38] $Au_{68}(SC_{18}H_{37})_{34}$,[39] $Au_{102}(SC_6H_{13})_{44}$,[18,39] and $Au_{144/146}(SC_6H_{13})_{60/59}$,[21,22,37] respectively. Figure adapted with permission from ref. 31. Copyright 1997 American Chemical Society.

Recent advances in MS methodologies for AuNP analysis

Through the discovery of the magic-sized MPCs, researchers had demonstrated that mass spectrometry could be a formidable tool for elucidating size distributions of small clusters. Ideally, mass spectrometric analysis of thiolate-protected AuNPs would yield not only information about the core size, but also the ligand composition

9

decorating the AuNP. However, because of the ubiquitous fragmentation of the ligands from the gold core, this ideal was not realized until the advent of improved MALDI- and ESI-based methodologies.

Matrix-assisted laser desorption/ionization

The use of traditional weak organic acid MALDI matrices have provided a means to measure the mass of the core of ligand-protected AuNPs; however, these matrices do not prevent extensive ligand fragmentation. Following the initial studies reported in the late 1990s, it was not until 2008 that the first MALDI spectra (Figure 4) of intact ligand-protected AuNPs was published by Dass *et al.*[40] Very recent work has extended the effective range of MALDI-MS AuNP characterization to 18 kDa for $Au_{68}(SCH_2CH_2Ph)_{34}$.[39] The success of these efforts was due to the use of a unique matrix, *trans*-2-[3-(4-*tert*-butylphenyl)-2-methyl-2-propenylidene] malononitrile (DCTB), which ionizes by electron transfer rather than the proton transfer of weak organic acid matrices.[41] In spite of this solution to the fragmentation problem, MALDI-MS analysis will be limited to small MPCs indefinitely due to the problems associated with larger AuNPs mentioned in the previous section.
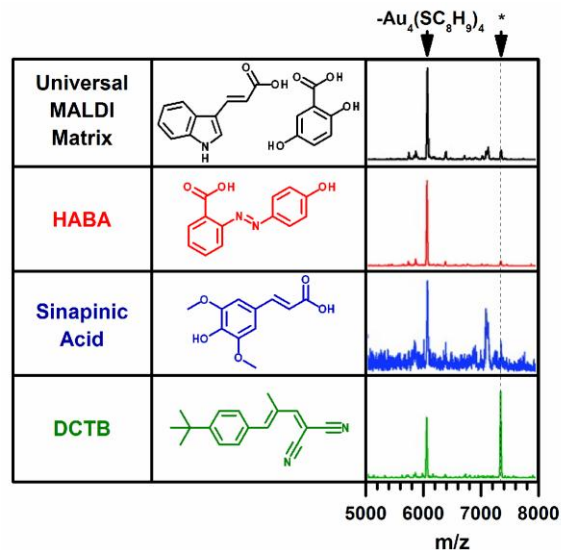
Figure 4. MALDI-MS spectra of $Au_{25}(SCH_2CH_2Ph)_{18}$ using various matrices, demonstrating the unique capability of the DCTB matrix to generate intact ligand-protected AuNP ions. The most prominent fragment shown corresponds to $Au_{21}(SCH_2CH_2Ph)_{14}$, resulting from a loss of $Au_4(SCH_2CH_2Ph)_4$. The peaks marked with an asterisk correspond to the intact $[Au_{25}(SCH_2CH_2Ph)_{18}]^+$ species. Adapted with permission from ref. 40. Copyright 2008 American Chemical Society.

The analysis of AuNPs with hydrophilic ligands has posed a problem for both MALDI and ESI. These ligands are necessary for applications which require water-soluble thiolate-protected AuNPs. For hydrophobic AuNPs, the relatively low-energy electron transfer is conducive to ionization without fragmentation. However, hydrophilic ligands of choice are commonly terminated with carboxylic acids, which at physiological pH exist in a carboxylate form. The steric confinement of high charge density results in significant Coulombic repulsion and fragmentation following ionization, particularly for larger particles with lower surface curvature and a higher charge density. No MALDI-MS spectra of intact hydrophilic ligand-protected AuNPs have been reported to date.

11

Electrospray ionization

The first unfragmented mass spectra were obtained using ESI,[29] due to its softness as an ionization technique; however, the electrospray process is not well-suited for AuNPs. Alkanethiolates are the most commonly used ligands, and are among the best ligands for generating magic-sized MPCs. Unfortunately, alkanethiolates are traditionally difficult to ionize in either the positive or the negative mode, but ionization can be enhanced through the use of ligand exchange. In 2007, Tracy *et al.*[42] reported the ligand exchange of methoxy penta(ethylene glycol)thiolate ligands onto $Au_{25}(SCH_2CH_2Ph)_{18}$ clusters, allowing observation of highly charged MPCs. More recently, Fields-Zinna and colleagues utilized quaternary amine ligands with an intrinsic charge to enhance the ionization of larger MPCs.[22]

A different approach was explored by Tsukuda and coworkers, who oxidized or reduced the clusters prior to ESI-MS analysis using $Ce(SO_4)_2$ or $NaBH_4$.[43] This approach allowed the observation of relatively large, intact MPCs (Figure 5).[44] Approaches which enhance the charge state of intact MPCs are significant for the future due to their applicability to larger AuNPs, and their ability to overcome the attenuated signal of high-mass ions.
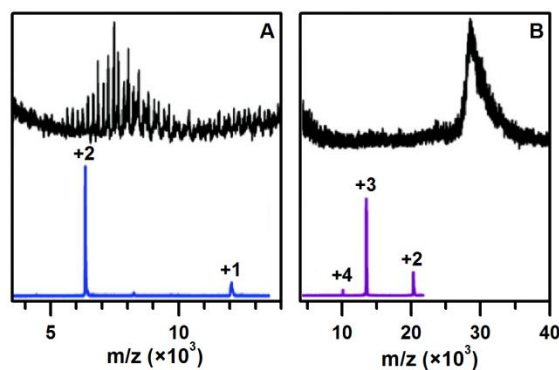
Figure 5. LDI and ESI mass spectra of $Au_{38}(SC_{12}H_{25})_{24}$ and $Au_{144}(SC_{12}H_{25})_{59}$ as obtained by Chaki *et al.* LDI is above, ESI below, while $Au_{38}(SC_{12}H_{25})_{24}$ and $Au_{144}(SC_{12}H_{25})_{59}$ are in panels A and B, respectively. Samples were oxidized with $Ce(SO_4)_2$ prior to analysis. Adapted with permission from ref. 44 Copyright 2008 American Chemical Society.

The first unfragmented AuNP mass spectrum reported was that of the small Au_{25} cluster protected by glutathione ligands (abbreviated SG here to highlight the thiolate bonding).[29] However, due to a large amount of chemical noise and an alternate molecular formula with a very similar mass, the ion was mistakenly identified as $Au_{28}(SG)_{16}$ until corrected in 2005.[14] This underscores two challenges of peak identification from intact AuNPs: multiple molecular formulae can be nearly isobaric, and a significant amount of chemical noise is often present due to impurities or ligand fragmentation. Improved sample quality, resolving power, and mass measurement accuracy increase the certainty of molecular formula assignments,[45] since the number of indistinguishable, nearly-isobaric permutations are decreased.

New applications and emerging trends

Apart from the characterization of synthesized nanoparticles, applications of MS-based AuNP analysis have included investigations into the nature and properties of

AuNPs, particularly the small MPCs. Two applications are detailed in this section, namely mixed-ligand and gold-thiolate complex analysis. Both have implications for routine MS-based AuNP characterization while also revealing new information about the nanoparticles.

Mixed-ligand analysis

With the ability to analyze intact MPCs, it is now possible to investigate variations in the stoichiometry of different ligands on the basis of mass, considering the gold core to be a constant mass. This has enabled the characterization of mixed-ligand AuNPs since, assuming one is comparing ligands of different masses, each population of ligands will correspond to a unique mass. Mass spectrometry alone allows the observation of ligand mixtures of discrete stoichiometry. Other techniques, primarily nuclear magnetic resonance (NMR) spectroscopy, provide population averages, yielding only the percent coverage of different thiolate ligands on an average nanoparticle.

The characterization of mixed-ligand AuNPs has significant implications in a wide range of applications, ranging from biological to electronic. While AuNPs are typically protected by a uniform monolayer of a single ligand species, a mixture of ligands is required for many applications where the demands of synthetic parameters, solubility, and chemical functionality require more than a single species can provide. For example, covering an entire nanoparticle with a given epitope for a vaccine would be costly, difficult, and likely render the nanoparticle insoluble. Thus, having multiple ligand species with different chemical roles is desirable. This can be accomplished

through the combination of a higher proportion of a shorter capping ligand to achieve the desired solubility properties with a smaller proportion of longer ligands containing the epitope moiety.[15]

Diverse mixtures of ligands can be placed on a nanoparticle through the presence of multiple thiols during the AuNP synthesis or through ligand exchange (also known as place-exchange) reactions. For some applications, it may be acceptable to know that the ligand of interest is present on the nanoparticle surface. Ideally, the relative amounts of nanoparticles featuring a given stoichiometry of ligands would be identified. This "ligand exchange distribution" can only be accurately observed using mass spectrometry if the ionization efficiency is the same for all nanoparticles, regardless of the specific mixture of ligands present. The amount of variation in ionization efficiency across mixed-ligand populations should be dictated by the specific chemical properties of the ligands present. However, ligand exchange distributions obtained by Murray and coworkers reveal symmetric distributions for different stoichiometries of phenylethanethiolate and hexanethiolate ligands, which seems to indicate a uniform ionization efficiency.[40]

The first MS-based mixed-ligand analysis focused on the ligand exchange kinetics of small $Au_{25}(SR)_{18-x}(SR')_x$ clusters.[46] The kinetics of ligand exchange for thiols on gold films has been thoroughly explored and extrapolated to three-dimensional nanoparticles.[47] An understanding of on/off rates for terraces, edges, and vertices based on self-assembled monolayers may conceptually be true for nanoparticles; however, the existence of semi-ring $Au(SR)_2$ and $Au_2(SR)_3$ structures on AuNP surfaces may complicate a direct extrapolation. Two thiolate positions – those

connected to the core and those that only bind to the outer "staple" gold atoms – are expected to have similar but distinct exchange rates. Further complexities arise from ligand-ligand intermolecular interactions. For example, three different types of interactions were identified in the crystal structure of $Au_{102}(p\text{-MBA})_{44}$.[18]

The work by Dass *et al.* explored ligand exchange kinetics for MPCs with mixtures of phenylethanethiol, hexanethiol, and thiophenol ligands.[46] Clusters with a mixture of hexanethiol and phenylethanethiol, generated both through post-synthesis ligand exchange (Figure 6A) and mixed-ligand synthesis (Figure 6B), agreed well with the predicted ligand exchange distribution. However, the ligand exchange distribution of place-exchanged thiophenol was much narrower than expected (Figure 6C). This may imply the existence of ligand-ligand interactions which more strictly control the number of ligands which can exchange. This work demonstrates the capabilities of MS-based ligand analysis, as well as providing future directions to investigate the variables of ligand exchange reactions for ligand-protected AuNPs.
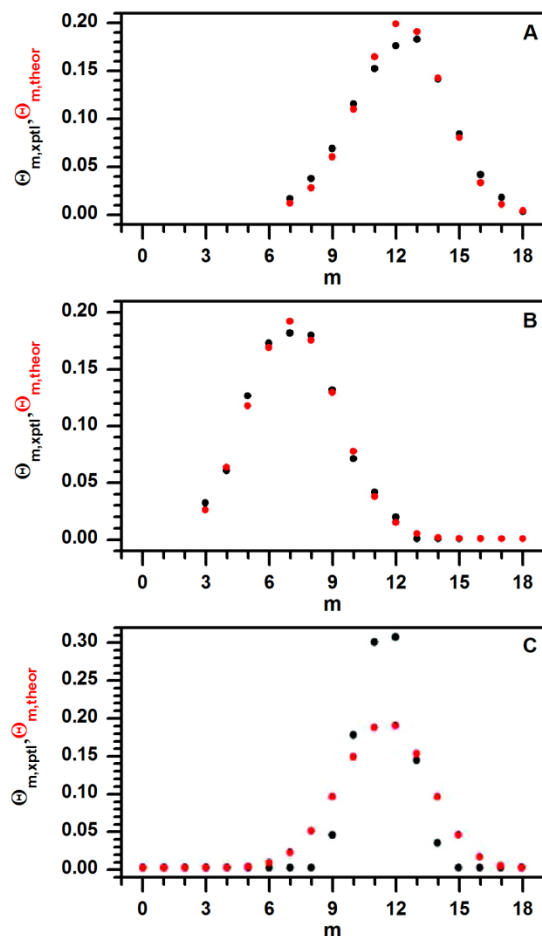
Figure 6. Comparison of theoretical and experimental ligand exchange distributions (red and black, respectively), where m is the number of phenylethanethiol ligands, $Au_{25}(SCH_2CH_2Ph)_m(SR)_{18-m}$, and Θ is the proportion of the entire cluster population featuring its respective value of m. Hexanethiol ligand exchange (A) and hexanethiol/phenylethane thiol mixed Brust synthesis (B) matched with calculated ligand distributions, but thiophenol ligand exchange (C) demonstrated a narrower ligand exchange distribution. Adapted with permission from ref. 46. Copyright 2008 American Chemical Society.

Gold-thiolate precursor complexes and capping structures

Complexes of cationic gold and thiols are well-known, having been used for medicinal purposes for some time.[17] The complexes form both ring and linear structures; aurophilic binding induce aggregation until, in many cases, they become insoluble. In the Brust synthesis, these complexes are generated and then reduced to

form ligand-protected AuNPs. An alternative case of cationic gold binding to thiolate ligands are self-assembled monolayers (SAMs), where a planar film of gold is oxidized by binding to the thiolate monolayer. It was long assumed that gold nanoparticles were a kind of three-dimensional SAM, with planar gold surfaces on every face of the nanoparticle.

The first experimental evidence of a distinct and discrete gold-thiolate capping structure arose in 2007, when Cliffel and coworkers analyzed tiopronin (Tio)-protected AuNPs using ESI-MS and found a dominant $Au_4(Tio)_4$ ion species.[48] This $Au_4(Tio)_4$ complex – which has been found to be a tetrameric ring structure[49] – was estimated to be a favorably eliminated structural formation present on the surface of the nanoparticle. The same tetrameric complex ion was obtained by ESI-MS analysis of a gold-tiopronin precursor complex, and more recently by MALDI-MS.[49,50] The two separate analyses which yielded a remarkably similar mass spectrum indicated that the surface of AuNPs was dominated by cationic gold-thiolate complexes not dissimilar to the precursor complexes prior to reduction.

Kornberg and colleagues' crystal structure of the $Au_{102}(p\text{-}MBA)_{44}$ cluster, published later in 2007, revealed the presence of semi-ring "staple" structures which capped a gold core.[18] In the 2008 MALDI-MS study of $Au_{25}(SCH_2CH_2Ph)_{18}$ by Dass and co-workers, the first major fragment upon raising laser fluence corresponded to a loss of $Au_4(SCH_2CH_2Ph)_4$, as shown in Fig. 3.[40] The same loss has been prominent in MALDI-MS spectra of $Au_{38}(SCH_2CH_2Ph)_{24}$ and $Au_{68}(SCH_2CH_2Ph)_{34}$.[39] Heaven *et al.* published the crystal structure of $[Au_{25}(SCH_2CH_2Ph)_{18}]^-$ later in 2008.[32] No $Au_4(SCH_2CH_2Ph)_4$ features were present on the cluster, suggesting that the feature

18

appears during ionization prior to elimination. This idea is strongly reinforced by Dass' recent observation of a similar elimination from $Au_{68}(SCH_2CH_2Ph)_{34}$ and $Au_{38}(SCH_2CH_2Ph)_{24}$.[39] It should be noted that the cluster in Heaven's crystal structure was negatively charged, while the tetramer loss is more prominent in the positive ion mode. Furthermore, tandem ESI-MS spectra obtained by Fields-Zinna *et al.* which shows a tetrameric ion generated from $[Au_{25}(SCH_2CH_2Ph)_{18}]^+$ after collision-induced dissociation (CID).[51] The well-known "staple" $Au_2(SR)_3$ capping structure of this MPC was also present in the spectrum. This staple feature was also present as a loss from the $Au_{146}(SR)_{59}$ cluster.[22] This work demonstrates the capabilities of CID to provide an interesting view into the gold-thiolate capping structures of MPCs.

The tetrameric $Au_4(SR)_4$ feature may an alternate capping structure to the "staple" for some nanoparticles. The tetrameric $Au_4(SCH_3)_4$ was observed on planar gold by Voznyy and coworkers.[52] For the $Au_{38}(SCH_3)_{24}$ nanoparticle, Häkkinen used density field theory to predict the existence of six $(AuSCH_3)_4$ rings surrounding the core.[53] The tetrameric ring structure was described as having a "convergence in stability and electronic properties."[54] Furthermore, computational work by Gronbeck *et al.* investigated the differences between staple complexes, as seen in crystal structures, and tetrameric cycles and linear multimers of gold-thiolate complexes when located on a metallic gold Au(111) surface.[55] The tetrameric ring complex was lower in energy than three-fold hollow thiolate binding, but higher in energy than staple structures. The prominence of these $Au_4(SR)_4$ ions suggests some degree of similarity between the architecture of gold-thiolate complexes and the cationic gold of AuNPs.

Investigations of the relationship between gold-thiolate complexes and AuNP structure have implications for improving AuNP syntheses. A recent study has suggested that the physical structure of a gold-glutathionate complex controls the size of the AuNPs formed by reduction.[56] Another study improved the yield of $Au_{25}(CH_2CH_2Ph)_{18}$ clusters by controlling the size of a gold-phenylethanethiolate precursor complex aggregate.[57] These reports indicate that the next step in improving AuNP syntheses may involve precise control of the gold-thiolate complex structure. A technique yielding precise structural information on an atomic level would be required to advance such research. Mass spectrometry provided the first indicator of unique AuNP structural capping phenomena, and the continuing investigation of the relationship between gold-thiolate complexes and AuNP structure may require the unique capabilities of an MS-based platform.

Conclusion

Mass spectrometry is a powerful analytical tool in part because of its capacity for revealing what would otherwise be unobtainable information. For this reason, mass spectrometry has played a prominent role in the discovery and application development of monolayer-protected AuNPs. While much of the progress detailed in this report has occurred since 2007, this progress has contributed greatly to our understanding of gold MPCs, thereby fueling interest in their unique properties and enabling potential applications.

However, the inherent properties of metallic NPs – the high mass of intact NPs, the molecular polydispersity present in the overwhelming majority of NP samples, and the extreme tendency toward fragmentation, particularly for NPs with hydrophilic ligands –

appear to place intrinsic size- and ligand-based limitations on the MS analysis of intact NPs. There is a growing need for an analytical platform which is well-suited for the routine characterization of monolayer-protected metal NPs, but without highly novel advances in the field, MS may remain an effective characterization platform for gold MPCs alone.

In addition to routine characterization, there are several questions remaining in this field which are highly relevant to both a thorough understanding of nanoscale monolayers on metallic nanoparticles and to the development of metal NP-based applications. For example, the nature of the metal-thiol interface has only been elucidated for small, hydrophobic, magic-sized gold MPCs with defined charge states (-1[32] or 0[18,58]). For nanoparticles composed of alternate metals (*i.e.*, Ag or Pd)[59] or water-solubilizing ligands,[59,60] with larger core sizes or different charge states, the metal-organic interface has not been sufficiently characterized experimentally. Extrapolation from available data on gold MPCs[61] and density functional theory (DFT) calculations on Au(111)[55,62] suggests that gold-thiolate complexes are present on AuNPs of all size, though corroborating experimental evidence is scant.[48] Furthermore, in recent years a number of reports have predicted[63] or asserted[25,64,65] the existence of phase segregation in monolayers on metal NPs, but an unequivocal confirmation of any has yet to emerge. The question of the existence of phase-segregation in nanoscale monolayers remains open.

The great majority of interest in monolayer-protected metal NPs is focused on their surfaces, which can occupy a large amount of chemical space through the use of diverse thiolates and mixtures of thiolates, some of which are expected to be capable of phase-

segregation. Thus, analytical platforms which can thoroughly characterize the metal NP surface would be the most useful tool in this field.

It has been clearly established in the literature that the gold-thiolate complexes which form the monolayer of gold MPCs can be desorbed from the MPC and by relatively low-energy in-source fragmentation processes (*e.g.*, ESI and MALDI at low laser intensities).[29,40,51] Therefore, I hypothesize that if metal-thiolate complexes which are observed in mass spectra correspond to pre-existing metal-thiolate complexes in the protecting monolayer, then observed complexes should reflect the monolayer characteristics of the parent nanoparticle. To test this hypothesis, three experiments can be performed. First, metal-thiolate complexes should be observed in the mass analysis of any monolayer-protected metal NPs on which they are known to exist. Second, the abundance of thiolate ligands within observed metal-thiolate complexes should correspond to the abundance of the ligands on the intact metal NP core, as measured by a non-destructive technique such as NMR spectroscopy. Third, phase-segregated ligands in the monolayer will create phase-segregated complexes; in other words, complexes will be more likely to contain only one of the thiolates in the mixture. These experiments also conveniently permit the investigation of mass spectrometry as a platform for the routine surface characterization of monolayer-protected metal NPs. The results of the experiments, and an appraisal of the use of mass spectrometry for NP characterization, are reported in the following chapters.

CHAPTER II

PRODUCTS OF MONOLAYER-PROTECTED METAL NANOPARTICLE
IONIZATION AND FRAGMENTATION

Introduction

As discussed in Chapter I, mass spectrometry is a powerful tool for the study of monolayer-protected metallic nanoparticles, providing the route to understanding the "magic" sizes as well as the gold-thiol interface. Combined with density functional theory (DFT) calculations,[53] the mass spectrometric evidence[48] led to a new interfacial model. This model was refined and validated by subsequent crystallographic[18,32,38] and theoretical[21,66,67] measurements. The discovery of the protecting gold-thiolate complex led to a reassessment of protection schemes for planar surfaces such as Au (111), with an emphasis on reconciling the gold-thiolate complex with previous measurements.[52,55,68,69]

For similar metals such as silver and palladium, the nature of the metal-organic interface at the surface of ligand-protected metallic nanoparticle cores has been explored through numerous approaches, theoretical and experimental.[9,70] Understanding these interfaces is crucial for developing the physical and electronic properties of metal NPs for applications in catalysis and other fields. However, very few reports have been published since the advent of the gold-thiolate protection model, and thus do not take a metal-thiolate theme into consideration. One exception is a recent computational study on palladium (111) surfaces,[71] which proposed an adlayer of palladium-thiolate complexes on a palladium-sulfide surface, in agreement with previous experimental findings.[72]

For thiolate-protected nanoparticles with Ag[59,73,74] or Pd,[59,75] cores, only one published report has investigated this interface, predicting the presence of bridging thiolate ligands for very small $[Ag_7(SR)_4]^-$ clusters.[76] The lack of investigation into the metal-thiol interface is surprising, considering the interest in the catalytic properties of palladium[75,77] nanoparticles and the known catalytic activity of gold clusters with protecting gold-thiolate moieties.[78]

This chapter presents data regarding the fragmentation of monolayer-protected Au, Ag, and Pd nanoparticles. For the latter two, we have found evidence for the existence of analogous protecting metal-thiolate complexes on silver and palladium nanoparticles. By performing an experiment on AgNPs and PdNPs which was somewhat analogous to previous work on AuNPs, we discovered silver- and palladium-thiolate complexes with some stoichiometric differences from their gold-thiolate counterparts. This evidence should lead to an improved understanding of the catalytic properties of thiolate-protected metal nanoparticles. Together with the published reports of other groups covered in Chapter I, the data presented here provide a synoptic view of monolayer-protected metallic nanoparticle fragmentation in different ionization sources.

Experimental Procedures

Reagents

All chemicals were purchased from Fisher Scientific or Sigma-Aldrich and used as received with the exception of tetrachloroauric acid, which was synthesized as described elsewhere.[79]

Tiopronin-protected AuNP synthesis

Tetrachloroauric acid (HAuCl$_4$•3H$_2$O) was combined with three equivalents of tiopronin in 85:15 MeOH:acetic acid at 0 ℃. The solution was stirred for 3 hours, after which sodium borohydride was added in a 10:1 NaBH$_4$:Au molar ratio. The nanoparticles were dialyzed for 3 days until observed to be clean by NMR spectroscopy, that is, free of any narrow peaks indicative of unbound tiopronin or other organic molecules.

Hexanethiolate-protected AuNP synthesis

Tetrachloroauric acid was dissolved in deionized water and combined with a slight molar excess of TOABr in toluene. Once the gold was completely transferred to the organic layer (evidenced by a red organic layer and clear aqueous layer), the aqueous layer was removed and three equivalents of hexanethiol were added. After the solution became clear, 10 equivalents of NaBH$_4$ were dissolved in cold deionized water and added to the solution. The generated nanoparticles were precipitated in methanol. The methanol was filtered off, and the product was washed three times each with water, ethanol, and acetone, followed by sonication in acetonitrile.

Tiopronin-protected AgNP synthesis

Silver nitrate (64.9 mg) was dissolved in 30 mL acetonitrile and combined with tiopronin (62.7 mg, 1:1 metal:ligand ratio) in 30 mL methanol. A yellow-green gel formed immediately, indicating the formation of silver-thiolate complexes. After 3 min sodium borohydride (143.2 mg, 10:1 reductant:metal ratio) dissolved in a minimal amount of methanol was added to the reaction mixture. Within a few seconds the solution

transitioned from yellow-orange to a deep orange-black color indicating the presence of nanoscale particles. After a few minutes, the color became black-red, with some precipitates on the walls of the flask. The mixture was allowed to stir for 30 min and then was transferred to culture tubes for centrifugation. The supernatant was discarded and deionized water was added. The sample was transferred to a flask and any remaining methanol was removed in a rotary evaporator at <30 °C. The remaining solution was dialyzed for 3 days.

Tiopronin-protected PdNP synthesis

Palladium acetate (101.2 mg) was dissolved in 20 mL acetonitrile and combined with tiopronin (36.3 mg, 2:1 metal:ligand ratio) in 10 mL acetonitrile. The mixture formed a cloudy orange precipitate within seconds, again indicating the formation of palladium-thiolate complexes. After 3 min sodium borohydride (168.9 mg, 10:1 reductant:metal ratio) was dissolved in a minimal amount of methanol and added to the reaction mixture. The solution immediately became black with some precipitation observed. The solution was evaporated under vacuum at >30 °C and deionized water was added. The nanoparticles were then dialyzed for 3 days.

Gold-thiolate synthesis

Gold-thiolate complexes were formed by combining tetrachloroauric acid with 3 molar equivalents of thiol ligand (glutathione, tiopronin, cysteine, 2-mercaptoethanol, or hexanethiol) in dry methanol (Fisher) at 0º C. The product was generally a clear solution, turning into a white precipitate over the course of seconds to hours

26

In a separate experiment, gold(I)-triphenylphosphinechloride was combined with mercaptoundecanoic acid in toluene with some sonication to enhance the solubility of the ligand. The solution was clear, with a cloudy white precipitate building over the course of several days.

MALDI-TOFMS characterization

Samples were prepared for MALDI analysis by the dried droplet method.[80] Tiopronin-protected AuNPs (3 mg/mL) were combined with DHB (gentisic acid, 0.07 M in water). For the hexanethiol-protected AuNPs, 20 µL of a 10 ug/mL solution of AuNPs in methylene chloride was combined with 20 µL of a saturated solution of sinapinic acid (Sigma Aldrich) in methylene chloride. Gold-thiolate complexes were combined with saturated α-cyano-4-hydroxycinnamic acid (CHCA, in methanol) and 1% mg sodium chloride. For each sample, a 1 µL aliquot was deposited on a stainless steel plate. Samples which contained precipitates were sonicated immediately prior to spotting. MS analysis was performed on an Applied Biosystems Voyager DE-STR with equipped a nitrogen laser (337 nm). Spectra were obtained in the negative ion mode for AuNPs, and positive ion mode for gold-thiolate complexes.

Electrospray-mass spectrometric (ESI-MS) characterization

Solutions of approx. 3 mg/mL nanoparticles in 1:1 H_2O:MeOH or an Au-thiol mixture in toluene were analyzed on Thermo-Finnigan LCQ Classic (Waltham, MA, USA). The sample was injected using a syringe pump operating at 4 µL/min. The source and

capillary voltage were set to 4.5 kV and 9.8 V, respectively, and the capillary temperature was 200 °C. Spectra were collected in the negative ion mode.

Results and Discussion

MALDI-MS analysis of monolayer-protected AuNPs

For tiopronin-protected AuNPs, the ion products were gold-sulfur clusters forming a polymer-like distribution from ~2-15 kDa (Figure 7). The Au:S ratio in these ions ranges from 2-3:1, roughly increasing with the mass of the ion. This ratio, which is similar to that of intact AuNPs, indicates that the primary fragmentation pathways involve carbon-sulfur bonds rather than gold-gold or gold-sulfur bonds. The most abundant ion, $[Au_{25}S_{12}]^-$, is common in mass spectra of $Au_{25}(SR)_{18}$.[81] This result suggests that tiopronin may form the $Au_{25}(SR)_{18}$ superatomic cluster in a similar fashion to glutathione[81] and phenylethanethiol.[82] Below 4 kDa, the pattern becomes convoluted with other unidentifiable ions, which may contain a mixture of fragmented and unfragmented tiopronin ligands.
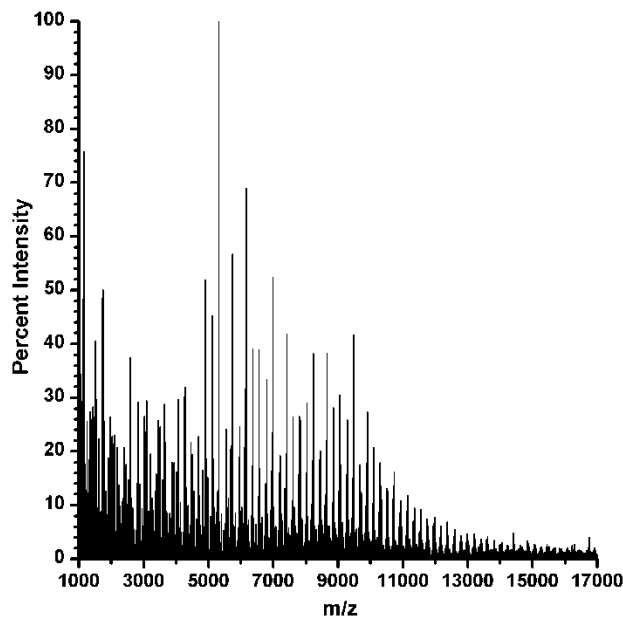
Figure 7. The mass spectrum of tiopronin-protected AuNPs, obtained in the negative ion mode on an Applied Biosystems Voyager DE-STR. The most abundant ions are gold-sulfur clusters, while ions below ~3 kDa contain some unfragmented thiolate ligands.

Notably, the resolution in this spectrum is poorer than expected (~500 at the base peak). The amount of energy deposited in AuNPs by this method is very large, cleaving every carbon-sulfur bond and generating a wide array of gold-sulfur fragment ions. Fast atom bombardment (FAB), an ionization technique which deposits much higher amounts of energy, generates similar gold-sulfur ions.[83] This suggests UV radiation imparts a uniquely high amount of internal energy to the AuNP, generating a wide array of fragments with a massive amount of mass lost. It is possible that this fragmentation may have a thermal element, since the effective temperature under similar conditions has been calculated to be well in excess of 10^4 K.[84] Thermal gravimetric analysis (TGA), another characterization method for AuNPs, is known to fully desorb the organic ligands, including the thiolate headgroups, by heating to temperatures on the order of 10^3 K over the course of 10^4 s.[28] The energy deposition and transition to the gas phase under high

vacuum is much more rapid during the MALDI process, thus any internal energy in each ion would not be dissipated easily. Furthermore, the cleavage of any carbon-sulfur bond appears to generate a radical AuNP anion and a neutral tailgroup.[30] The UV radiation of AuNPs and the subsequent cleavage of *every* carbon-sulfur bond should therefore lead to a heavily-charged ion with a very high internal energy. As all ions observed here are singly charged, as is common for ions generated by MALDI, each ion may be passivated by a number of protons donated by the acidic matrix. This variety in stoichiometry – as well as the behavior of the ion in an electric field during extensive gas-phase chemistry – likely causes the unusual broadness of each gold-sulfur peak.

The hexanethiol-capped AuNPs studied exhibited extremely broad peaks centered on 13, 22, and 28 kDa (Figure 8). These broad peaks correspond to "magic sized" $Au_{68}(SC_6H_{13})_{34}$,[27] $Au_{102}(SC_6H_{13})_{44}$,[18,27] and $Au_{144/146}(SC_6H_{13})_{60/59}$.[30,32] (Figure 3) The small peak at ~10.5 kDa may correspond to $Au_{55}(SC_6H_{13})_{31}$.[85] Because the ions are more massive gold-sulfur clusters than those observed from tiopronin-protected AuNPs, there should be a greater number of gold-sulfur stoichiometries present, causing extremely broad peaks ($R \approx 10$).
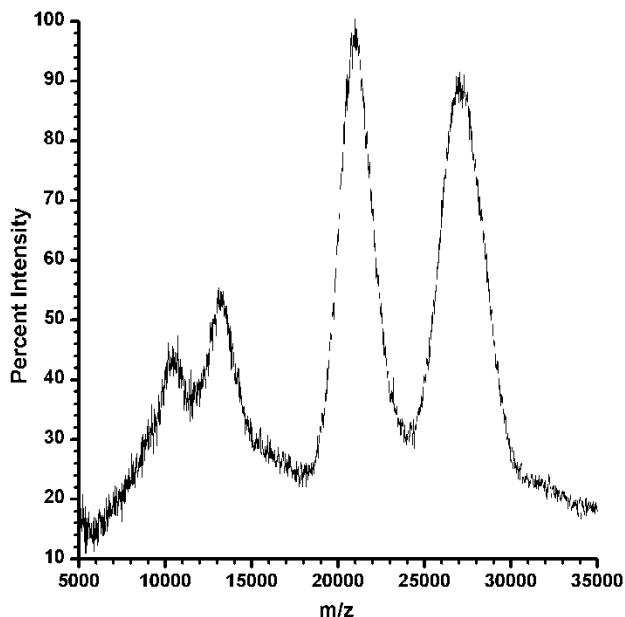
Figure 8. Mass spectrum obtained from hexanethiolate-protected AuNPs. Data was smoothed using a Savitzky-Golay (150-point quadratic) method. Data is comparable to Figure 3F, an unfractionated sample of dodecanethiolate-protected AuNPs. Broad peaks centered at approximately 13, 21, and 28 kDa correspond to gold-sulfur cluster fragments of $Au_{68}(SC_6H_{13})_{34}$,[27] $Au_{102}(SC_6H_{13})_{44}$,[18,27] and $Au_{144/146}(SC_6H_{13})_{60/59}$,[30,32] respectively. The small peak at ~10.5 kDa may correspond to $Au_{55}(SC_6H_{13})_{31}$.[85]

MALDI- and ESI-MS analysis of gold-thiolate complexes

As discussed in Chapter I, an investigation of the gold-thiolate complexes which serve as precursors to the reductive formation of AuNPs may lead to new advances in synthetic methodologies, improving product monodispersity and the ability to target specific size ranges. In the case of tiopronin-protected AuNPs, recent improvements in understanding the stoichiometry and structure of the gold-tiopronin complex has established a way forward. Mass spectrometry played a prominent role in the discovery process, elucidating the unique tetrameric Au_4L_4 stoichiometry and pointing to a cyclic structure, as recently confirmed by X-ray techniques.[49] Following on the work of Cliffel and coworkers,[48] we

characterized the complex by MALDI in order to compare its solvated and crystalline structure (Figure 9).
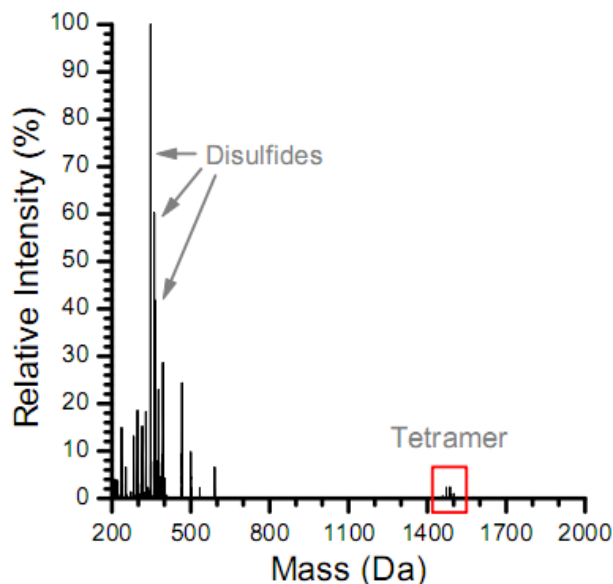
Figure 9. Positive ion LDI-TOF mass spectrum of gold-tiopronin complex. The sample was taken directly from the synthetic solution. The only peaks corresponding to gold-tiopronin bonding are the tetrameric ions. The most intense peaks correspond to tiopronin disulfides.

A large amount of the signal are organic ions, primarily disulfides. A small portion at a higher mass consists of the Au_4L_4 stoichiometry, coordinated to different numbers of sodium atoms. The ligands are not fragmented as observed for the MALDI products of AuNPs, pointing to a significant difference in ionization mechanisms and ion internal energy despite the similar energy imparted to the sample.

As a broader experiment, gold-thiolate complexes with a variety of ligands were formed and characterized by MALDI-TOFMS. The products of each were a series of low-mass complexes, but the stoichiometry of the different complexes differed greatly (Table 1). Less-polar ligands and those with a smaller steric profile (alkanethiols and ω-

32

functionalized n-alkanethiols) appear to prefer larger and more diverse Au_xL_{x-1} stoichiometries, while bulkier, more polar ligands prefer smaller Au_xL_{x-1} or Au_xL_x stoichiometries.

$Au_x(SR)_y$	SR=				
x,y	Glutathione	Tiopronin	Cysteine	2-Mercapto-ethanol	Hexanethiol
4,3	97%	-	89%	2%	-
4,4	-	100%	-	4%	5%
5,4	3%	-	11%	4%	7%
6,5	-	-	-	62%	51%
7,6	-	-	-	17%	25%
8,7	-	-	-	10%	11%

Table 1. The preference of various gold-thiolate complexes for given stoichiometries, measured as a percent of total positive gold-thiolate ion signal obtained by MALDI-TOFMS for that complex. Bulkier and more polar ligands favor smaller, more discrete stoichiometries. Less polar and less bulky ligands prefer larger, more diverse stoichiometries.

The influence of ligand sterics likely reflects the variability of the dihedral bond angles in the gold-sulfur backbone.[54] The bulkier ligands force sharper angles, terminating the backbone more abruptly. Terminal carboxylic acids or amines may also interact with the terminal gold atoms, decreasing the extension of the backbone by inhibiting a gold-sulfur interaction. This would have the second effect of making the stoichiometry more discrete, as observed. Less bulky and polar ligands will be more likely to extend away from the gold-sulfur backbone, permitting longer and more linear complexes.

A recent report by Lennox and coworkers[86] investigated the precursor molecules to the Brust synthesis[1] which are formed in toluene. The authors asserted that gold-thiolate complexes are not formed in nonpolar solvents. In order to test this assertion, we combined gold(I) chlorotriphenylphosphine and one molar equivalent of thiol in toluene and observed the products by mass spectrometry. The ions which were generated by MALDI and electrospray ionization were all gold-thiolate products with Au_xL_{x+1} stoichiometries (Figure 10). This establishes the fact that gold-thiolate complexes can be formed in a nonpolar solvent. The result obtained by Lennox and coworkers likely reflects the interaction of gold with a quaternary amine surfactant, preventing the generation of gold-thiolate complexes.
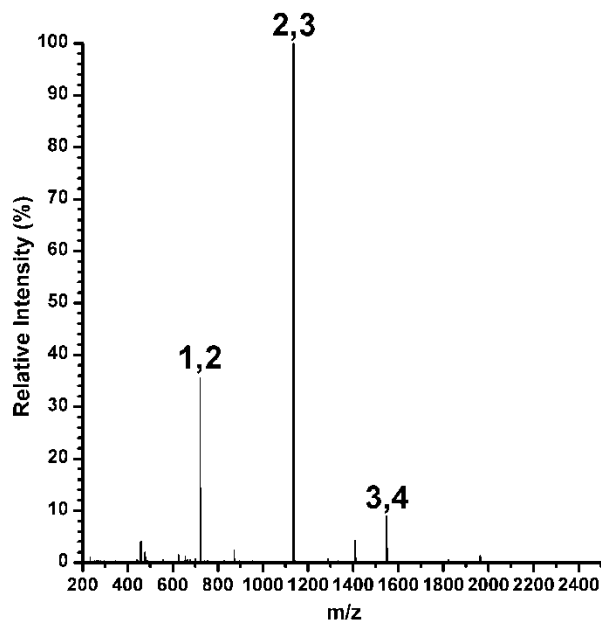
Figure 10. Mass spectrum of Au^I-mercaptoundecanoic acid complex formed in toluene. Their $Au_x(MUA)_y$ stoichiometries are notated (*x*,*y*). Each of the ions is coordinated to a relatively large number of sodium atoms (2 or 4). An equivalent spectrum obtained without matrix assistance is similar, but produces abundant ions with fragmented ligands.

Preliminary studies have indicated that Au(III) does not form gold-thiolate complexes in toluene in the presence of a tetraoctylammonium (TOA) counterion, but gold chlorotriphenylphosphine does form complexes despite the presence of TOA (Table 2). Remarkably, this initial evidence suggests that the gold-thiolate complexes formed by combining gold chlorotriphenylphosphine and mercaptoundecanoic acid in the presence of TOA are stoichiometrically different from complexes formed in the absence of TOA. This may shed light on the results of a recent comparison of syntheses with and without TOA.[87] Together, these data indicate that TOA is not as attracted to the less ionic gold chlorotriphenylphosphine as to chloroaurate, but still plays a pivotal role in restricting gold-thiolate formation in the Brust synthesis.

Mixture	Au-MUA Complex?
Au^{III} + MUA	✓
Au^{III} + TOA^+ + MUA	✗
Au^{I} + MUA	✓
Au^{I} + TOA^+ + MUA	✓

Table 2. The formation of Au-MUA complexes from various combinations of metal and ligand in the presence of a tetraoctylammonium cation. The results indicate that gold-thiolate complexes can be formed in a nonpolar solvent, but that the TOA cation interferes with their formation.

Notably, in all mass spectra the gold-thiolate ions observed were coordinated to multiple sodium atoms, normally 3 or 4. This was unexpected, since no component of the mixture contained any significant amount of sodium. The polar gold-thiolate complex appears to attract ionic species from the nonpolar medium, eventually precipitating as a cloudy white solid as observed.

ESI-MS analysis of tiopronin-protected silver and palladium NPs

The mass spectrum obtained from the electrospray ionization of each metal nanoparticle is shown in Figure 11. It should be noted that both silver and palladium induce a unique isotopic pattern for each metal-thiolate ion, which makes the ions easy to distinguish from organic ions. In the case of silver, the isotopic envelope allows measurement of the number of silver atoms in the ion, enhancing molecular formula assignment.[50] Nearly all observed ions were metal-thiolate ions, and all were singly charged as observed in previous ESI analyses of gold-thiolate complexes.[51] The lack of ligand fragmentation, similar to the gold-thiolate ions generated by MALDI, indicates the low internal energy relative to the gold-sulfur ions generated by MALDI.
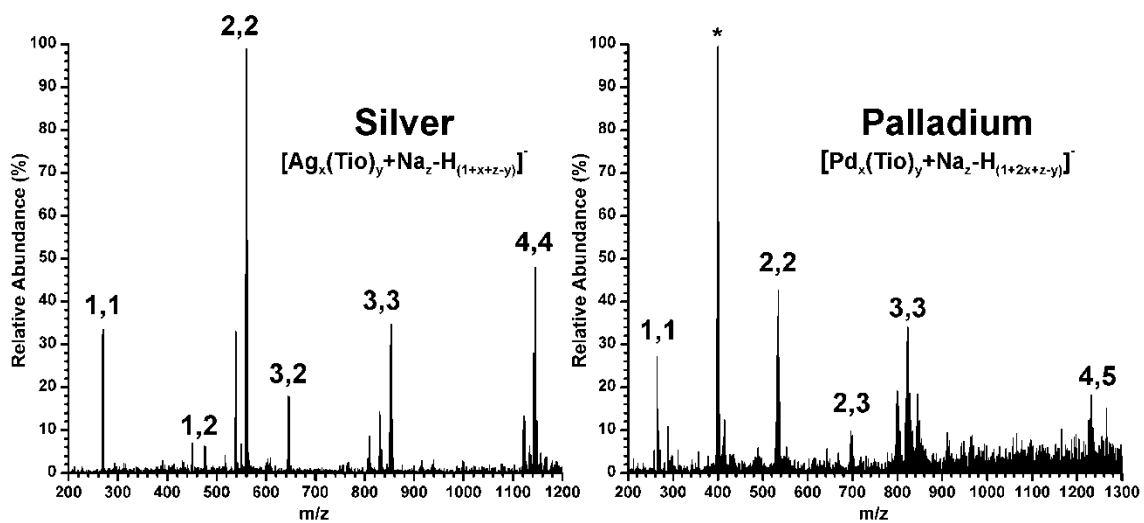
Figure 11. Electrospray-mass spectra of tiopronin-protected silver and palladium nanoparticles, obtained in negative mode. The peak notation is *x,y*, where *x* is the number of metal atoms and *y* is the number of tiopronin ligands. The general *x:y* stoichiometry of 1:1 is similar to that observed in gold, though the ions observed are smaller (i.e., for most ions *x* and *y* < 4).

The mass spectrum on the left is that of monolayer-protected silver nanoparticles. The primarily 1:1 silver:tiopronin stoichiometry is similar to that of gold, as is be expected due to their similar chemistries. Such complexes are natively neutral, with the silver bearing a formal positive charge and the sulfur of the thiol ligand bearing a formal negative charge. However, these complexes are generally smaller than their gold counterparts, and display more diverse stoichiometries compared to gold.[48]

In the case of palladium (II), the results are more surprising. Their d^8 electronic structure, which leads to a +2 formal charge state, should make complexes which are more cationic relative to gold and silver. There were no palladium-thiolate observed ions in the positive mode, and the negative ions revealed a surprising pattern: each of the tiopronin molecules were deprotonated at least once, and some twice. The first deprotonation occurs at its most acidic site, the carboxylic acid. The second most acidic

37

site on tiopronin is expected to be its central amide bond, though the pKa of this group should be relatively high, making the deprotonation surprising. It is possible that the palladium may induce some reaction which oxidizes the ligand, removing protons; tandem MS analysis proved inconclusive with respect to the possibility of ligand modifications. This finding is even more surprising in light of the single charge observed on all metal-thiolate ions. Apparently the energy needed to deprotonate a relatively basic site such as an amide bond is less than the energy needed to preserve a metal-thiolate structure intact with multiple charges. This may be relevant to studies of the electronic structures of the metal-thiolate structure, which have indicated an aromatic element along the gold-sulfur backbone of analogous complexes[88] as well as influence over electron localization in the organic portion of the ligands,[54] potentially affecting their acidity.

From a structural standpoint, the results presented here are highly relevant to any understanding of the metal-thiol interface of these nanoparticles. The scarce studies which have explicitly taken a metal-thiolate capping structure into account have both demonstrated them to be energetically favored.

Conclusion

The ionization of monolayer-protected metal nanoparticles is unique, producing a mixture of unfragmented nanoparticle ions, protecting metal-thiolate complex ions, and gold-sulfide clusters, depending on the nature of the nanoparticle and the ionization technique. The observation of gold-sulfide clusters, in which all carbon-sulfur bonds have been photolytically cleaved, suggests a highly efficient transmission of photon energy to the internal energy of the nanoparticle. Nevertheless, low-mass metal-thiolate fragments

can be observed which have not undergone C-S bond scission, indicating a separate and lower-energy ionization pathway which precedes the generation of gold-sulfide clusters. Mass spectrometry was also utilized to investigate the presence or absence of gold-thiolate complexes under various circumstances, leading to new mechanistic insights into the seminal synthesis of AuNPs

In this chapter, mass spectrometric data has been presented which provides a great deal of information on the products of AuNP fragmentation in MALDI and ESI sources, the existence of gold-thiolate complexes under various conditions, the determining factors for gold-thiolate complex stoichiometry, and the nature of the metal-thiol interface for silver and palladium nanoparticles. In addition, the existence of previously unknown $Au_{25}(Tiopronin)_{18}$ clusters is suggested by mass spectral fragmentation patterns. This wide range of investigations – including those discussed in Chapter I, such as core size and charge measurement – all of which are relevant to metal nanoparticle chemistry, illustrates the power of mass spectrometry as an analytical platform.

Acknowledgements

Vanderbilt College of Arts and Sciences, the Vanderbilt Institute of Chemical Biology, and the Vanderbilt Institute for Integrative Biosystems Research and Education.

ION MOBILITY-MASS SPECTROMETRIC ANALYSIS OF HOMOLEPTIC MONOLAYER-PROTECTED METAL NANOPARTICLES

Introduction

The full characterization of any ligand-protected AuNP, *i.e.*, non-averaging measurement of size and molecular composition, is not currently possible in a single analytical platform. Mass spectrometry (MS) has shown considerable promise as a characterization technique, whereby gold cores less than 2 nm in diameter have been sized by MS,[31] and intact AuNP analysis is theoretically capable of providing both size and molecular composition information.[40] However, AuNP characterization by MS is currently effective only for hydrophobic ligand-protected AuNPs up to *ca.* 2 nm in diameter[44] and hydrophilic AuNPs with 39 gold atoms or less (*ca.* 1.1 nm in diameter).[89] The investigation of low-mass AuNP fragments (<3000 m/z), such as the $Au_4(SR)_4$ ion, is likely to yield a greater understanding of the capping structural motifs of AuNPs, as discussed in Chapters I and II. Unfortunately, significant chemical noise from synthesis byproducts, other impurities, matrix molecules, and fragmented gold-sulfide clusters can create a continuous background signal which obscures diagnostically important signals.

A complementary technique which has been used for the analysis of ligand-protected AuNPs in the gas-phase is ion mobility spectrometry (IMS). The physical property providing separation selectivity in IMS is ion size, specifically ion surface area. Briefly, in IMS ions are injected into a gas-filled drift tube where they experience numerous low-energy collisions

with a background gas which separates ions based on the ion-neutral collision cross section (CCS). Smaller ions elute faster than larger ions which experience more collisions. IMS was used for measuring the diameter of ligand-protected AuNPs,[90] but the majority of IMS work relevant to this report has focused on small gold clusters generated from gold surfaces. Following the work of Jarrold *et al.*,[91,92] in 2002 Kappes and colleagues published two reports on positively[93] and negatively[94] charged gold clusters (< 25 atoms). The ion CCS of each cluster yielded a determination of their respective geometries. The ability to distinguish between various three-dimensional geometries for very small gold clusters illustrates the structural capabilities of IMS for small inorganic clusters.

Building on this foundation, we report the first application of combined ion mobility-mass spectrometry (IM-MS) to the analysis of ligand-protected AuNPs. By integrating mass and ion CCS separation, gold-thiolate ions can be isolated from nearly isobaric but larger organic ions (*i.e.*, chemical noise). Furthermore, the structural measurement capabilities of IM-MS, which have been well-documented for biomolecules,[95] could theoretically be applied in order to obtain an unprecedented amount of structural information from these ions. Because of the two advantages of signal-to-noise enhancement and structural characterization capability, IM-MS is well-suited for the study of low-mass fragments generated from ligand-protected AuNPs. The samples used in this work consisted of AuNPs protected by tiopronin or phenylethanethiolate as well as gold-tiopronin and gold-phenylethanethiolate precursor complexes for comparison using MALDI-IM-MS.

Experimental Procedures

Synthesis

Tiopronin- and phenylethanethiolate-protected AuNPs were synthesized using previously reported protocols.[48,57] The tiopronin-protected AuNPs were found to be 3.0 ± 0.8 nm in diameter by transmission electron microscopy. Gold-tiopronin and gold-phenylethanethiolate precursor complexes were formed by combining tetrachloroauric acid with 3 molar equivalents of tiopronin ([(2-mercaptopropanoyl)amino]acetic acid, Sigma-Aldrich) and phenylethanethiol (98%, Aldrich) respectively in dry methanol (Fisher) at 0° C. The gold-phenylethanethiolate complex aggregated immediately and became insoluble, creating a slurry; gold-tiopronin created a cloudy solution. After 30 min., 100 μL aliquots of the gold-tiopronin solution and gold-phenylethanethiolate complex slurry were collected.

Sample preparation

Samples were prepared for MALDI analysis by the dried droplet method.[80] The samples were combined with matrix in solution and $0.5 - 1.5$ μL of the sample was deposited on a stainless steel plate. Tiopronin-protected AuNPs were saturated in 50 μL of deionized H_2O and combined with 50 μL of dry methanol. Each sample was combined with 30 mg α-cyano-4-hydroxycinnamic acid (Sigma), and 1 mg sodium chloride (certified A.C.S., Fisher) was added to all samples except for the gold-phenylethanethiolate in order to obtain better signal from sodium-coordinated species. To a 3 mg sample of phenylethanethiol-protected AuNPs was added 100 μL acetone (Fisher) and combined with 30 mg *trans*-2-[3-(4-*tert*-butyl-phenyl)-2-methyl-2-propenylidene]malononitrile (DCTB, Fluka).[40] Each mixture was sonicated immediately prior to spotting on the MALDI plate.

Sample analysis

All spectra were obtained on a Synapt HDMS ion mobility-mass spectrometer (Waters Corp., Manchester, UK) equipped with a MALDI ion source. A travelling wave (T-wave)-ion mobility cell[96] was utilized for ion mobility separation in nitrogen gas. The ion guide T-wave was operated at 300 m s^{-1} and linearly ramped in amplitudes ranging from 1-17 V to 5-20 V for each experiment. The transfer guide T-wave was operated at 248 m s^{-1} with a constant 3 V amplitude. Trap and transfer ion injection voltages were set at 6 and 4 V, respectively. MassLynx 4.1 software (Waters Corp., Milford, MA) was used for instrument control and data processing.

Results and Discussion

Interpreting IM-MS spectra

Figure 12 is a diagram of a typical two-dimensional IM-MS spectrum, in which the abscissa axis is m/z and the ordinate axis represents drift time, which correlates to CCS. The plot can be viewed as a density map, with the upper-left quadrant being low mass and high drift time, or effectively low density. The lower right quadrant contains ions of high mass and low drift time, thus having a relatively high density. Chemical noise, composed of extensively fragmented and adducted organic ions, is present in a band of roughly constant density that spans from the lower left quadrant to the upper right. Incorporation of a gold atom within the ion increases the mass by 197 Da while increasing the CCS by a small amount. This effect creates an ion mobility shift to regions of higher density, similar to the effect of covalently bound ion mobility shift reagents utilized by McLean and co-workers.[97,98] Greater numbers of gold atoms in the ion impart a corresponding increase in

density. The cumulative pattern of gold-thiolate ions in ion mobility-mass spectrometry is the presence of multiple bands which are nearly parallel. Each band, counting from left to right, corresponds to the number of gold atoms present in the ions of that band. Within a given band, ions with a greater number of bound ligands will show up higher in the band, while ions with fewer will show up at the bottom of the band. These gold-thiolate ion trend lines are slightly inflected with respect to the organic ion trend line. A higher organic content dilutes the increased density effect and brings the overall density closer to that of the organic ion trend.
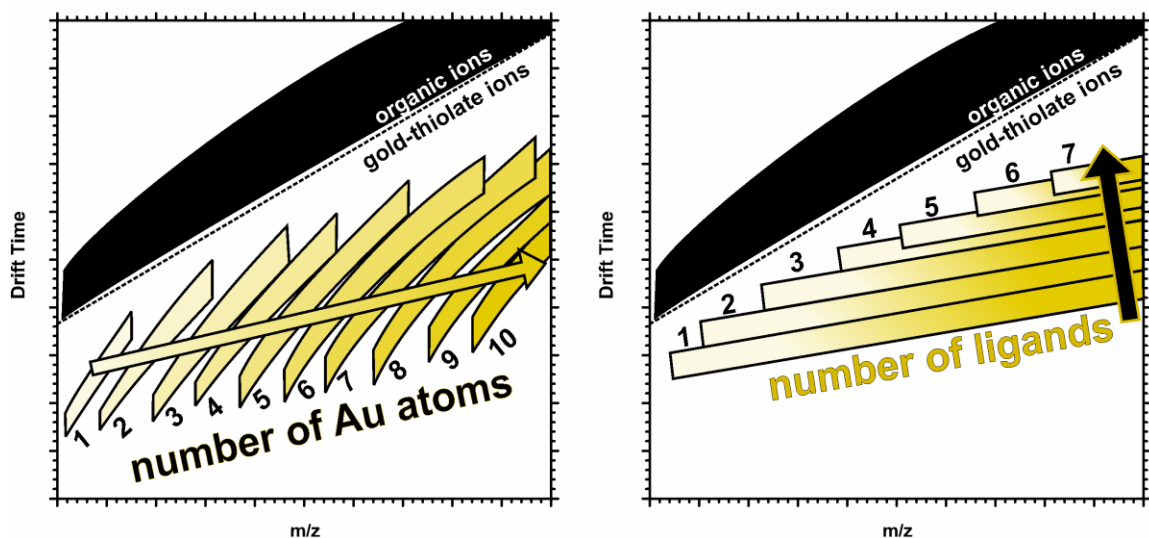
Figure 12. An illustration of a typical two-dimensional ion mobility-mass spectrum of gold-thiolate ions fragmented from monolayer-protected AuNPs in the ionization source. A broad band in the top-left of the spectrum is composed of organic ions. The small bands below and to the right of the major organic ion band correspond respectively to the number of gold atoms contained in the ions of that band. Ions higher in each band correspond to species with a greater number of thiolate ligands, bearing a higher organic content. The lowest ions in each band are the products of more extensive fragmentation, generally suffering photolytic S-C bond cleavage.

Tiopronin-protected AuNPs

Figure 13A is a two-dimensional plot of positive ions generated from tiopronin-protected AuNPs. The gold-thiolate ion species are gold-thiolate complexes, in which the gold and sulfur atoms have formal charges of +1 and -1, respectively, although the gold-sulfur bonds have a covalent character and the electrons are delocalized throughout the gold-sulfur sequence. These ions are products of dissociation from the AuNP surface which are proton- or sodium-coordinated, primarily the latter. Negative ions (Figure A 1) are products of carboxylic acid deprotonation or C-S thiolate bond cleavage. Methyl esterified ions are also present as M+14 peaks. The methyl esterification is present due the high concentration of methanol and acid during synthesis. The lower portion of each band is generally composed of ions with fragmented ligands, most of which are products of thiolate C-S bond cleavage. A wide range of gold/tiopronin stoichiometries can be observed, including ions with much larger numbers of gold atoms than thiolate ligands (*e.g.*, $Au_{13}(Tio)_8$); however, the majority of ions observed contain an equal amount of gold and ligands, $Au_x(Tio)_x$, one less gold than ligands, $Au_x(Tio)_{x+1}$, or one more gold atom than ligands, $Au_{x+1}(Tio)_x$. As in previously reported work,[51] these structures have charges of 0, -1, and +1, respectively.
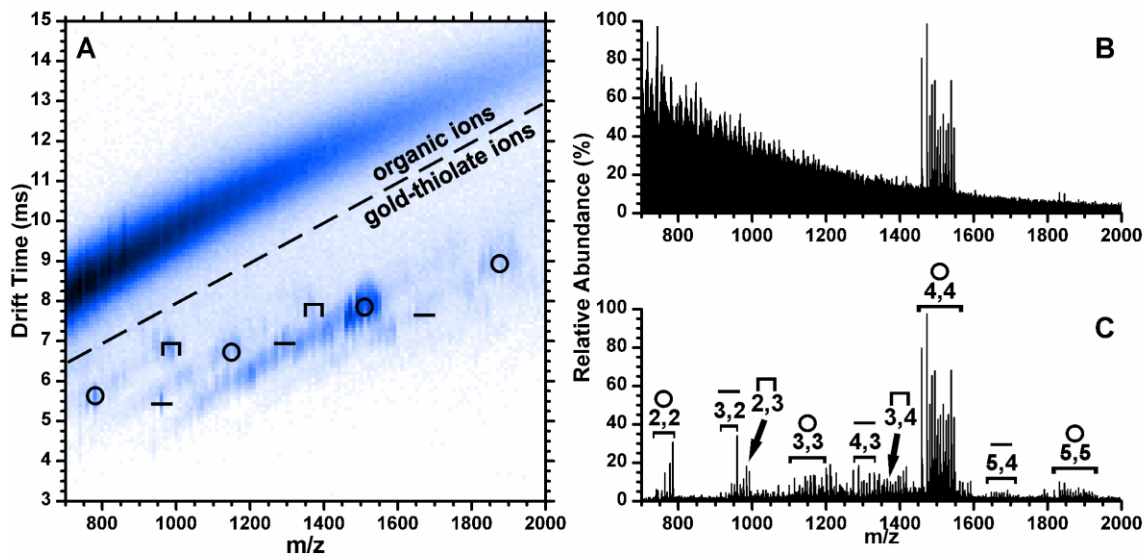
Figure 13. Ion mobility-mass spectrum of tiopronin-protected AuNPs in positive ion mode (A), and the total (B) and extracted (C) mass spectrum. Extracted signal is from the outlined region of the two dimensional plot. The symbols above the ion species in the IM-MS plot indicate their assigned structure: ring (○), linear (–), and staple (Π). In panel C, species are labeled by their molecular formula x,y for $Au_x(Tio)_y$.

It is reasonable to assume that the $Au_x(Tio)_x$ species is cyclical in light of other experimental[49] and computational[54] work; the strong preference of these species for x = 4 suggests a discrete, closed structure. Cycles are known structures for gold-thiolate complexes;[17] among these cycles, tetramers are somewhat favored.[54,99,100] The $Au_x(Tio)_{x+1}$ ions correspond to the semi-ring "staple" capping structures which have been intensively studied in recent years.[52,55,68] The structure of the $Au_{x+1}(Tio)_x$ species is not as clear, but is likely influenced by the same types of structures previously found for the first two motifs. For the sake of clarity, these species will be referred to as linear since gold-thiolate complexes are known to form linear, open chain structures.[17]

The most notably absent ion species are staple $Au_x(Tio)_{x+1}$ ions where x > 3. This reflects the desorption of staple capping motifs from the AuNP surface, which are known to exist in x

= 1,2 states crystallographically.[18,32] The presence of an x = 3 ion species may be evidence of the existence of longer staples in tiopronin-capped AuNPs. In comparison, the largest $Au_x(Tio)_x$ and $Au_{x+1}(Tio)_x$ species (including ions with ligand fragmentation) have x = 8 and 9, respectively. These larger ions are much more likely to have ligand fragmentation; the largest cyclical and linear ion species with unfragmented ligands are $Au_6(Tio)_6$ and $Au_5(Tio)_4$, respectively.

The utility of separating chemical noise by IM-MS is illustrated by the signal-to-noise enhancement shown in panels B and C. Panel B shows the mass spectrum integrating signals over all IM-MS conformation space, *i.e.*, what would be obtained without IM separation. Only the high intensity $Au_4(Tio)_4$ ion species are visible, but through IM separation, signals can be extracted from the gold-thiolate ion region as outlined in Fig. 3.2A. Note that noise is greatly reduced and low intensity signals can be observed, as shown in Fig. 3.2C. Clearly, low intensity signals corresponding to other cyclical, linear, and staple species would not be observed in the presence of the continuous chemical noise background. In comparison with the negative ion mode spectrum (Figure A 1), the preference for the cyclical ion is much stronger. The $[Au_4(Tio)_4+Na]^+$ ion is the most abundant among the gold-thiolate ion species.[39,40] The $Au_2(Tio)_3$ and $Au_3(Tio)_4$ ion species are present in very low abundance, and are the only $Au_x(Tio)_{x+1}$ ion species observed. Since the $Au_x(SR)_{x+1}$ species correspond to the only capping motif which has been proven to date, their presence in a mass spectrum generated from AuNPs is not unexpected. There is evidence in the literature that capping structures can be directly desorbed from the AuNP surface: the crystallographically demonstrated $Au_2(SR)_3$ staples of the $Au_{25}(SR)_{18}$ cluster have been observed by ESI-MS/MS.[51]

Given that capping motifs can be desorbed from the AuNP surface, the dominance of the tetrameric cycle in these spectra raises the possibility of a capping motif different from the RS-(AuSR)$_x$ complex. In the literature, the tetrameric Au$_4$(SR)$_4$ can be found as a neutral loss from small AuNPs,[39,40] and have been observed on planar Au (III) by scanning tunneling microscopy (STM).[52] The observation of abundant [Au$_{21}$(SCH$_2$CH$_2$Ph)$_{14}$]$^+$, [Au$_{34}$(SCH$_2$CH$_2$Ph)$_{20}$]$^+$, and [Au$_{64}$(SCH$_2$CH$_2$Ph)$_{30}$]$^+$ ions,[39] each reflecting this loss, suggests that the elimination of the tetramer may be driven by a common dissociation pathway. The natively neutral tetramer can also be observed as an ion through coordination to sodium, as revealed in recent tandem MS spectra of the Au$_{25}$(SR)$_{18}$ cluster.[51] Because the structure of this cluster is known,[32,58] the authors noted that the Au$_4$(SR)$_4$ motif is not seen in the crystal structure of this cluster. This implied that rearrangement may occur within the cluster prior to fragmentation. The tetramer was observed as a product of rearrangement for phenylethanethiolate-protected AuNP mass spectra obtained using an ESI source with collision-induced dissociation, so we next explored the extent of rearrangement present in the phenylethanethiolate-protected AuNP MALDI spectra.

Phenylethanethiolate-protected AuNPs

Results of the analyses of the structurally characterized Au$_{25}$(SCH$_2$CH$_2$Ph)$_{18}$ cluster using MALDI-IM-MS are shown in Figure 14. The most prominent peaks correspond to linear Au$_{x+1}$(SCH$_2$CH$_2$Ph)$_x$ ion species, the [Au$_4$(SCH$_2$CH$_2$Ph)$_4$]$^+$ ion, and a low-abundance Au$_2$(SCH$_2$CH$_2$Ph)$_3$ staple ion species. Since previous ESI and MALDI spectra show the loss of the tetramer as a neutral, the [Au$_4$(SCH$_2$CH$_2$Ph)$_4$]$^{+\cdot}$ ion abundance in Figure 14 may be small compared to the amount of tetramer lost as a neutral. Otherwise, the abundances of the

ions appear to correspond to the efficiency of cationization, *i.e.*, the natively positive linear ion species are high in abundance, while the cyclic and anionic staples are lower in abundance. Thus the types and abundances of the ions generated from $Au_{25}(SCH_2CH_2Ph)_{18}$ do not reflect only the crystallographically observed structural components of the cluster,[32] implying potential rearrangements during the fragmentation process. It is likely that other AuNPs also undergo such rearrangements during ionization.
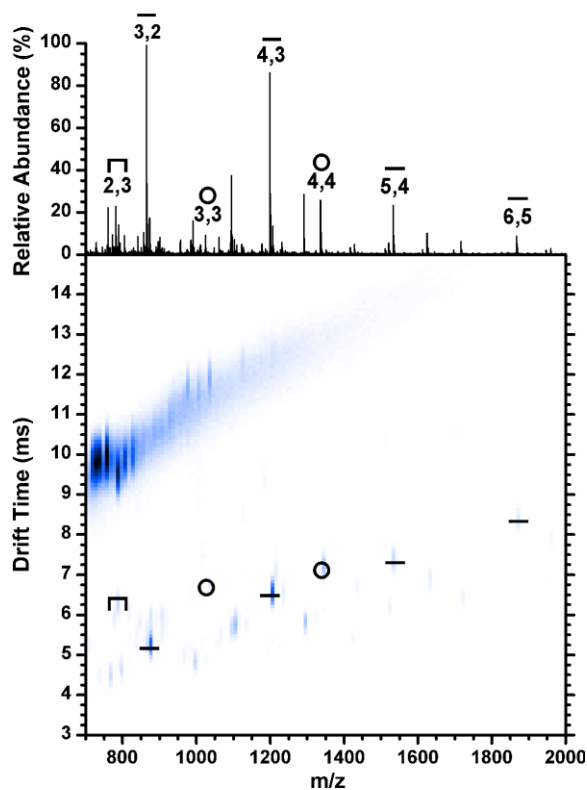
Figure 14. Positive ion mobility-mass spectrum of phenylethanethiolate-protected AuNPs and the extracted mass spectrum (above). The highest intensity ions correspond to linear structures, but the tetrameric $[Au_4(SCH_2CH_2Ph)_4]^+$ is present, as well as the $Au_2(SCH_2CH_2Ph)_3$ staple species.

Comparison to gold-tiopronin complexes

Another aspect of IM-MS is the ability to characterize both gold-thiolate precursor complexes and the corresponding AuNPs in positive and negative mode, making this

experimental technique a powerful method for the interactions of gold-thiolate complexes with the AuNP core. Figure 15 contains spectra generated from the gold-tiopronin precursor complex (top) and from tiopronin-protected AuNPs (bottom) in both the positive (left) and negative (right) ion modes. A careful analysis of the spectra shown in Figure 15 reveals three important patterns.
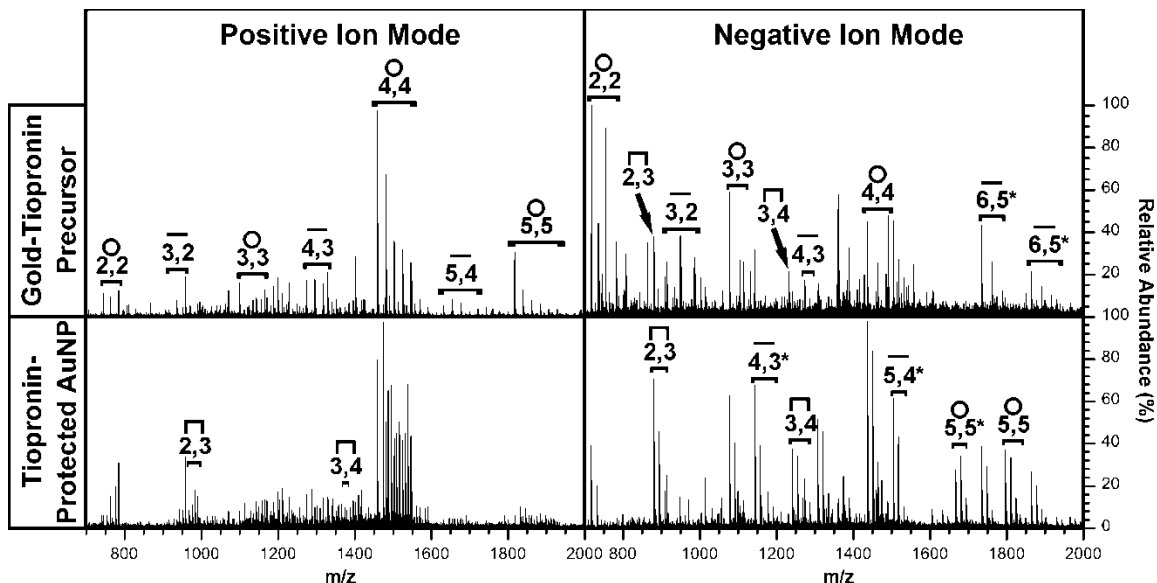
Figure 15. Extracted mass spectra of gold-tiopronin precursor complexes and tiopronin-protected AuNPs (above and below, respectively) in positive (left) and negative (right) ion mode. Structural assignment and stoichiometries are indicated as in previous figures. All assignments in above spectra are applicable to spectra underneath, with notable differences marked in the lower spectra.

The first notable pattern observed in Figure 15 is the abundance of the $Au_x(Tio)_{x+1}$ staple ions. This pattern is significant because, as previously discussed, these ions reflect the desorption of protecting gold-thiolate complexes from the AuNP surface without rearrangement. While they are not observed in the positive ion spectrum of the gold-tiopronin precursor complex, they are present in the spectrum of the corresponding AuNPs. Furthermore, in the negative ion mode these staple ions are much more abundant from the AuNP surface than from the corresponding precursor complex. Thus, overall the

staple ion species are much more abundantly generated from AuNPs than precursor complexes. This strongly implies the existence of $Au_x(Tio)_{x+1}$ capping structural motifs on the AuNP surface.

The second pattern observed in Figure 15 is the abundance of the cyclic ions. These ions are dominant, being the base peak among the gold-thiolate ions for each spectrum. The tetramer is the most abundant in the positive ion mode, in agreement with results obtained by an analogous ESI-MS experiment.[48] This agreement suggests that the dominance of the $Au_4(Tio)_4$ tetramer in the analysis of the gold-tiopronin complex is not based on sample preparation or ionization conditions, and that it is present in both in solution and in the solid phase. However, the tetramer is less dominant in the negative ion mode, particularly in the spectrum of the gold-tiopronin complex. As the smaller species are much more dominant in this spectrum, these species may be products of the fragmentation of the larger cycles into smaller species. It is important to note that, in the negative ion spectra, ionization is achieved by deprotonation or ligand C-S bond cleavage.

The final pattern concerns the conditions under which high abundances of these ions are observed. The tetrameric cycle, which appears to be the dominant form of the precursor gold-tiopronin complex, is most abundant in the positive ion mode and in the negative ion spectrum of tiopronin-protected AuNPs. The staple ion species, which correspond to capping structural motifs which have been both predicted from theory[55,66,68] and observed experimentally,[18,32,52] are also abundant in the spectra generated from AuNPs, particularly in the negative mode. Thus, it appears that negative ion products from AuNPs reflect more accurately the capping motifs of AuNPs, while positive ion products reflect a rearrangement that favors precursor-like ions. It may be significant to note that the linear ion species, which

could possibly represent staple structures with the two "anchoring" gold atoms desorbed together, are more abundant in the negative ion spectrum of the AuNPs. The high abundance of the linear ion species in this spectrum is particularly unexpected considering its natively positive charge. While the negative ion products largely reflect desorption with less rearrangement, the abundance of the negatively charged tetramer generated from AuNPs is noteworthy.

Given the abundance of tetrameric and larger ions observed in our studies, it is possible that larger AuNPs have larger substructures as capping motifs than the conventional 1 and 2 gold staples currently seen in the crystal structures of small AuNPs. Tetrameric species were observed on Au (111) by Voznyy et al. using STM.[52] Grönbeck *et al.* reported density functional calculations that compared a variety of capping structural motifs, including the cyclical tetramer, open linear chains, and staples with regard to their relative energies.[55] The cyclic tetramer was 0.53 eV/unit cell higher in energy than the staple capping motif, suggesting the preference for staple motifs. However, the energy difference between *cis-* and *trans-* orientations for staples with short SCH_3 ligands was calculated to be 0.69 eV/unit cell. This suggests that ligand interactions may have a substantial effect on the potential energy landscape of gold-thiolate capping motifs. While the typical ligand used for computational studies has been methanethiolate,[52,55,68] the hydrophilicity and hydrogen bonding availability of tiopronin should increase the degree of ligand interactions, and the corresponding effect on the gold-sulfur structures which support them.

More recent evidence supports the idea of capping structure heterogeneity. Crystal structures have been achieved for clusters with a uniform monolayer of $Au(SR)_2$ or $Au_2(SR)_3$ staples, but recent mass spectrometric reports on a larger AuNP have observed multiple

molecular formulae for what was thought to be a single, discrete "magic size:" $Au_{144}(SR)_{59}$,[44] $Au_{144}(SR)_{60}$,[22,37] and $Au_{146}(SR)_{59}$.[22] The close proximity of these assignments suggests that the difference between them may be in part from differences in the capping structural motifs. Indeed, tandem MS of the $Au_{146}(SR)_{59}$ cluster revealed a product ion corresponding to a loss of $Au_2(SR)_3$,[22] a staple structure not predicted for the $Au_{144}(SR)_{60}$ cluster.[21] In addition, the $Au_{68}(SR)_{34}$ cluster has been predicted to be formulated as $Au_{19+30}(Au(SR)_2)_{11}(Au_2(SR)_3)_4$; *i.e.*, an Au core with 11 $Au(SR)_2$ staples and 4 $Au_2(SR)_3$ staples. In light of the emerging evidence for capping structural heterogeneity, it is possible that cyclical and staple capping motifs could be present on the AuNP surface together for larger AuNPs.

Conclusion

We have demonstrated the capability of MALDI-IM-MS to analyze low-mass fragments generated from thiolate-protected AuNPs. This study underscores the advantages of structural separation prior to MS, and also provides a foundation for the facile characterization of thiolate-protected AuNP surfaces and gold-thiolate complexes. These surfaces are difficult to characterize using traditional experimental methods. This report highlights some of the advantages of the IM-MS approach by analyzing the product ions of thiolate-protected AuNPs and gold-thiolate complexes. We have demonstrated how the energetic ionization of AuNPs in the MALDI process produces positive fragment ions which are nearly identical to the gold-thiolate precursor complex. These similarities reveal an unexpected but rational reversal of the reduction of the precursor complex, and highlight the role of gold-thiolate complexes in the capping of AuNPs. The negative ions generated in the same process more

strongly correlate to capping structural motifs that are well-established in the literature. Using this technique, we have explored capping structural motifs of larger, hydrophilic AuNPs, revealing known staple capping motifs and possible cyclical capping structures.

Acknowledgements

CHAPTER IV

STOICHIOMETRIC ANALYSIS OF LIGAND MIXTURES IN MONOLAYERS
ON GOLD NANOPARTICLES

Introduction

The inclusion of multiple functionalities within the same monolayer is becoming increasingly important for AuNP applications. The most common route to mixed-monolayer AuNPs involves synthesizing monolayer-protected AuNPs with a given ligand X, followed by a ligand exchange reaction in which an alternate ligand Y is added. In the simplest cases, ligand X is chosen for reproducible syntheses and nanoparticle solubility, while ligand Y bears a functionality chosen specifically for the desired application. For example, peptides,[101] glycans,[102] and DNA[103] give specific biological functionality, poly(ethylene glycol) has been used for solubility modification,[104] and ligands with conjugated functionality yield enhanced conductivity.[105] The rate, extent of exchange, and even the placement of exchanged ligands on the AuNP surface[106] can be controlled through a number of experimental parameters: exchange time, choice of initial and alternate ligands, AuNP and ligand concentrations,[46] temperature, and AuNP oxidation state.[107] Other modification routes for monolayer-protected AuNPs involve ligand coupling reactions, such as those involving amide bond formation.[101]

Efficient analytical characterization strategies are a necessary counterpoint to these advanced synthetic and modification techniques,[108] providing experimental feedback for protocol fine-tuning and ensuring that the final AuNP product is ready for use.

Unfortunately, the rapid development of synthesis and modification methodologies has highlighted the weaknesses of current characterization strategies. Most of these methods, such as high-performance liquid chromatography (HPLC), infrared (IR) spectroscopy, and nuclear magnetic resonance (NMR) spectroscopy, measure based on ligand functionalities. This dependency makes each of these techniques impracticable for ligand mixtures which do not have extremely different functionalities. Furthermore, in the case of HPLC and IR, resolution and sensitivity limit the relative quantitation to rough estimates.[109,110]

Among these three, NMR has the most quantitative capacity, and therefore is the dominant technique in the characterization of mixed-ligand AuNPs. After identifying at least one fully-resolved and ligand-specific peak for each ligand in the mixture, the relative peak areas can be compared to obtain the relative quantity of each ligand.[47] However, in some cases, peak assignment can be complicated by interactions between the ligand and the gold core.[28] Specifically, characteristic peaks for an unbound ligand become shifted, broadened, and in some cases split when the same peak is bound to an AuNP.[111-113] The shifting and splitting of peaks increases the potential for erroneous assignments. The broadening of peaks leads to increased signal convolution, especially for large, complex, or structurally similar ligands. One way to enhance the deconvolution of the peaks is to oxidize the monolayer-protected AuNPs by the addition of iodine, which results in dissociation of all ligands as disulfide species. However, peak convolution still remains for many ligand combinations, and the proton signals closest to the disulfide linkage will be shifted yet again. Thus even under optimal conditions for

NMR measurements – dissociative oxidation and ligands with sufficiently unique functionalities – precise quantitation can be difficult.

One alternative strategy to NMR for the analysis of mixed monolayer-protected AuNPs is mass spectrometry (MS). Two different approaches have been reported: the ionization of thiols and disulfides dissociated from the AuNP surface,[114-116] and the ionization of intact AuNPs.[22,40,46,51,117] The ionization of thiols and disulfides from AuNPs follows on a large body of work using LDI to study self-assembled monolayers on two-dimensional gold surfaces.[118] This appears to be an effective method to identify the presence of an AuNP bearing a given thiol by observing certain "mass barcodes,"[114] but this strategy is only semi-quantitative.[116] Moreover, the presence of any residual disulfides from AuNP synthesis or modification can bias quantitative measurement of the bound ligands. The low mass of these molecules places the signal in an inherently noisy portion of the mass spectrum and effectively prohibits any potential use of an assisting matrix. This matrix, while not necessary for these analyses, provide a softer ionization technique with greater sensitivity and less ligand fragmentation, which is prone to take place at the carbon-sulfur bond of the thiol.[119]

The MS analysis of intact AuNP ions is a powerful method for the absolute quantitation of ligands on the AuNP surface, with the ability to simultaneously analyze the ligands and the core without population averaging. Each distinct population of AuNPs with different amounts of ligand exchange (*e.g.*, $Au_n(SR)_x(SR')_y$, $Au_n(SR)_{x+1}(SR')_{y-1}$…) can be observed and quantified directly, enabling the measurement of exchange dispersity.[46] Unfortunately, this strategy is predicated upon the ability to obtain intact, unfragmented AuNP ions. This is a severe limitation, since the ionization of intact

AuNPs has only been accomplished for small (<1.7 nm core diameter) monolayer-protected clusters (MPCs).[119] Water-soluble AuNPs are particularly prone to fragmentation, perhaps due to increased Coulombic forces. Because of these problems, mass spectrometric analysis of intact AuNPs is not currently a viable strategy for the characterization of the larger AuNPs (> 1.7 nm) which are used in many applications, particularly those which are water-soluble.

In this report we describe the use of structural separations by ion mobility-mass spectrometry (IM-MS) for the relative quantitation of ligands on AuNPs, a rapid and facile strategy for the characterization of mixed-ligand AuNPs (Figure 16). As with other MS-based methods, each ion has a unique mass depending on the number and identities of the thiolate ligands within the ion. However, there are distinct advantages of our strategy over NMR and other MS quantitation strategies. With regards to NMR spectroscopy, this method is not limited to ligand mixtures with different functionalities, since measurements are based on ligand mass. This strategy is therefore useful for a wide range of hydrophobic and hydrophilic ligand mixtures, from peptides and poly(ethylene glycol) to small molecules. Compared to MS techniques, the addition of IM separation appears to have two beneficial effects. The first, the separation of gold-thiolate ions from organic ions confirms the identities of observed ligands as being bound to the AuNP surface, enhancing the signal-to-noise ratio and eliminating quantitative measurement bias from free thiols or disulfides.[50] The second is an apparent preservation of diverse gold-thiolate ions from disintegration, perhaps through greater collisional cooling of the gold-thiolate ions.[120] Since gold-thiolate ions are generated from small MPCs and larger

59

AuNPs (>1.7 nm) alike,[50] this quantitation strategy is useful for the characterization of AuNPs which cannot be ionized intact for MS analysis.
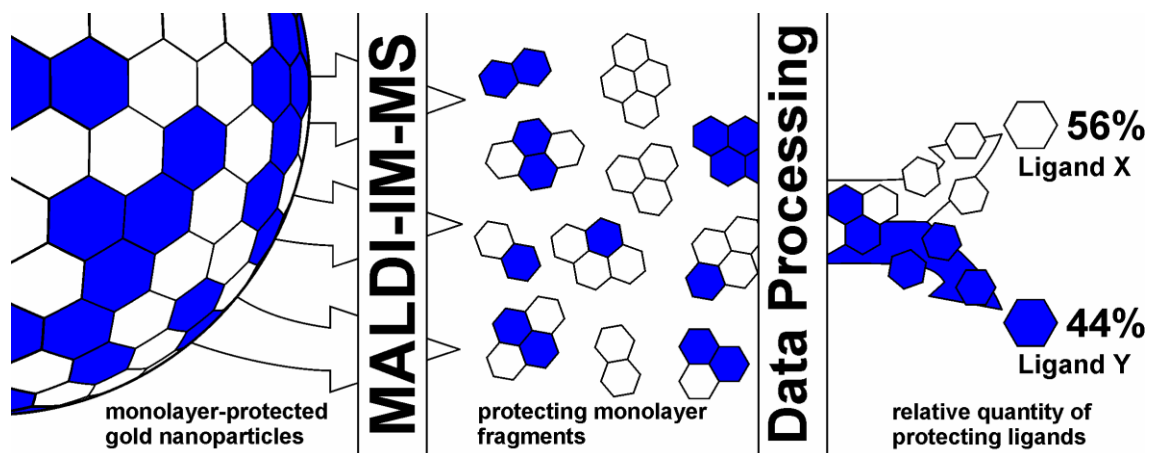
Figure 16. An experimental design for the relative quantitation of ligand mixtures. Portions of the protecting gold-thiolate monolayer are desorbed from the AuNP surface, ionized, and observed by IM-MS. Using data processing, the observed ions allow a measurement of the relative amounts of each ligand in a mixture in the monolayer of the AuNP.

Experimental Procedures

Reagents

Methanol (Fisher, 99.9%), ethanol (Optima, Fisher), acetone (>99.5%, Sigma-Aldrich), acetonitrile (>99.5%, Sigma-Aldrich), toluene (HPLC grade, Fisher), chloroform (≥99.8%, Sigma-Aldrich), acetic acid (glacial, Fisher), L-glutathione (reduced, Sigma-Aldrich, 99%), N-(2-mercaptopropionyl)glycine (tiopronin, Sigma-Aldrich), glacial acetic acid (certified ACS, Fisher), sodium chloride (certified ACS, Fisher), sodium borohydride (98+%, Acros), tetraoctylammonium bromide (TOABr, Fluka), octanethiol (98.5+%, Aldrich), decanethiol (96%, Aldrich), 11-mercaptoundecylpoly(ethylene glycol) (MUPEG, Sigma-Aldrich), *trans*-2-[3-(4-*tert*-butyl-phenyl)-2-methyl-2-

propenylidene]malononitrile (DCTB, Fluka), 2 nm "bare" AuNPs (nanoComposix), and α-cyano-4-hydroxycinnamic acid (CHCA, Sigma-Aldrich) were used as received.

Tiopronin AuNP Synthesis

Tetrachloroauric acid (HAuCl$_4$•3H$_2$O) was combined with three equivalents of tiopronin in 85:15 MeOH:acetic acid at 0 ℃. The solution was stirred for 3 hours, after which sodium borohydride was added in a 10:1 NaBH$_4$:Au molar ratio. The nanoparticles were dialyzed for 3 days until observed to be clean by NMR spectroscopy, that is, free of any narrow peaks indicative of unbound tiopronin or other organic molecules.

Octanethiol AuNP Synthesis

Tetrachloroauric acid (HAuCl$_4$•3H$_2$O) was dissolved in deionized water and combined with a slight molar excess of TOABr in toluene. Once the gold was completely transferred to the organic layer (evidenced by a red organic layer and clear aqueous layer), the aqueous layer was removed and three equivalents of octanethiol were added. After the solution became clear, 10 equivalents of NaBH$_4$ were dissolved in cold deionized water and added to the solution. The generated nanoparticles were precipitated in methanol. The methanol was filtered off, and the product was washed three times each with water, ethanol, and acetone, followed by sonication in acetonitrile.

Ligand Exchange

For mixed tiopronin:glutathione monolayer-protected AuNPs (Tio:GS AuNPs), unexchanged Tio AuNPs were combined with glutathione in deionized water or borate

buffer, depending on the solubility of the product. For tiopronin:11-mercaptoundecylpoly(ethylene glycol) (Tio:MUPEG) AuNPs, unexchanged Tio AuNPs were combined with MUPEG in deionized water. Octanethiol (OT) AuNPs were combined with decanethiol in chloroform. For each experiment, the time scale of the ligand exchange and the concentrations of the AuNPs and alternate ligand were varied in order to produce AuNPs with a wide range of ligand:ligand ratios (Table A 1).

Characterization

Transmission electron microscopy (TEM) images were obtained on a Phillips CM20 electron microscope. Thermal gravimetric analysis (TGA) was performed on an ISI TGA 1000 (Instrument Specialists Inc., Twin Lakes, WI). UV-Vis spectra were obtained on a Cary 100 Bio UV-Vis spectrophotometer in the range of 350-700 nm. Four samples of Tio:GS AuNPs were analyzed on an Applied Biosystems Voyager DE-STR with equipped a nitrogen laser (337 nm). Average molecular formulas were calculated as described elsewhere.[60] Briefly, the number of gold atoms per AuNP is calculated from the average diameter as measured by TEM, and the number of ligands is calculated from the percent mass lost measured by TGA.

Quantitative NMR Analysis

Tio:GS AuNPs were dissolved in D_2O and analyzed on a 400 MHz Bruker NMR, collecting at least 40 scans with a d1 delay of 1.5 seconds. A double WATERGATE pulse program was used for water suppression. The amount of tiopronin and glutathione

present on the nanoparticles was measured by comparing deconvoluted peak areas (Figure A 5).

Sample Preparation and IM-MS Analysis

Eight samples of Tio:GS AuNPs with different degrees of ligand exchange were obtained. A saturated sample of each in 10 µL deionized H_2O was combined with 100 µL of saturated CHCA and 1% NaCl in MeOH or an H_2O:MeOH mixture, depending on AuNP solubility. Six of these samples were soluble in these solutions, and were independently prepared and analyzed in duplicate to estimate preparation and instrumental variability. The remaining two samples, those with the highest glutathione abundance, were poorly soluble together with the matrix, and were thus prepared and spotted as slurries. A 1 µL portion of each was deposited on a stainless steel plate using the dried droplet method,[80] with sonication immediately prior for the poorly soluble samples. Tio:MUPEG AuNPs were prepared in the same manner.

For OT:DT AuNPs, the sample was dissolved in acetone and combined with DCTB matrix in an approximately 400:1 matrix/analyte ratio. All MALDI-IM-MS analyses were performed using a Synapt HDMS (Waters Corp., Manchester, UK), equipped with a frequency-tripled Nd:YAG (355 nm) laser operated at a pulse repetition frequency of 200 Hz. All spectra were acquired in the positive ion mode at laser energy settings approximately 10% above threshold values.

Peak Identification and Assignment

Gold-containing ion signals were extracted and identified using the MassLynx 4.1 (Waters Corp.) software package. Processed spectra were exported to Microsoft Excel, in which a custom spreadsheet was constructed for the remainder of the data processing. A template of this spreadsheet is available in Supporting Information. Each spectrum was compared to a list of possible m/z values constructed from expected gold-thiolate peaks. This list contained monoisotopic ions following the three stoichiometries identified previously, namely: $Au_{x+1}L_x$, Au_xL_x, and Au_xL_{x+1}.[50] Within these stoichiometries, an appropriate list of permutations was constructed with every possible combination of ligands and modifications such as sodium coordination and methyl esterification. Protons were added or subtracted as necessary to achieve a +1 charge state. Each processed spectra was filtered by abundance, with any signal below 1% relative abundance with respect to the base peak discarded in order to reduce false positive identification. The remaining peaks were compared to the expected gold-thiolate ion list. Any observed peak within 30 ppm mass accuracy of an expected peak were matched and used for quantitation.

As with any automatic peak matching strategy, there can be some erroneous assignments for samples which are more complex, such as those with more diverse ligand mixtures, multiple alkali metals, or more possible modifications. As such, making the expected peak list as parsimonious as possible reduces false positive identifications. For AuNPs with hydrophobic ligands, the gold-thiolate complexes can undergo apparent electron loss rather than proton or sodium coordination leading to ionization, yielding radical cationic species. Thus it is useful to check the results of the matching against the

original IM-MS spectrum when first attempting to quantify the ligands. The number of gold atoms in any given ion can be rapidly assessed,[50] providing a simple method to check the accuracy of most assignments. Once any necessary adjustments have been made to the expected gold-thiolate ion list, subsequent analyses can generally be performed in a few minutes.

Data Processing for Quantitation.

Since the expected peak list was generated with monoisotopic ions, matched peaks were normalized to the expected monoisotopic abundance for each respective ion. This method was chosen since isotopic resolution was achieved throughout each spectrum, and for more complex samples the isotopic patterns were regularly convoluted by multiple peaks within several m/z units of each other. After this normalization, Eqn. 1 was used:

$$\left(\frac{X}{X+Y}\right)_{AuNP} = \frac{\sum C_{X,Y}(X)}{\sum C_{X,Y}(X+Y)}$$

For a nanoparticle with a binary ligand mixture, X and Y, the term on the left denotes the mole fraction of ligand X on the entire nanoparticle. On the right, the numerator is the sum of the multiples of the ion count ($C_{X,Y}$) and the number of X ligands present in each respective peak. The denominator is the sum of the multiples of the ion count ($C_{X,Y}$) and the total number of ligands ($X+Y$) present in each respective peak. Together, these represent a mole fraction of the ligand X present on the nanoparticles. For example, if only two ions are observed corresponding to $Au_4X_1Y_3$ and $Au_4X_2Y_2$ species, having an ion count of 200 and 300, respectively:

$$\left(\frac{X}{X+Y}\right)_{AuNP} = \frac{200(1)+300(2)}{200(4)+300(4)} = 40\%$$

The calculated overall percent coverage of ligand *X* would be 40%. In the spreadsheet, this was performed by calculating the sum of the numerator and denominator of the fraction separately, then dividing to obtain the final percent coverage. A sample spreadsheet is available in the Supporting Information.

Results and Discussion

Nanoparticles with tiopronin (Tio) and octanethiol (OT) protecting ligands were synthesized and characterized by TEM (Figure A 2), UV-Vis (Figure A 3), and TGA (Figure A 4) in addition to IM-MS as described here. Tio AuNPs had an average core diameter of 2.5 ± 0.6 nm, and the OT AuNPs had an average core diameter of 3.6 ± 1.5 nm. Six samples of mixed octanethiol:decanethiol (OT:DT) AuNPs with various OT:DT coverage ratios were characterized, in addition to unexchanged OT AuNPs (Table 3). This set of ligands was chosen for two reasons. The first is to illustrate the effect of varying ligand ratios on the mass spectrum of the gold-thiolate ions. The second is to demonstrate the use of IM-MS for a sample in which NMR cannot effectively distinguish between the two ligands. In such cases, NMR cannot be used for quantitation measurements.

66
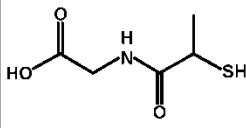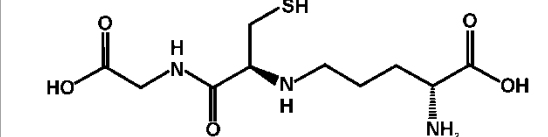
Octanethiol (OT): Decanethiol (DT)	Tiopronin (Tio): Glutathione (GS)		Tiopronin (Tio): (MUPEG)
IM-MS	IM-MS	NMR	IM-MS
100:0	99:1	100:0	100:0
78:22	86:14	85:15	86:14
53:47	83:17	83:17	60:40
42:58	78:22	79:21	33:67
38:62	56:44	54:46	
28:72	56:44	53:47	
16:84	46:54	44:56	
	10:90	12:88	
	4:96	5:95	

Table 3. All mixed monolayer-protected AuNPs characterized in this chapter and the ligand composition of each as measured by NMR or MALDI-IM-MS. For all IM-MS measurements, relative ligand abundances were measured using all observed gold-thiolate ions. The structures of tiopronin and glutathione are shown in the bottom portion.

Octanethiol:decanethiol AuNPs

Figure 17A presents a typical two-dimensional IM-MS plot, generated from 38:62 OT:DT AuNPs. As described in our previous report,[50] the two dimensions of ion drift time (ordinate axis) and m/z (abscissa) roughly form a density plot, in which large, lighter ions appear higher and to the left, while smaller, heavier ions appear lower and to the right. Because of the high mass and relatively low cross-section of gold atoms, gold-thiolate ions appear in a high-density portion of the two-dimensional plot, separate from the lower-density organic ions. In the mass range investigated here, the organic ions visible in Figure 17A have not been identified, but the regular spacing of the ions suggests that the ions are large clusters of free ligands, disulfides, and/or matrix

molecules which have undergone fragmentation or rearrangement processes. The number of possible permutations for these ions is indicated by the continuous nature of the organic ion signal in Figure 17A, in which very few ions stand out. The separation of gold-thiolate ions from these organic ions, which can be termed chemical noise, markedly increases the signal-to-noise ratio for the extracted gold-thiolate mass spectra.[50] This separation of gold-thiolate ions from organic contaminants is particularly significant for the routine characterization of AuNPs, since it virtually eliminates interference due to matrix, residual reagents, or modification materials. Thus extensive sample purification is not required as it is for other characterization methods.
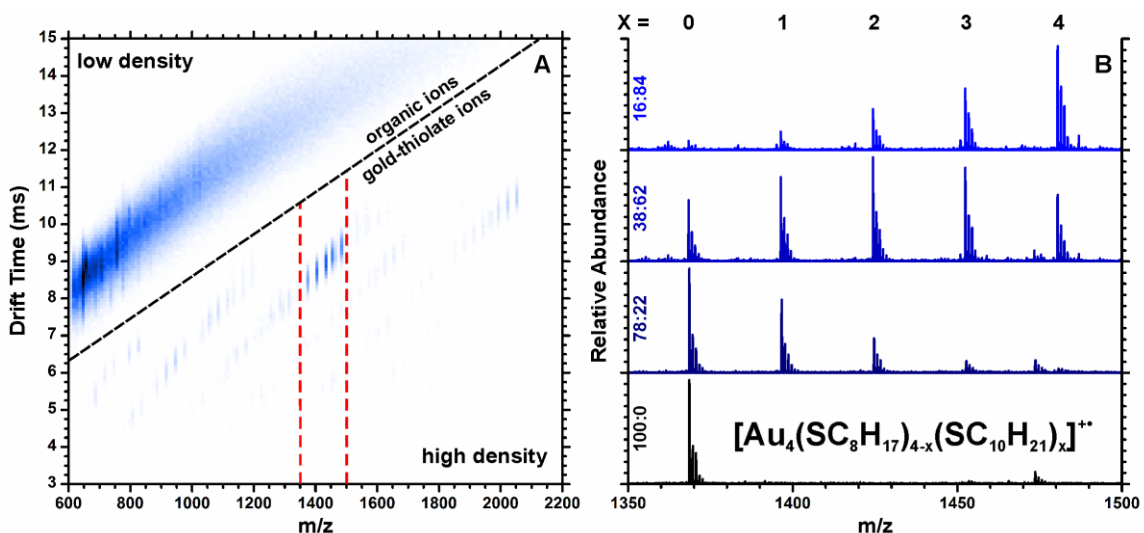
Figure 17. Ion mobility-mass spectra and extracted mass spectra for OT:DT AuNPs. Panel A reveals the separation of gold-thiolate ion signal from organic chemical noise. Panel B shows a portion of the extracted mass spectra, highlighting the Au_4L_4 stoichiometry, for four AuNP samples with varying OT:DT ligand coverage. The five peaks, corresponding to different numbers of OT and DT (*x*), roughly form a binomial distribution which reflects the overall coverage of OT and DT on the AuNP.

The most abundant gold-thiolate ions in Figure 17A are species with the Au_4L_4 stoichiometry, as seen in previous MALDI and ESI analyses of low-mass AuNP

fragments.[48,50,51,121] These ions are shown after extraction in Figure 17B. The lowest mass spectrum in Figure 17B is that of unexchanged OT AuNPs, and those above represent AuNPs with higher DT abundance (shown along the ordinate axis). The transition from homogeneous to heterogeneous ligand mixtures can be observed in the emergence of serial, uniformly spaced peaks within the Au_4L_4 stoichiometry, reflecting the five permutations of OT:DT mixtures in the four ligands of the ion. The increased amount of DT leads to the emergence of higher-mass peaks with increased numbers of DT ligands indicated across the top of the panel. The abundance of each peak varies with the overall abundance of OT and DT on the AuNP surface, forming a distribution which roughly follows the binomial model in a similar fashion to that found in intact AuNP ions by Murray and coworkers.[46]

Tiopronin:glutathione AuNPs

A second experiment using tiopronin:glutathione (Tio:GS) AuNPs allows for experimental validation with a more complex, and therefore potentially more error-prone sample. Since tiopronin and glutathione can be easily distinguished in an NMR without iodine-induced ligand dissociation, the same sample can be characterized by NMR and MALDI-IM-MS. In this case, the many permutations of possible ion modifications, namely cation coordination and esterification,[50] make the spectra much more complex than that shown in Figure 17. Eight samples of Tio:GS AuNPs were characterized in addition to unexchanged Tio AuNPs (Table 3). The results from the analysis of 56:44 Tio:GS AuNPs are shown in Figure 18. The upper portion is the mass spectrum of the extracted gold-thiolate ion region after software processing as described in the

experimental section. The mass spectrum is shown after this processing in order to clearly differentiate between ions used in the quantitation calculations (black) and those which are not (red). Even in a relatively complex mass spectrum, a large majority of the ion signals can be identified. Many of the ions which were not considered were products of C-S thiolate bond cleavage, thereby being rendered unusable in quantitation calculations.
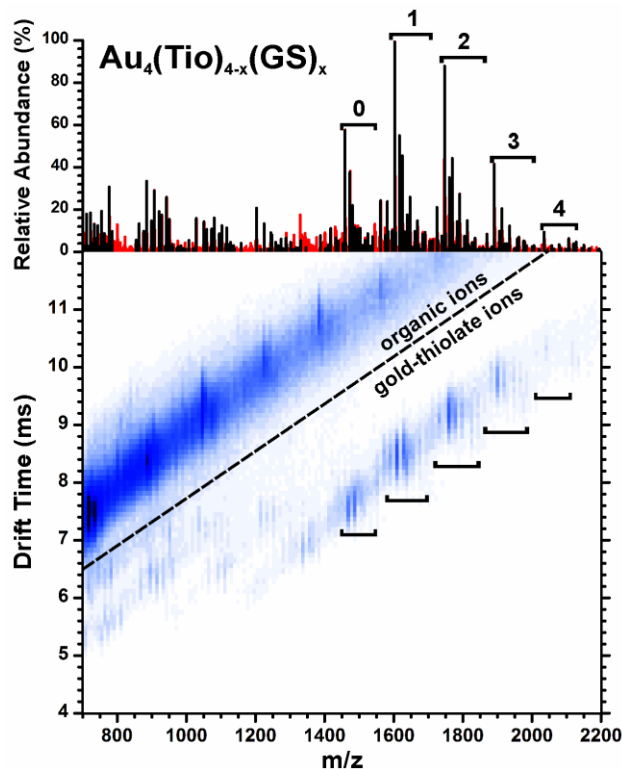
Figure 18. Ion mobility-mass spectrum of 56:44 Tio:GS AuNPs, and a mass spectrum showing the peaks from the extracted gold-containing region (above). Black peaks represent ions which were used for the quantitative calculations, red peaks were disregarded. The Au_4L_4 ions with different numbers of tiopronin and glutathione (x) are indicated by brackets.

By using the calculations detailed in the experimental section, the spectrum for each Tio:GS AuNP was used to calculate the Tio:GS ratio in the protecting monolayer. Each spectrum was processed identically by comparing the extracted and calibrated mass spectrum to a peak list generated from all expected gold-thiolate ions. The tiopronin

AuNP sample served as a control, since any peaks which were identified as containing glutathione would be erroneous. This allows for a rough estimate of error estimated in the abundance ratios that are obtained due to false identifications, in this case 1.4%.

Comparison of relative abundance measurements to NMR

A parallel NMR experiment was performed using the same samples, by measuring the integrated intensity of peaks corresponding to tiopronin and glutathione in the ^{1}H NMR spectrum (Figure A 5). Two methods were used to compare the NMR and MALDI-IM-MS measurements. In the first (Figure 19A), a regression plot measures the amount of correlation between the two strategies. The closeness of the regression to a line of equality (slope of 1, intercept of 0) is remarkable. The second and more useful method is a Bland-Altman plot (Figure 19B),[122] which is used to compare a new measurement strategy against an existing standard. As one might expect from the regression plot, the average difference between NMR and IM-MS measurement is less than 1% in terms of glutathione abundance. The limits of agreement for the two techniques are -3.0 to 3.5% molar percentage. The good agreement between these two techniques is particularly striking since the two quantitation strategies focus on different physical properties: proton magnetic moment and angular momentum for NMR, and the abundance of fragmented and ionized gold-thiolate complexes for MALDI-IM-MS.
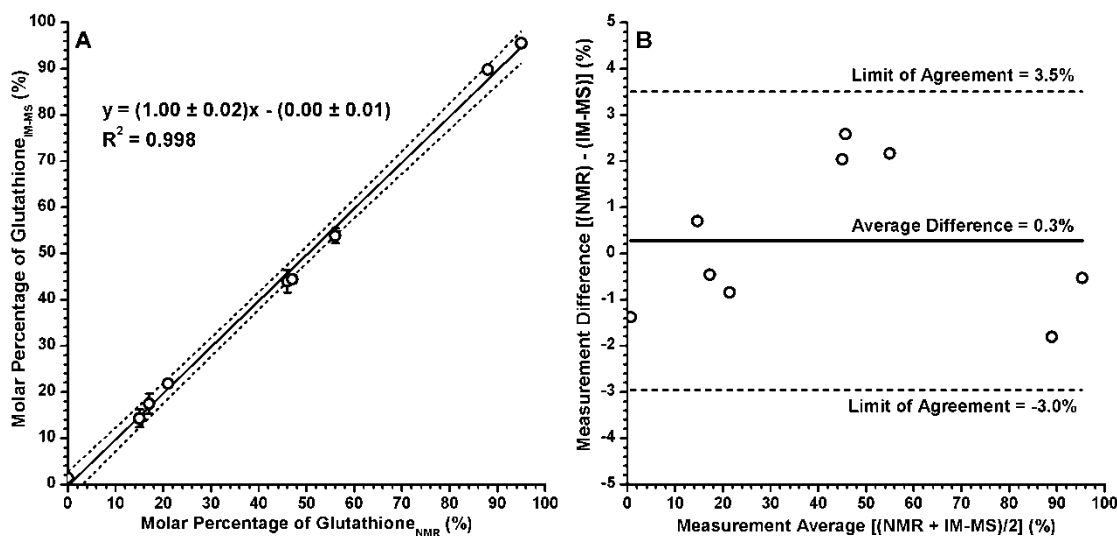
Figure 19. Two plots comparing NMR and MALDI-IM-MS measurements of Tio:GS ratios, expressed as a molar percentage of glutathione. Panel A is a simple regression plot comparing IM-MS results (ordinate) to those obtained by NMR spectroscopy (abscissa). The measurements are closely correlated regression is near the line of equality (slope of 1, intercept of 0), the dashed lines indicate the 98% confidence interval. Error bars represent $\pm 1\sigma$ (n = 2). Panel B is a Bland-Altman plot showing the difference between the IM-MS and NMR measurements (ordinate) for each sample against the average between the two measurements (abscissa). The average difference between the two measurements and their limits of agreement ($\pm 1.96\sigma$) are shown as lines.

The ions with Au_4L_4 stoichiometry were the most abundant for all the AuNPs characterized in this study (Figure 17 & Figure 18). It was observed that roughly similar quantitative results could be obtained from these ions alone, raising the possibility of using this limited data set to match with greater speed and lower false identification probability. Regression and Bland-Altman plots were generated for comparison of NMR measurements and IM-MS measurements using only Au_4L_4 ions (see Figure A 6). Briefly, the correlation between the two measurements was poorer ($R^2 = 0.988$) and the limits of agreement were broader (-4.0% to 10.2%, 3.1% average difference between NMR and IM-MS).

72

In addition to OT:DT and Tio:GS AuNPs, tiopronin:11-mercaptoundecylpoly(ethylene glycol) (Tio:MUPEG) AuNPs were quantitatively analyzed in order to demonstrate the use of this technique with PEGylated ligands (Figure A 7), which are commonly used *in vivo*.[123,124] The results of the quantitative analysis are shown in Table 3. Since the diagnostic NMR spectroscopic peaks were convoluted, validation experiments could not be successfully performed for the OT:DT and Tio:MUPEG AuNPs. It is also relevant to note here that corrections for ionization efficiency cannot be made, but differences in ionization efficiencies for these ligands are not expected to be significant.[46] For ligand combinations with more extreme differences in ionization efficiency than those shown here, the accuracy of this method will doubtless be decreased.

The best method for validation will be an entirely different technique which functions independently of these complexities, namely NMR spectroscopy. For Tio:GS AuNPs, no evidence was found for significant differences in ionization efficiency. For all AuNPs, it was observed that the relative abundance of the alternate ligand increased with greater exchange time, higher AuNP concentrations, and greater alternate:original ligand feed ratios as expected, with no anomalous behavior (Table A 1).

Comparison to one-dimensional mass spectrometry

It is worthwhile to compare these results to those obtained using MS without ion mobility separation. In a parallel experiment, some of the Tio:GS AuNPs were analyzed in a mass spectrometer using the same preparative protocol. Gold-thiolate ions were not observed for the 46:54 and 4:96 Tio:GS AuNPs, and only a single gold-thiolate ion species was observed for 14:86 and 56:44 Tio:GS AuNPs (Figure A 8). This is a strong

difference from our IM-MS strategy, for which every monolayer-protected AuNP studied has produced a significant amount of gold-thiolate ions. One possible cause for this difference may be the higher pressures utilized in the source and travelling wave regions of the IM-MS instrument. The operating source pressure was on the order of 10^{-2} Torr in the Synapt IM-MS instrument, compared to $<10^{-6}$ Torr for the Voyager. At higher source pressures the collisional cooling of ions is increased,[120] dissipating the internal energy of the gold-thiolate complexes and reducing the tendency towards ion fragmentation or decay. To ensure that the additional pressure did not produce gold-thiolate ions in a gas-phase reaction, a control experiment was performed in which bare gold AuNPs and free tiopronin ligand were spotted together on the stainless steel plate and immediately dried, preventing any significant amount of gold-ligand binding in solution. Analysis of the dried mixture by IM-MS revealed no gold-thiolate ion signal (Figure A 9).

It is also possible to investigate gold-thiolate ions generated by tandem MS without ion mobility separation, as demonstrated by Murray and coworkers.[51] However, the use of tandem MS requires precursor ion selection, at which point the absolute ligand abundances would likely already be known. Furthermore, in this approach the fragmentation product ions do not appear to accurately reflect the relative ligand abundances of the precursor MPC ion.[51] This may be due to differences between MALDI in-source decay and CID-promoted fragmentation pathways, the differences between the fragmentation of small, "magic-sized" clusters and larger AuNPs, or the difference in pressure and collisional cooling leading to the preferential decay of some ions, as suggested by our MS results (Figure A 9).

Many other ligand mixtures have been successfully characterized stoichiometrically. To name a few especially relevant examples, binary mixtures of tiopronin with two different peptide epitopes (RGD and a portion of the protective antigen of *B. anthracis*), mixtures of alkanethiolates with highly conjugated "molecular wires," and a quaternary cysteamine:glutathione:*para*-mercapobenzoic acid:3-mercaptopropanesulfonic acid system used by Feldheim and coworkers to identify antibiotics[125] were all successfully analyzed and quantified using the protocol described here. These results are shown in Figures A10-A12. Many of these ligand mixtures cannot be quantified by any other analytical method.

Conclusion

In this report we have demonstrated the use of MALDI-IM-MS for the relative quantitation of AuNP-bound thiolate ligands for AuNPs with three different binary ligand mixtures (Tio:GS, OT:DT, and Tio:MUPEG). Results for Tio:GS AuNPs are validated by NMR spectroscopy, revealing less than 1% deviation in relative abundance between the two techniques. AuNPs with OT:DT and Tio:MUPEG ligand mixtures were analyzed by MALDI-IM-MS for quantitation purposes, an analysis that is difficult or impossible using NMR quantitation strategies. Comparison with a normal MS platform reveals that the diverse gold-thiolate ions observed here are not observable by MS. Thus, a strategy based on MALDI-IM-MS is uniquely capable of discriminating for a wide variety of gold-bound ligands and measuring their relative abundances. This general mixed-ligand AuNP characterization strategy should be scalable to the synthesis and characterization of a

broader class of complex mixed monolayer-protected AuNPs, as evidenced by a preliminary examination of quaternary ligand mixtures.

Acknowledgements

CHAPTER V

IDENTIFICATION OF SUPRAMOLECULAR STRUCTURES

Introduction

The ligands on monolayer-protected gold nanoparticle (AuNP) surfaces are known to be capable of spontaneously separating into nanoscale domains[25] based on ligand-ligand interactions and entropic energy gains,[63] creating uniquely organized nanomaterials. This organization can be harnessed to generate unique physical and chemical properties, from nonmonotonic solubility[126] to non-destructive membrane transport.[26] Understanding these unique properties and the driving forces behind microphase separation requires a methodology for characterizing the patterning of ligands on the AuNP surface.

Beyond the measurement of these unique physical processes and properties, AuNPs with reproducibly ordered surfaces are a versatile and powerful scaffold for use in biological systems.[127,128] In this context, AuNPs are somewhat analogous to a biomacromolecule, with a highly tunable nanoarchitecture inducing specific chemical interactions. Because of this, AuNPs with a mixture of ligands in the protecting monolayer have quickly emerged as a new class of drugs with a vast range of combinatorial chemistry possibilities.[125] Specific ligand combinations could form supramolecular assemblies with biological activity unique to the mixed-ligand AuNP, but unfortunately there is no available experimental strategy for observing the presence or absence of these assemblies. As with any application targeted to a biological system, a characterization protocol which gives molecular detail for a wide variety of ligand types

is required.[108] Established techniques for characterizing AuNPs with discrete supramolecular structures, such as scanning tunneling microscopy[25,129] and other spectroscopic techniques,[64,130] only work under very specific circumstances and are thus unable to probe a wide variety of heterogeneous ligand mixtures.

Here we propose that ion mobility-mass spectrometry (IM-MS) is a suitable tool for both the routine characterization of AuNPs with ordered ligands, and for investigations of the nanoscale processes which drive this ordering. In addition to serving as a simple probe for AuNP-bound ligands,[50,125] this strategy was recently demonstrated to be effective in the relative quantification of binary ligand mixtures.[131] In a typical experiment, mixed-monolayer-protected AuNPs are fragmented in a matrix-assisted laser desorption/ionization (MALDI) source, liberating portions of the protecting gold-thiolate complex monolayer. These liberated complexes are ionized and separated in the gas phase, first by effective surface area and then by the mass-to-charge ratio. The effect of separating by both size and mass generates a two-dimensional density map in which gold-thiolate ions are clearly separated from purely organic matter.[50] This allows for the extraction of a one-dimensional mass spectrum which exclusively contains gold-thiolate ions from the two-dimensional signal, allowing for highly sensitive mass-based measurements of the gold-thiolate complexes which protect AuNPs.

To experimentally establish this claim, we have predicted the mass spectral "fingerprint" for different types of ordering. This fingerprint region is comprised of the Au_4L_4 ion species, cyclical tetrameric complexes of gold and thiolate ligands which are either directly desorbed from the AuNP surface, or are products of rearrangement of "staple" Au_xL_{x+1} species.[18] In either case, each gold-thiolate complex ion desorbed from

the AuNP will contain the ligands present in a given portion of the AuNP surface. The complex monolayer-protected AuNP surface can be simplified as a grid pattern on a sphere, in which each block represents one ligand. For binary ligand mixtures, each block can either be L or L'. Since the $Au_4L_{4-x}L'_x$ ion species contain four total ligands and are known to be ring-shaped, these species will be assumed to roughly represent four-ligand portions of that grid. If one randomly samples a four-ligand portion of the AuNP surface, there will be a given probability of finding each of the five possible combinations of L and L': Au_4L_4, Au_4L_3L', $Au_4L_2L'_2$, etc. The probability of finding each of these combinations will vary depending on the ordering of the ligands.

In this context, the Au_4L_4 and $Au_4L'_4$ ion species represent pockets of each ligand, while the other three ion species represent an interface between the two ligands, regions where portions where the ligands are mixed. The abundances of the pocket and interface ions will vary according to the type of ordering on the surface, allowing for a somewhat quantitative investigation of ligand ordering (Figure 20). The percentages of surface coverage expected for each ordering type can be calculated mathematically. The binomial probability distribution model can be used to predict the outcome for randomly distributed ligands. Each ion provides four trials ($N = 4$), one trial for each ligand in the ion, to answer the binary question: L or L'? The probability of finding either ligand (p) is determined by the relative quantity of the two ligands. For example, for a 50:50 mixture of two ligands there will be a few four-ligand pockets of ligand 1 or 2, but the large majority of the surface (86%) will be comprised of an "interfacial" region, due to the highly mixed nature of the ligands. As the ligands become organized into patchy or striped domains, the proportion of the AuNP surface which contains only ligand 1 or 2

increases and the area of the interfacial region decreases. The degree to which this occurs will reflect the number and size of the ordered ligand domains, thus the striped/patchy AuNPs are predicted to yield a range of results. The most extreme case of order on the AuNP surface, the Janus structure, contains only one large pocket each of L and L'. In this case, the amount of area comprised of pockets will be high, while the amount of interfacial ions will be at a minimum.
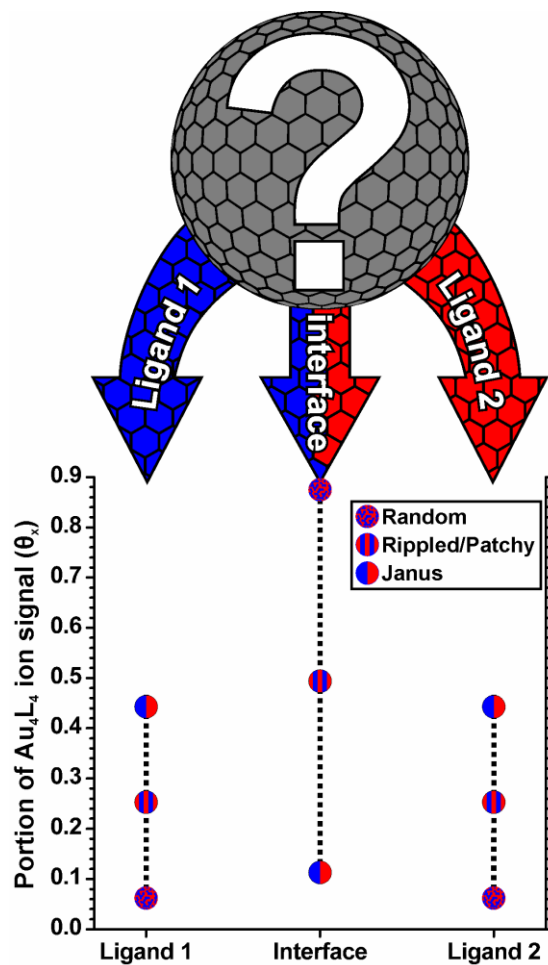
Figure 20. An illustration of the expected results for varying degrees of microphase separation. For AuNPs with no separation in the monolayer, the randomly distributed ligands will cause a large "interfacial" region, whose abundance can be predicted by the binomial distribution. For rippled or patchy AuNPs, the moderate microphase separation will yield some deviation, with interfacial area declining and pocket area increasing. Janus AuNPs which exhibit complete microphase separation will have a maximal pocket area and minimal interfacial area.

Experimental Procedures

Reagents

All chemicals were purchased from Fisher Scientific or Sigma-Aldrich and used as received with the exception of tetrachloroauric acid, which was synthesized as described elsewhere.[79]

Nanoparticle synthesis and purification

Gold nanoparticles protected by a monolayer of mercaptotetra(ethylene glycol) (MTEG), tiopronin, or octanethiol were synthesized and modified by ligand exchange reactions as described in Chapters III-IV. In addition, the MTEG AuNPs were combined with tiopronin, mercaptoundecanol (MUO), or mercaptohexanol (MHO); tiopronin AuNPs were combined with dPEG acid® or mercaptoundecanoic acid, with the final intended ligand:ligand ratios being 1:1.

Mercaptoundecanoic acid, tiopronin:mercaptoundecanoic acid (Tio:MUA), tiopronin:octanethiol (Tio:OT), mercaptopropionic acid:octanethiol (MPA:OT), and nonanethiol:methylbenzenethiol (NT:MBT) were synthesized according to the following procedure. Chloroauric acid (~100 mg) and one molar equivalent of the chosen thiol were combined in 20 mL methanol with stirring at room temperature. For synthesis with a mixture of ligands, one-half molar equivalents of each were used for a total of one molar equivalent with respect to gold. After 3 minutes, 10 molar equivalents of $NaBH_4$ dissolved in a minimal amount of methanol were added. In each case the solution turned black and some precipitation could be observed. The solution was stirred for at least 30

min, followed by centrifugation for 5 min at 3000 rpm. The supernatant was discarded and fresh methanol was added, followed by sonication and another 5 min of centrifugation. If the nanoparticles did not fully precipitate after 5 min, the centrifugation continued up to 30 min. If precipitation did occur, the nanoparticles were washed repeatedly by this method, up to four times total. After the final centrifugation, the supernatant was discarded and a minimal amount of water or dichloromethane was added (≤10 mL), depending on the hydrophilicity of the nanoparticle. AuNPs which could be easily suspended in water were dialyzed in snake skin dialysis tubing (MWCO = 30 kDa) for 3 days. Core measurements were not made at the time of this writing, but samples ranged from exhibiting no to a very small surface plasmon band, indicating average diameters from ~2-3.5 nm. All samples were stored in solution.

Sample preparation and analysis

To a 100 µL solution of dichloromethane containing roughly 0.5 mg of NT:MBT AuNPs, 5 mg of DCTB matrix was added. A Pasteur pipet was used to deposit roughly 1 µL of the solution using capillary action. It is important to use glassware rather than any form of plastic, since a significant amount of polymer will enter the sample, creating undesired chemical noise in the ion mobility-mass spectrum.

For the remaining samples, a modified sandwich crystallization method[132] was utilized. For each sample, 0.5 µL of a saturated solution of CHCA matrix was deposited on a stainless steel plate. After drying, a 0.5 µL aliquot of the concentrated sample solution was deposited and dried, followed by another 0.5 µL spot of matrix solution. Using this technique appears to allow for greater sensitivity to gold-thiolate species at lower laser

fluences. All spectra were obtained on a Waters Synapt G2 in the positive ion mode. Laser intensity was generally set at 20% above threshold, the travelling wave velocity was fixed at 300 m/s while the wave height was ramped from 9 to 16 V. Data was collected over 60 sec for each spectrum.

Data processing and calculations

Mass spectra were extracted from the gold-thiolate region of the ion mobility-mass spectrum using Driftscope v2.1 software (Waters Corp.). Peaks were identified and calibrated using MassLynx 4.1 software (Waters Corp.). The processed spectra were exported in text format to Microsoft Excel using a similar system to that described in Chapter IV. The peak identification cutoffs were placed at 0.5% abundance relative to the base peak and 10 ppm mass accuracy. These cutoffs are more stringent than those reported in Chapter IV, since improvements in instrumentation and sample preparation technique allow for greater sensitivity and mass accuracy.

The abundances of the monoisotopic peak were corrected as described in Chapter IV, and all ions with an Au_4L_4 stoichiometry were selected for comparison to a binomial model. For each ligand-ligand combination (*i.e.*, each possible value of x for $Au_4SR_xSR'_{4-x}$), the ion abundances were summed and divided by the total abundance of all Au_4L_4 ions to obtain θ_x. The binomial distribution was calculated using Microsoft Excel (function "BINOMDIST") with the values $n = 4$, $0 \leq x \leq 4$, and

$$p = \sum \frac{x \cdot C_x}{n}$$

where C_x is the sum of ion counts for a given value of x. Residuals were calculated as the square root of the sum of the squared differences between each observed and calculated values.

Results and Discussion

Having predicted the fingerprint of the three types of ordering (Figure 20), we synthesized a variety of nanoparticles with binary ligand mixtures (Table 4). Ligand pairs with disparate lengths and chemical functionalities were chosen in order to probe the role of microphase separation and conformational entropy. A previously studied binomial mixture, tiopronin:glutathione (Tio:GS), serves as a useful control establishing the baseline measurement of no to very little microphase separation. Figure 21 illustrates how a completely random distribution of ligands results in very little deviation from the binomial distribution. The average calculated residual for Tio:GS AuNPs with various ligand:ligand ratios is 4%, with lower values at low molar percent glutathione in the monolayer, and greater deviation from the binomial distribution at higher amounts of glutathione (>50%). Other mixed-ligand AuNPs with similar residual values are Tio:MUA (3%, obtained by mixed ligand synthesis), NT:MBT (5%),[106] Tio:OT (5%), Tio:dPEG acid® (6%), and MPA:OT (6%).

Figure 21. A comparison of observed ion abundances for $Au_4(Tio)_{4-x}(GS)_x$ and predicted ion abundances for a random distribution of ligands. Very little difference is observed between the two, indicating the validity of the binomial distribution for predicting ion abundances and the random distribution of Tio:GS AuNPs.

Moderate separation can be observed on some nanoparticles (Figure 22), indicated by positive deviation from the binomial distributions at $x = 0, 4$ and negative deviations for $x = 1-3$, which represent ligand pockets and interfaces, respectively. Average residuals for these AuNPs range from 10-50% depending on the degree of microphase separation. Ligand mixtures falling in this range include MTEG:Tio (17%) and OT:DT (19%).[63]

Figure 22. A comparison of observed ion abundances for $Au_4(OT)_{4-x}(DT)_x$ and predicted ion abundances for a random distribution of ligands. Positive deviation for ions derived from OT and DT pockets and negative deviation for ions derived from an interface indicate the presence of microphase separation.

As microphase separations become complete, two distinct phases emerge, forming Janus AuNPs (Figure 23). Compared to AuNPs with some microphase separations, such as those discussed above, the deviations will simply be amplified to a certain maximum deviation. At this maximum deviation, the interfacial region of the two phases will be minimal, as will the ions derived from this area. Tio:MUTEG AuNPs exhibited this pattern, with a residual ranging from 45% to 69%.
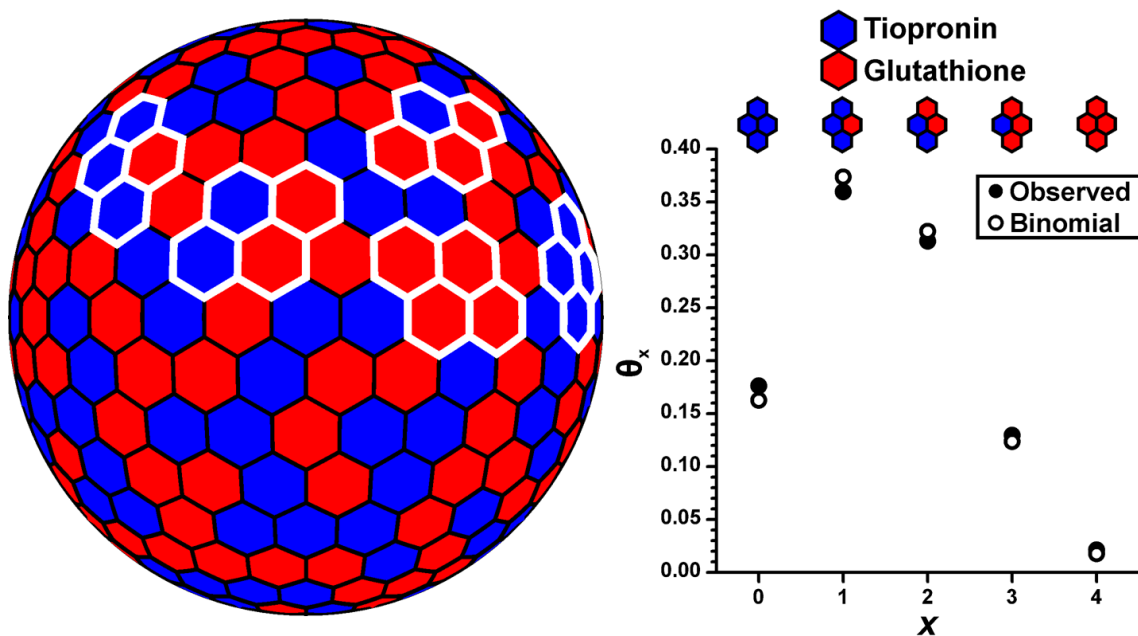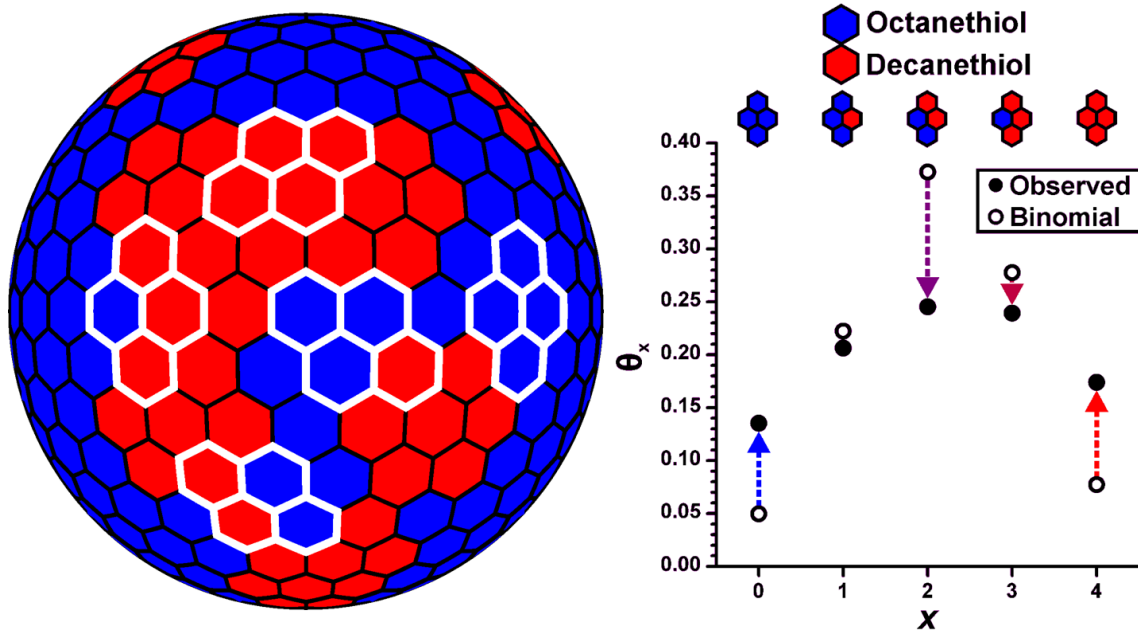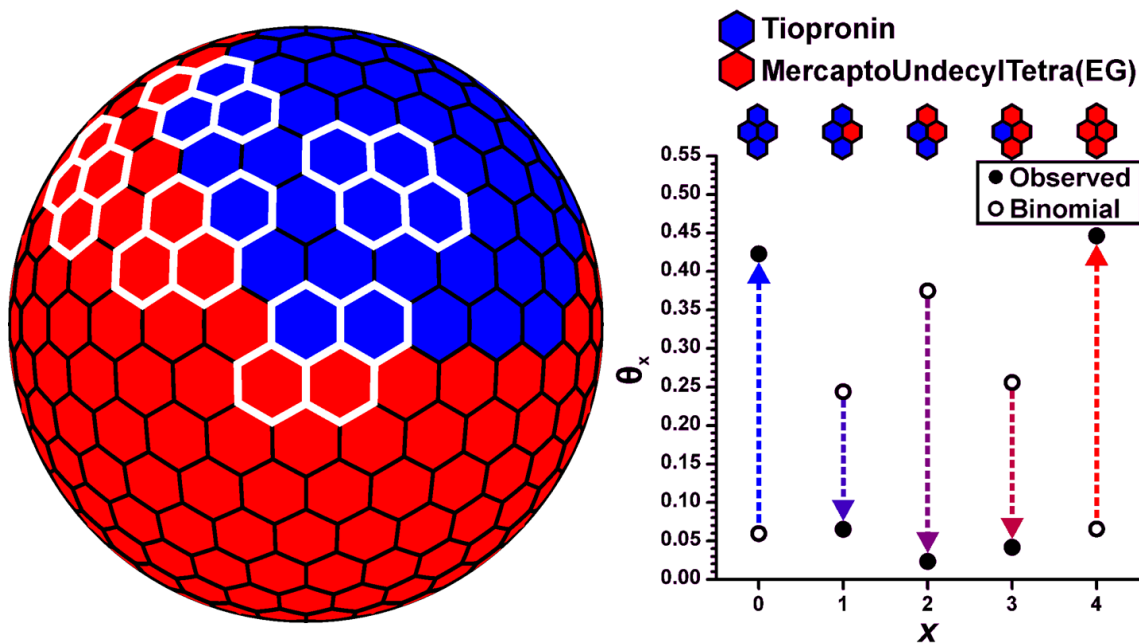
Figure 23. A comparison of observed ion abundances for $Au_4(Tio)_{4-x}(MUTEG)_x$ and predicted ion abundances for a random distribution of ligands. Very positive deviation for ions derived from Tio and MUTEG pockets and very negative deviation for ions derived from an interface indicate a complete microphase separation.

In cases where microphase separation is observed, rather than seeing a uniform decrease for each of the interface ions, the ions which are expected to have the highest abundance decrease the most, while those expected to be least abundant decrease the least, and even increase in some cases. This creates a surprising inverse trend with respect to the relative quantity of the alternate ligand: at high relative quantities of a given ligand SR', ions with a higher number of SR' ligands deviate more negatively than ions with a low number of SR' ligands. The observed behavior is certainly counterintuitive, but it provides confirmation of microphase separation. If each of the ions with a mixture of ligands is derived from a common interfacial region, the abundance of those ions should not differ as significantly as those in a random distribution. This common source region

produces an equalization effect on the "interfacial" ions, causing their abundances to be more equal than would be expected for a random mixture of ligands.

Another type of deviation from the binomial distribution was observed for MTEG:MHO and MTEG:MUO along with methyl-esterified Tio:MUA AuNPs. In this type of deviation, each of the ions remains the same intensity or is reduced while a single ion, containing three of one ligand and one of another, deviates positively by a significant amount (Figure 24). There are few plausible explanations, the most likely of which is the existence of a supramolecular structure which favors isolation of certain ligands, reducing any pockets of ligands and increasing the interfacial ions, particularly the one containing only one of the isolated ligand. It is unclear why these specific ligand mixtures evidence this type of supramolecular structure, especially the Tio:MUA AuNPs which were roughly 50% methyl-esterified. Tio:MUA AuNPs which were not esterified or were 100% ethyl- or butyl-esterified did not display any significant deviation from the binomial distribution.
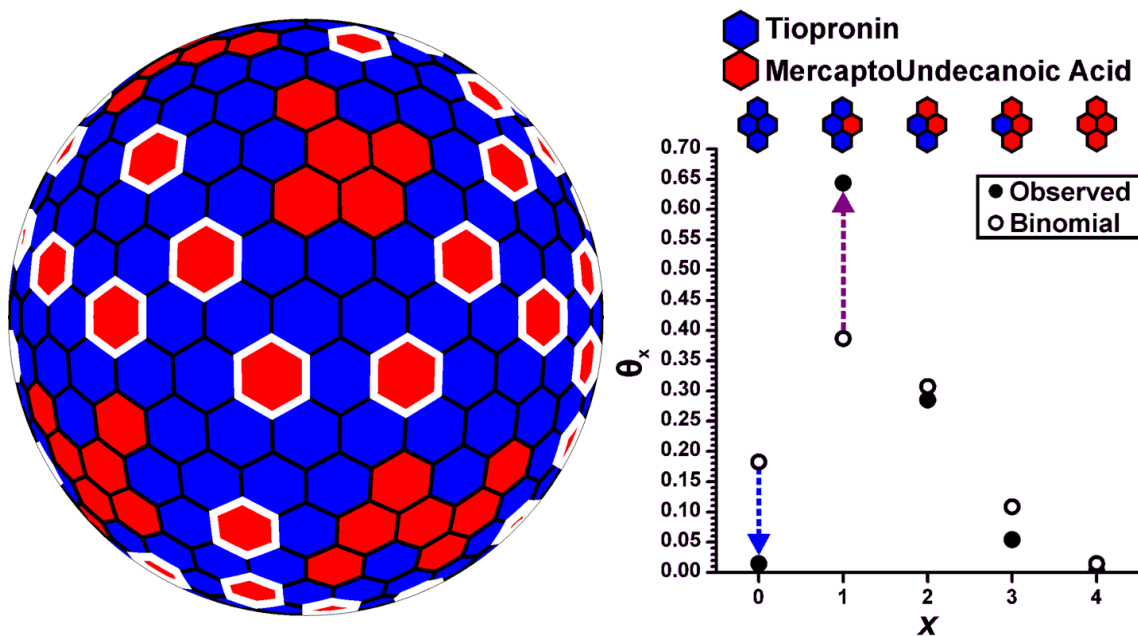
Figure 24. A comparison of observed ion abundances for $Au_4(Tio)_{4-x}(MUA)_x$ (where both tiopronin and MUA are ~50% methyl-esterified) and predicted ion abundances for a random distribution of ligands. No change or a negative deviation was observed for every ion except the one corresponding to $Au_4(Tio)_3(MUA)$, which was much more abundant than expected. This result may indicate a previously unknown type of supramolecular structure involving the isolation of one of the ligands in the mixture.

One of the advantages of this methodology is the ability to observe the emergence or disappearing of supramolecular structures at various ligand:ligand ratios. Figure 25 illustrates this ability by comparing the proportion of ion signal associated with pockets (red or blue data points) or interfaces (half-red, half-blue data points) to the expected values for pockets (red and blue lines) and interfaces (purple lines) taken from the binomial distribution. On the right, the alternate set of lines indicates a rough prediction of results for Janus AuNPs. For each of the AuNPs, deviation from a random distribution seems to peak around 60% abundance of the place-exchanged ligand.
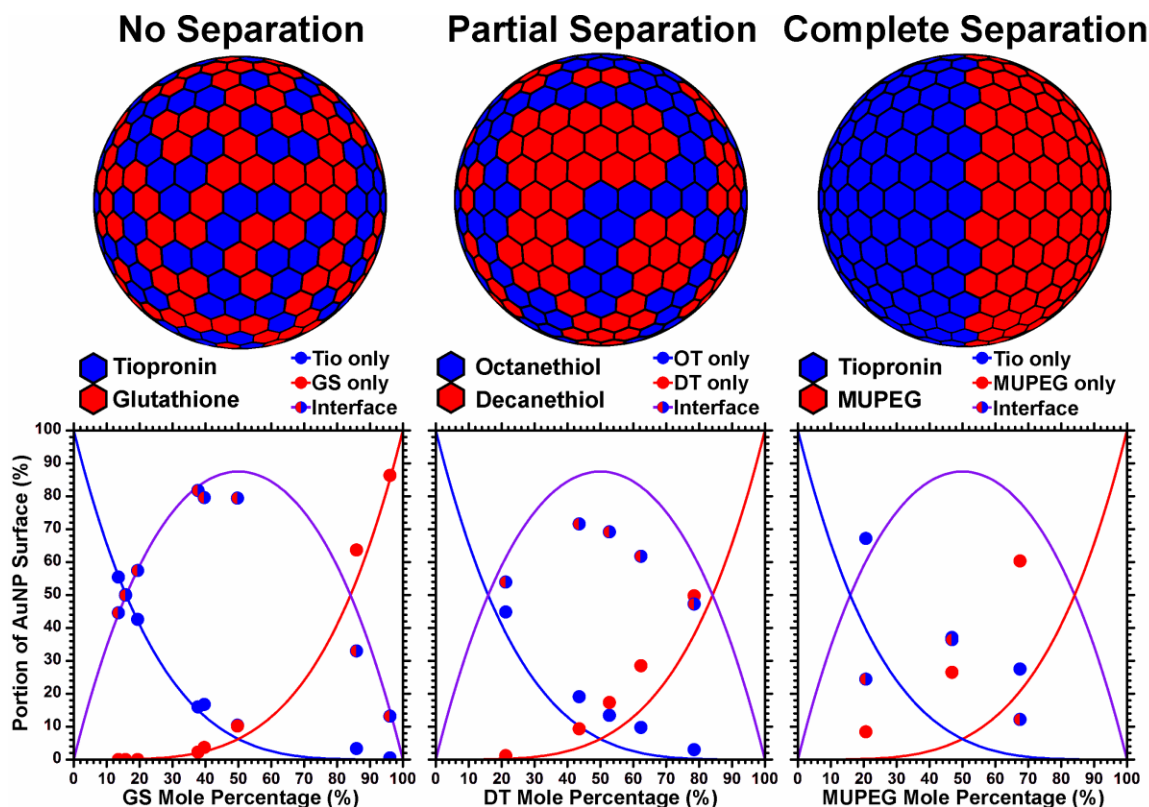
Figure 25. A representation of the measurement of microphase separations across multiple ligand-ligand ratios. Data points correspond to observed ion abundances for pocket or interfacial species, while lines correspond to expected abundances for randomly distributed ligands (left) or Janus AuNPs (right). Results reveal that deviation from the binomial model tends to be greatest between 40-80% alternate (red) ligand, reaching a maximum around 60%.

Table 4 summarizes the data presented here. A few trends are worth noting. First, ligand mixtures which have been obtained by place-exchange appear to be more likely to exhibit supramolecular structure. This is somewhat intuitive, since steric effects and ligand-ligand interactions are much more likely to determine the final structure of the monolayer. However, this is in direct opposition to the recent work of other groups who have described the formation of striped AuNPs through mixed ligand syntheses.[25,106,133,134] Indeed, limited attempts to form striped NT:MBT AuNPs have not revealed any significant degree of deviation from a random ligand distribution. It is

possible that delicate forms of supramolecular structure could be effectively "blurred out" and thus not observable, but it remains clear that any microphase separation on these AuNPs is essentially nonexistent.

Ligand Mixture (SR:SR')	Supramolecular Structure	Average Residual
Tio:MUPEG	Separation (Janus)	66%
Tio:MUA [w/ ~50% methyl esterfication]	Isolation	25%
MTEG:MHO	Isolation	21%
OT:DT	Separation (patchy)	21%
MTEG:Tio	Separation (patchy)	17%
MTEG:MUO	Isolation	13%
MPA:OT	-	4%
Tio:dPEG acid®	-	4%
Tio:OT	-	4%
Tio:GS	-	2%
NT:MBT	-	2%
Tio:MUA [w/ 0 or 100% butyl or ethyl esterfication]	-	2%

Table 4. All characterized ligand mixtures, their type of supramolecular structure and the degree of deviation from the random distribution (expressed as a residual from the binomial). Ligand mixtures in red were predicted to exhibit microphase separations, those in italics were obtained by place exchange reactions.

A second noteworthy trend is the degree of difference between nominally similar AuNPs. For example, MTEG:Tio AuNPs formed by exchanging tiopronin onto MTEG AuNPs exhibit microphase separation, while Tio:dPEG acid® (which is identical to MTEG with an additional ethanoic acid group at the ligand terminus) AuNPs formed by adding dPEG acid® to tiopronin AuNPs exhibits no microphase separation. In a similar fashion, non-esterified Tio:MUA does not form any observable supramolecular structure from a mixed-ligand synthesis, while Tio:MUA which is formed by place exchange

shows moderate microphase separation and Tio:MUA which is 50% methyl esterified forms an "isolation" supramolecular structure. These cases illustrate the power of IM-MS to investigate essentially isomeric AuNPs, observing differences which would not be observable by any other analytical platform.

As a final note, the data presented here may give some evidence of more unique structural properties of AuNPs and their gold-thiolate counterparts. Figure 26 demonstrates how the amount of place-exchanged decanethiol on OT:DT AuNPs appears to correlate to the relative abundance of $Au_{x+1}L_x$ ions generally and Au_6L_5 ions specifically. Furthermore, the larger stoichiometries tended to feature greater abundances of decanethiol, while smaller stoichiometries tended to favor octanethiol. One possible explanation is the coexistence of AuNPs with free gold-thiolate complexes created during the place-exchange process. Both of these are observed in the data for OT:DT and Tio:GS AuNPs. If this is the case, the free gold-thiolate complexes would increase in abundance with more ligands exchanged, and would tend to favor the exchange ligand over the original ligand. Another possible explanation would be the preference of certain ligands for certain stoichiometry. For example, in the case of OT:DT, the OT could prefer the Au_4L_4 stoichiometry while DT prefers Au_6L_5. However, this seems unlikely given the general preference of alkanethiols for $Au_{x+1}L_x$ stoichiometries (Table 1). In light of this fact, the dominance of the Au_4L_4 appears to reflect a favored stoichiometry prior to its ionization, *i.e.* while still bound to the gold core. This is potentially an experimental confirmation of the presence of tetrameric gold-thiolate species on AuNP surfaces which was proposed in Chapter III. This data opens the door for investigations of the presence

of free gold-thiolate complexes created during place exchange reactions as well as the stoichiometry of gold-thiolate complexes on AuNP surfaces.
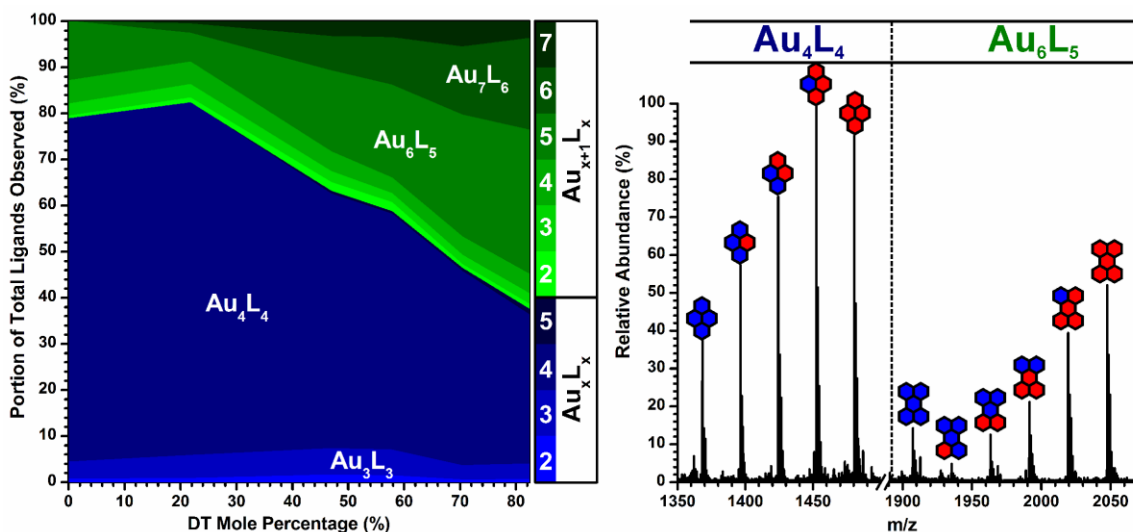
Figure 26. The relative abundance of ions with different Au_xL_y stoichiometries (left), and a comparison between the distributions observed for the Au_4L_4 and Au_6L_5 stoichiometries within the same spectrum (right).

Conclusion

Using ion mobility-mass spectrometry, we have developed a methodology by which qualitative and semi-quantitative assessments of supramolecular structure in AuNP-protecting monolayers can be carried out. The data reveals ideal pathways to obtaining supramolecular structure as well as a previously unknown type of supramolecular structure involving the isolation of one of the ligands in a mixture. The complexity of the data obtained reveals a unique and powerful approach to studying the monolayer-protected AuNP surface. A more complete understanding the processes at work in microphase separation and monolayer fragmentation could enable the reverse engineering of the AuNP surface, generating an image from mass spectral distributions. The ordering of ligands on the AuNP surface has been demonstrated to have a powerful effect on

AuNP properties, from unique reactivity[26,27,106,133,135] to solubility[126] and biocompatibility.[26] The potential of a technique which could allow a more precise investigation of patterned monolayer-protected AuNPs should not be understated.

Acknowledgements

CHAPTER VI

CONCLUSION AND FUTURE DIRECTIONS

Conclusion

Mass spectrometry is a powerful analytical method which has enabled structural investigations of molecules as diverse as peptides, molecular gases, and organometallic compounds. For small monolayer-protected gold clusters (MPCs), intact AuNPs can be ionized, allowing precise molecular formulas to be measured. This allows investigation of fundamental AuNP properties, such as the size and native charge of the favored "magic" sized clusters. During the ionization process, AuNPs commonly fragment to gold-sulfide clusters and/or gold-thiolate complexes, depending on the ionization method.

In the first experiment to confirm the foundational hypothesis, gold-thiolate complexes were indeed desorbed from gold MPCs, ionized, and observed successfully. These gold-thiolate ions are generated from the smallest MPC and from larger, more polydisperse AuNPs. Furthermore, metal-thiolate complexes can be observed as in-source fragmentation products of monolayer-protected silver and palladium nanoparticles. The observation of metal-thiolate complexes on nanoparticles of various metals and sizes leads to the conclusion that metal-thiolates are a ubiquitous capping structure for monolayer-protected metal NPs. In addition to gold-thiolate ions derived from AuNP surfaces, analogous gold-thiolate complexes formed in solution can be characterized. These results will lead to an enhanced understanding of the relationship between metal-thiolate complexes and metallic nanoparticles, the products of their reduction.

The combination of mass spectrometry with a second gas-phase separation technique based on ion mobility permits the separation of metal-thiolate ions from isobaric chemical noise, enhancing the sensitivity of metal-thiolate ion observations. The use of ion mobility creates higher gas pressures in the source region, which also reduces the internal energy of the ionized metal-thiolate complexes, virtually eliminating the formation of gold-sulfide ions and preserving more fragile metal-thiolate ions. Through these two properties, MALDI-IM-MS can be used to detect a diverse array of metal-thiolates. The two-dimensional separation allows for the extraction of metal-thiolate ion signal, leading to more sensitive measurements of the diverse gold-thiolate stoichiometries than possible using mass spectrometry alone.

For mixed-monolayer AuNPs, a measurement of ion abundances for gold-thiolate complexes containing various ligands yields ligand abundances which agree with NMR measurements taken on intact AuNPs. This second experiment also confirms the foundational hypothesis. The result also indicates the utility of MALDI-IM-MS for the measurement of relative ligand abundances. As a technique with only one clear alternative, NMR spectroscopy, IM-MS has several clear advantages: essentially zero probability of peak convolution, the ability to characterize ligand mixtures with no differences in functionality, and the ability to analyze complex ternary or quaternary ligand mixtures.

Within a given Au_xL_y stoichiometry, the abundances of ions corresponding to different numbers of the thiolates in the mixture can be compared to a binomial model, permitting a novel approach to investigating supramolecular structures on AuNP surfaces. The observation of gold-thiolate complexes which reflect the phase-segregated nature of the

parent AuNP surface provides the third and final confirmation of the hypothesis. This new approach has been utilized to shed light on previously reported structures, and to illustrate a previously unknown supramolecular structure. Compared to other analytical techniques which have very limited reported uses, a MALDI-IM-MS-based strategy is relatively quick, simple, and effective.

With three affirmative experiments, the hypothesis – that observed metal-thiolate ions reflect the monolayer-protected metal nanoparticle surface from which they are derived – is confirmed. Beyond the confirmation of the hypothesis, the IM-MS platform offers great promise for the characterization of monolayer-protected metallic NPs, particularly AuNPs. Compared to other analytical platforms, IM-MS offers the most information about the most relevant properties of metallic NPs, namely their surface properties. Furthermore, IM-MS is useful for a more diverse array of metal NPs than other techniques. It shares the capabilities of MS for the analysis of small MPCs while enabling the surface characterization of larger, more polydisperse, and hydrophilic AuNPs. For these reasons, IM-MS could easily become a new standard for the characterization of monolayer-protected AuNPs.

Future directions

Fundamental studies of AuNP chemistry

The vast chemical space which monolayer-protected AuNPs can occupy has led to a number of publications exploring simple AuNP chemistry, particularly the structure and behavior of the monolayer.[18,25,70] Some of the most high-impact publications of recent years have dealt with fundamental AuNP properties. IM-MS offers an unparalleled

platform for investigating the chemistry of gold-thiolate complexes both when in solution and when bound to gold cores. For example, IM-MS could be utilized for investigating place-exchange kinetics, finding which metals are on the surface in alloyed monolayer-protected nanoparticles, and the effective cross-section of magic-sized AuNPs, which would prove more informative than TEM core diameter measurements. It could perhaps be even more useful than crystallographic measurements, which only exist for AuNPs protected by two different sets of ligands. Another route that may prove useful to the AuNP synthetic community would be a study correlating gold-thiolate stoichiometries generated under given synthetic conditions with their eventual size and any other relevant properties.

Perhaps the most immediately pertinent fundamental study which could be made would involve the possible direct desorption of protecting gold-thiolate species from AuNPs, *i.e.* the observation of gold-thiolate stoichiometries on AuNP surfaces. The data presented in Figure 15 and Figure 26suggest a unique ability to investigate the stoichiometries present on larger AuNPs with ligands larger than SCH_3, a study which has been remarkably missing from the literature. It is unclear why each computational or experimental study of gold-thiolate complexes on Au has only utilized SCH_3, but it may be a major blind spot for researchers studying such complexes. For this purpose as well as cross-section measurements of intact AuNPs, collaboration with those familiar with density functional theory (DFT) calculations for studying gold-thiolate complexes and AuNPs[53-55,61,66,68] could prove invaluable.

Development of a new standard protocol for AuNP characterization

With the number of ion mobility-mass spectrometric instruments increasing, the methodologies developed here should garner a large number of users who are interested in fundamental metal nanoparticle chemistry or applications based on those nanoparticles. A combination of IM-MS and UV-visible spectroscopy provides a simple and relatively quick characterization method: average size can be determined to within ~1-2 nm by looking for the presence of discrete optical absorbance bands (1-2 nm AuNPs) or the presence and size of surface plasmon bands compared to the scattering region closer to ultraviolet frequencies (3+ nm), while IM-MS can provide a general estimate of sample purity (ESI is excellent for this purpose, since there are no matrix interference effects and no radiation-induced ionization enhancement or fragmentation) and a more precise measurement of surface stoichiometries. The development of IM-MS coupled with NMR or UV-vis spectroscopy as a technique for the common nanomaterials lab could be highly productive, especially for collaborative work.

The question of ionization efficiency is very important to the development of a relative quantitation protocol. More detailed analyses of various mixed-ligand AuNPs with varying expected ionization efficiencies could be compared to NMR measurements, and controls could potentially be developed by utilizing gold-thiolate complexes formed in solution with specific ligand:ligand ratios.

The current methodology for analyzing spectra using MassLynx and Microsoft Excel software, while effective and sufficiently robust for an experienced user, could benefit greatly from the development of simpler, more robust, and user-friendly software. This would almost definitely require collaboration with a more programming-oriented lab,

optimally one developing proteomic tools. The greatest challenge is the unusual composition of the ions observed: organometallic products with a wide array of stoichiometries, functionalities, and modifications are highly unfamiliar territory for the average proteomics-minded student. In spite of the great difficulties this would pose, the development of such software is likely a *sine qua non* for the popularization of IM-MS in this field.

APPENDIX
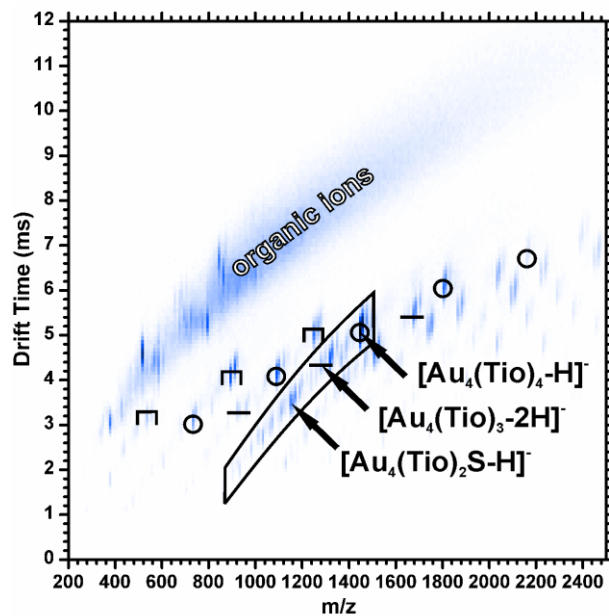
Figure A 1. An ion mobility-mass spectrum of tiopronin-protected AuNPs in negative ion mode. The symbols above the ion species in the IM-MS plot indicate their assigned structure: ring (Au_xL_x, ○), linear ($Au_{x+1}L_x$, −), and staple (Au_xL_{x+1}, Π).
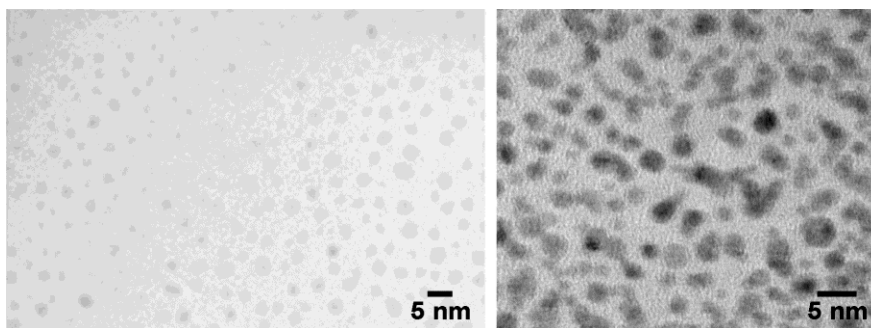
Figure A 2. Transmission electron microscopy images of Tio and OT AuNPs. Average core diameters were measured to be 2.5 ± 0.6 and 3.6 ± 1.5 nm, respectively.
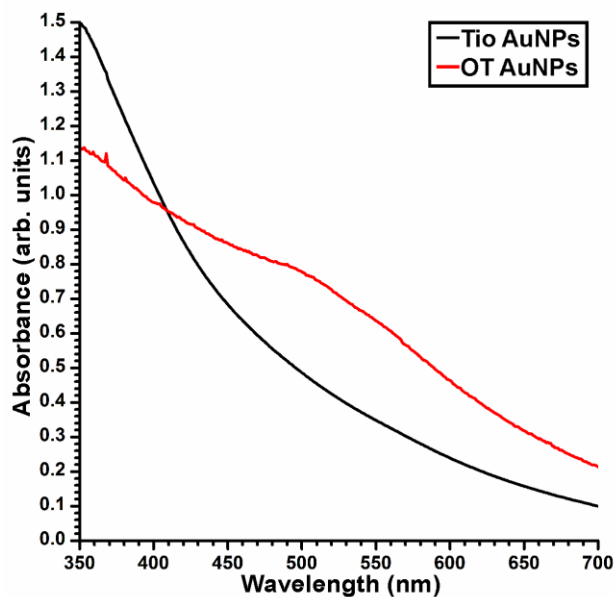
Figure A 3. UV-Vis spectrum of Tio and OT AuNPs. A surface plasmon band (centered at approximately 520 nm) was observed for OT AuNPs, but not for Tio AuNPs.
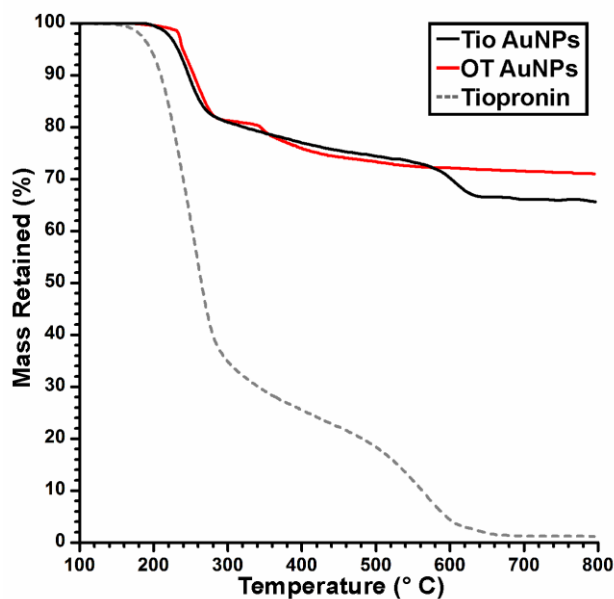
Figure A 4. Thermal gravimetric analysis of Tio and OT AuNPs. The organic mass fraction of the two samples were measured to be 35.3% and 29.0%, respectively. The results for pure tiopronin is shown for comparison. The two-stage decomposition of the tiopronin and AuNPs do not represent impurity; each AuNP sample was inspected for purity by NMR prior to usage.
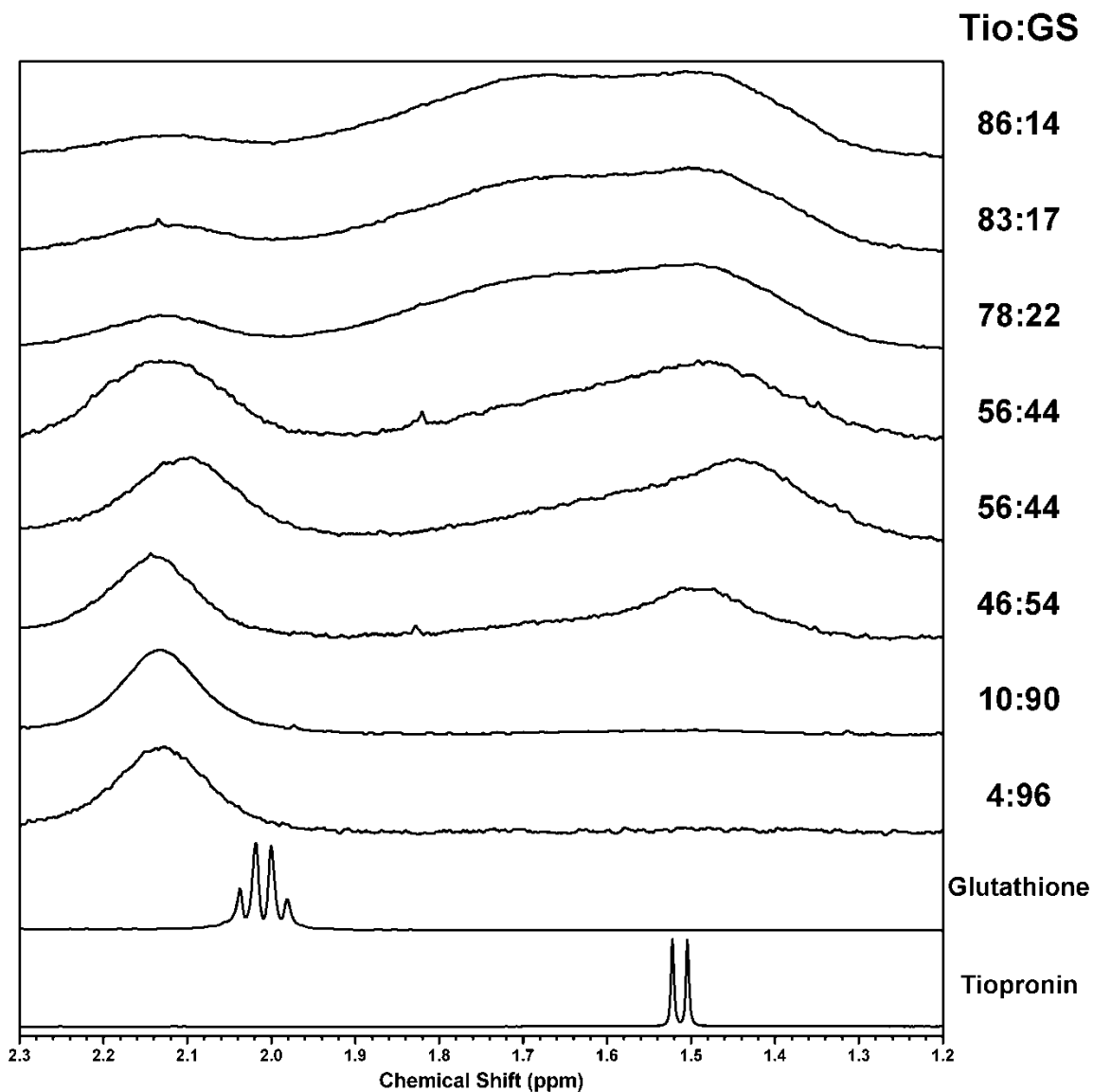
Figure A 5. NMR spectra of Tio:GS AuNPs, free glutathione, and free tiopronin. This portion of the NMR spectrum was used for relative quantitation of tiopronin and glutathione on the monolayer-protected AuNP surface. The peak between 1.9 and 2.3 corresponds to glutathione, the peak below 1.9 corresponds to tiopronin. Integration was performed for each peak starting from the outside edge of the peak to the minimum between the two.

103

$y = (0.99 \pm 0.04)x - (0.03 \pm 0.02)$
$R^2 = 0.988$
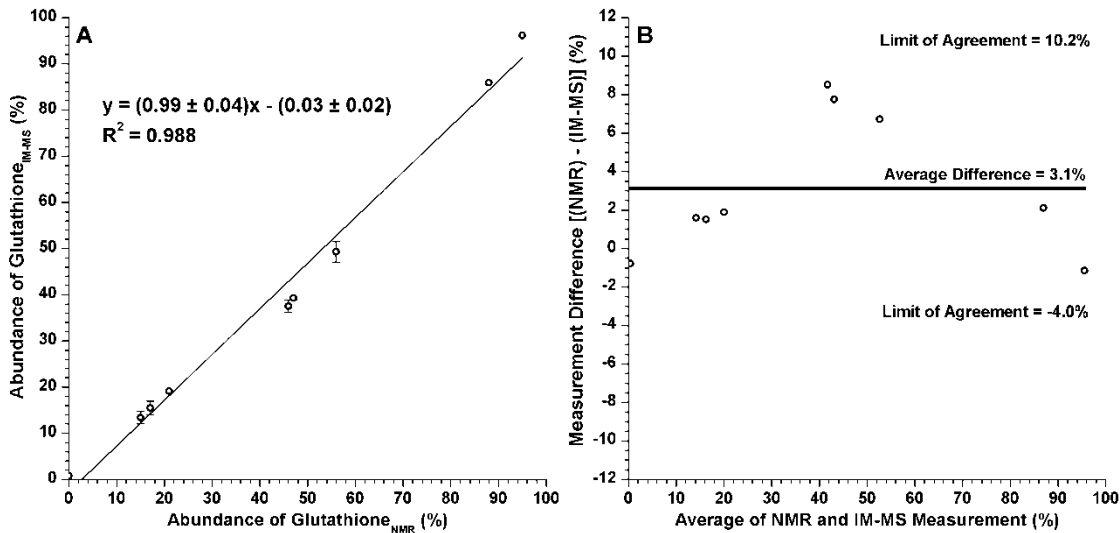
Figure A 6. Regression and Bland-Altman plots (left and right, respectively) comparing NMR and MALDI-IM-MS measurements of Tio:GS ratios using only Au_4L_4 ions, expressed as a molar percentage of glutathione. Using only Au_4L_4 ions makes the quantitation measurement quicker and more facile, but yields poorer results than using all gold-thiolate ions (Figure 19).
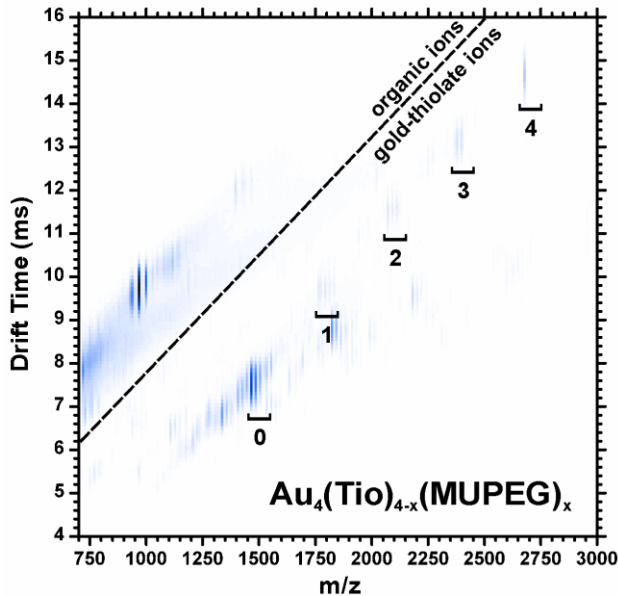
Figure A 7. Ion mobility-mass spectrum of 86:14 Tio:MUPEG AuNPs.
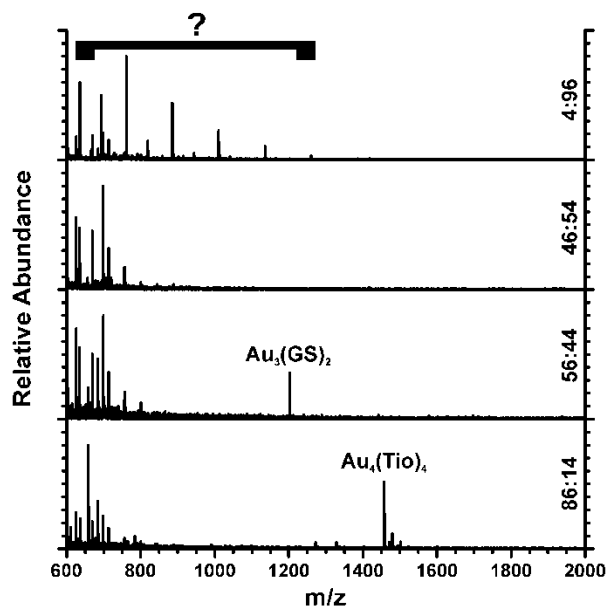
Figure A 8. Mass spectra of selected Tio:GS AuNPs, with ratios shown on the right. AuNPs with low amounts of glutathione tend to yield only the most dominant ion from the equivalent IM-MS spectrum. Peaks below 1200 m/z are unidentified ions, likely organic cluster ions or fragmented and rearranged gold-thiolate ions.
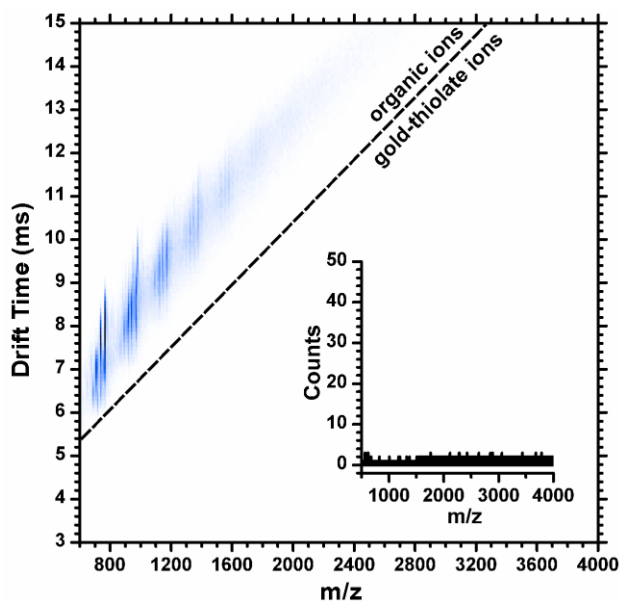
Figure A 9. Ion mobility-mass spectrum of a mixture of 2 nm bare gold AuNPs and free tiopronin, with the mass spectrum of the extracted gold-thiolate region shown inset. The solution was spotted and dried immediately after combination to prevent gold-thiol bonding in solution. No signals are seen in the gold-thiolate ion region, establishing that the gold-thiolate complexes investigated here do not form in the gas phase.
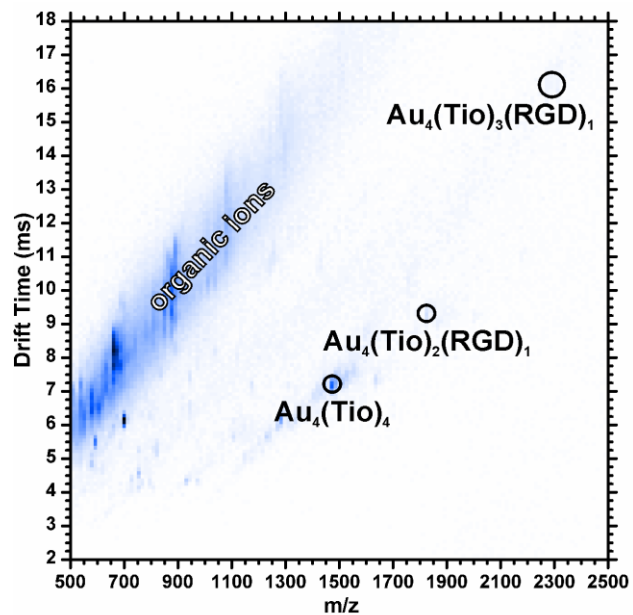
Figure A 10. Ion mobility-mass spectrum of 78:22 Tio:RGD epitope AuNPs.
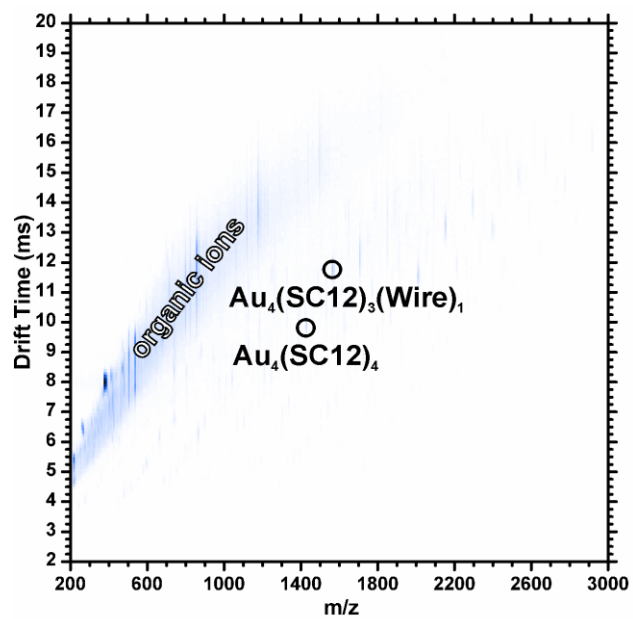
Figure A 11. Ion mobility-mass spectrum of dodecanethiol:phenylacetylene "molecular wire" AuNPs.
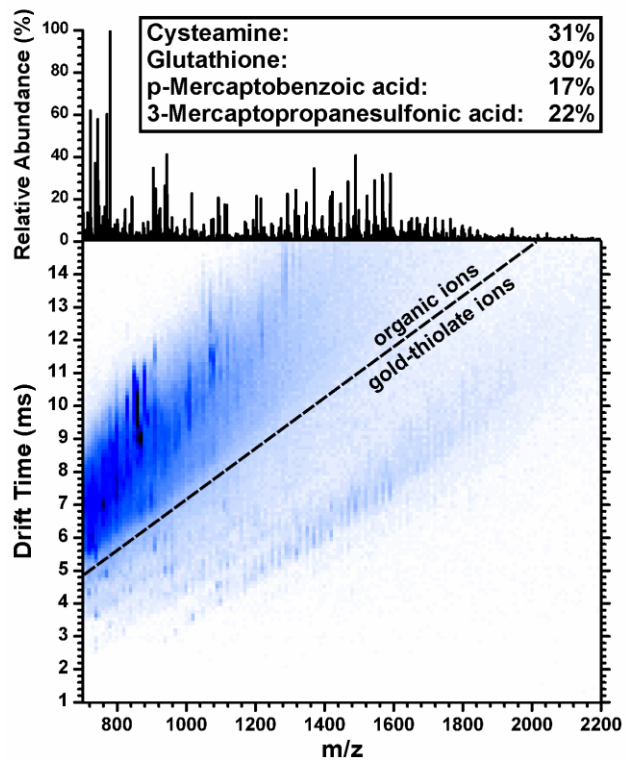
Figure A 12. Ion mobility-mass spectrum of AuNPs with a quaternary ligand system. Measured molar percentages of the four ligands are shown above.

Octanethiol (OT): Decanethiol (DT)		Tiopronin (Tio): Glutathione (GS)		Tiopronin (Tio): (MUPEG)	
Feed Ratio	Time	Feed Ratio	Time	Feed Ratio	Time
1:1	8h	7:1	1h	4:1	3d
1:1	24h	5:1	1h	1:1	3d
1:2	24h	3:1	1h	1:4	3d
1:5	8h	1:1	1d		
1:5	24h	1:1	1d		
1:10	24h	1:2	3d		
		1:60	7d		
		1:60	7d		

Table A 1. Feed ratio (original ligand:alternate ligand, as listed in headings) and time elapsed for place exchange reactions in Chapter IV. Amount of original ligand estimated from TEM and TGA data. Listings are ordered from least exchange (top) to most exchange (bottom), for comparison to Table 3. A comparison of feed ratios to measured ratios on the final AuNP product reveals a generally incomplete exchange, with the original ligand being favored in the final product. The only exceptions are Tio:GS AuNPs at low amounts of glutathione added.

BIBLIOGRAPHY

1.   Brust, M., Walker, M., Bethell, D., Schiffrin, D. J. and Whyman, R. (1994) Synthesis of Thiol-Derivatized Gold Nanoparticles in a 2-Phase Liquid-Liquid System. *J Chem Soc, Chem Commun*, 801-802.

2.   Cervera, J., Manzanares, J. A. and Mafe, S. (2009) Synchronization of coupled single-electron circuits based on nanoparticles and tunneling junctions. *J Appl Phys*, **105**, 074315-074315-074314.

3.   Pasquato, L., Pengo, P. and Scrimin, P. (2004) Functional gold nanoparticles for recognition and catalysis. *J Mater Chem*, **14**, 3481-3487.

4.   Wilson, R. (2008) The use of gold nanoparticles in diagnostics and detection. *Chem Soc Rev*, **37**, 2028-2045.

5.   Manea, F., Bindoli, C., Fallarini, S., Lombardi, G., Polito, L., Lay, L., Bonomi, R., Mancin, F. and Scrimin, P. (2008) Multivalent, Saccharide-Functionalized Gold Nanoparticles as Fully Synthetic Analogs of Type A Neisseria meningitidis Antigens. *Adv Mater (Weinheim, Ger)*, **20**, 4348-4352.

6.   Faraday, M. (1857) The Bakerian Lecture: Experimental Relations of Gold (and Other Metals) to Light. *Philos Trans R Soc London*, **147**, 145-181.

7.   Thompson, D. (2007) Michael Faraday's recognition of ruby gold: the birth of modern nanotechnology. *Gold Bull*, **40**, 267-269.

8.   Nuzzo, R. G. and Allara, D. L. (1983) Adsorption of bifunctional organic disulfides on gold surfaces. *J Am Chem Soc*, **105**, 4481-4483.

9.   Templeton, A. C., Wuelfing, W. P. and Murray, R. W. (2000) Monolayer-Protected Cluster Molecules. *Acc Chem Res*, **33**, 27-36.

10.   Thaxton, C. S. and Mirkin, C. A. DNA-Gold-Nanoparticle Conjugates In *NanoBiotechnology*; Niemeyer, C., Mirkin, C., Eds.; Wiley-VCH Verlag GmbH & Co. KGaA: Weinheim, Germany, 2004, pp 288-307.

11.   Cliffel, D. E., Turner, B. N. and Huffman, B. J. Nanoparticle-based biologic mimetics In *Wiley Interdiscipl Rev: Nanomed and Nanobiotechnol*; Baker, J. R., Ed.; John Wiley & Sons, Inc.: Hoboken, New Jersey, 2009; Vol. 1, pp 47-59.

12.   Chen, S. W., Ingram, R. S., Hostetler, M. J., Pietron, J. J., Murray, R. W., Schaaff, T. G., Khoury, J. T., Alvarez, M. M. and Whetten, R. L. (1998) Gold

nanoelectrodes of varied size: Transition to molecule-like charging. *Science*, **280**, 2098-2101.

13.   Alvarez, M. M., Khoury, J. T., Schaaff, T. G., Shafigullin, M. N., Vezmar, I. and Whetten, R. L. (1997) Optical absorption spectra of nanocrystal gold molecules. *J Phys Chem B*, **101**, 3706-3712.

14.   Negishi, Y., Nobusada, K. and Tsukuda, T. (2005) Glutathione-protected gold clusters revisited: Bridging the gap between gold(I)-thiolate complexes and thiolate-protected gold nanocrystals. *J Am Chem Soc*, **127**, 5261-5270.

15.   Gerdon, A. E., Wright, D. W. and Cliffel, D. E. (2005) Hemagglutinin Linear Epitope Presentation on Monolayer-Protected Clusters Elicits Strong Antibody Binding. *Biomacromolecules*, **6**, 3419-3424.

16.   Novak, J. P., Brousseau, L. C., Vance, F. W., Johnson, R. C., Lemon, B. I., Hupp, J. T. and Feldheim, D. L. (2000) Nonlinear Optical Properties of Molecularly Bridged Gold Nanoparticle Arrays. *J Am Chem Soc*, **122**, 12029-12030.

17.   Shaw, C. F. (1999) Gold-based therapeutic agents. *Chem Rev (Washington, DC, U S)*, **99**, 2589-2600.

18.   Jadzinsky, P. D., Calero, G., Ackerson, C. J., Bushnell, D. A. and Kornberg, R. D. (2007) Structure of a thiol monolayer-protected gold nanoparticle at 1.1 angstrom resolution. *Science*, **318**, 430-433.

19.   Schmidbaur, H. (2000) The aurophilicity phenomenon: A decade of experimental findings, theoretical concepts and emerging applications. *Gold Bull*, **33**, 3-10.

20.   Jin, R. (2010) Quantum sized, thiolate-protected gold nanoclusters. *Nanoscale*, **2**, 343-362.

21.   Lopez-Acevedo, O., Akola, J., Whetten, R. L., Gronbeck, H. and Hakkinen, H. (2009) Structure and Bonding in the Ubiquitous Icosahedral Metallic Gold Cluster Au-144(SR)(60). *J Phys Chem C*, **113**, 5035-5038.

22.   Fields-Zinna, C. A., Sardar, R., Beasley, C. A. and Murray, R. W. (2009) Electrospray Ionization Mass Spectrometry of Intrinsically Cationized Nanoparticles, [Au144/146(SC11H22N(CH2CH3)3+)x(S(CH2)5CH3)y]x+. *J Am Chem Soc*, **131**, 16266-16271.

23.   de Gennes, P. G. (1992) Soft Matter (Nobel Lecture). *Angew Chem Int Ed*, **31**, 842-845.

24.   Walther, A. and Müller, A. (2008) Janus particles. *Soft Matter*, **4**, 663-668.

25. Jackson, A. M., Myerson, J. W. and Stellacci, F. (2004) Spontaneous assembly of subnanometre-ordered domains in the ligand shell of monolayer-protected nanoparticles. *Nat Mater*, **3**, 330-336.

26. Verma, A., Uzun, O., Hu, Y., Hu, Y., Han, H.-S., Watson, N., Chen, S., Irvine, D. J. and Stellacci, F. (2008) Surface-structure-regulated cell-membrane penetration by monolayer-protected nanoparticles. *Nat Mater*, **7**, 588-595.

27. Hung, A., Mwenifumbo, S., Mager, M., Kuna, J. J., Stellacci, F., Yarovsky, I. and Stevens, M. M. (2011) Ordering Surfaces on the Nanoscale: Implications for Protein Adsorption. *J Am Chem Soc*, **133**, 1438-1450.

28. Terrill, R. H., Postlethwaite, T. A., Chen, C. H., Poon, C. D., Terzis, A., Chen, A. D., Hutchison, J. E., Clark, M. R., Wignall, G., Londono, J. D., Superfine, R., Falvo, M., Johnson, C. S., Samulski, E. T. and Murray, R. W. (1995) Monolayers in three dimensions: NMR, SAXS, thermal, and electron hopping studies of alkanethiol stabilized gold clusters. *J Am Chem Soc*, **117**, 12537-12548.

29. Schaaff, T. G., Knight, G., Shafigullin, M. N., Borkman, R. F. and Whetten, R. L. (1998) Isolation and selected properties of a 10.4 kDa Gold : Glutathione cluster compound. *J Phys Chem B*, **102**, 10643-10646.

30. Arnold, R. J. and Reilly, J. P. (1998) High-resolution time-of-flight mass spectra of alkanethiolate-coated gold nanocrystals. *J Am Chem Soc*, **120**, 1528-1532.

31. Schaaff, T. G., Shafigullin, M. N., Khoury, J. T., Vezmar, I., Whetten, R. L., Cullen, W. G., First, P. N., Gutierrez-Wing, C., Ascensio, J. and Jose-Yacaman, M. J. (1997) Isolation of Smaller Nanocrystal Au molecules: Robust Quantum Effects in Optical Spectra. *J Phys Chem B*, **101**, 7885-7891.

32. Heaven, M. W., Dass, A., White, P. S., Holt, K. M. and Murray, R. W. (2008) Crystal structure of the gold nanoparticle [N(C8H17)(4)][Au-25(SCH2CH2Ph)(18)]. *J Am Chem Soc*, **130**, 3754-3755.

33. Whetten, R. L., Khoury, J. T., Alvarez, M. M., Murthy, S., Vezmar, I., Wang, Z. L., Stephens, P. W., Cleveland, C. L., Luedtke, W. D. and Landman, U. (1996) Nanocrystal gold molecules. *Adv Mater (Weinheim, Ger)*, **8**, 428-433.

34. Alvarez, M. M., Khoury, J. T., Schaaff, T. G., Shafigullin, M., Vezmar, I. and Whetten, R. L. (1997) Critical sizes in the growth of Au clusters. *Chem Phys Lett*, **266**, 91-98.

35. Schaaff, T. G. (2004) Laser desorption and matrix-assisted laser desorption/ionization mass spectrometry of 29-kDa Au : SR cluster compounds. *Anal Chem*, **76**, 6187-6196.

36. Wu, Z., Suhan, J. and Jin, R. C. (2009) One-pot synthesis of atomically monodisperse, thiol-functionalized Au-25 nanoclusters. *J Mater Chem*, **19**, 622-626.

37. Qian, H. and Jin, R. (2009) Controlling Nanoparticles with Atomic Precision: The Case of Au144(SCH2CH2Ph)60. *Nano Lett*, **9**, 4083-4087.

38. Qian, H., Eckenhoff, W. T., Zhu, Y., Pintauer, T. and Jin, R. (2010) Total Structure Determination of Thiolate-Protected Au38 Nanoparticles. *J Am Chem Soc*, **132**, 8280-8281.

39. Dass, A. (2009) Mass Spectrometric Identification of Au68(SR)34 Molecular Gold Nanoclusters with 34-Electron Shell Closing. *J Am Chem Soc*, **131**, 11666-11667.

40. Dass, A., Stevenson, A., Dubay, G. R., Tracy, J. B. and Murray, R. W. (2008) Nanoparticle MALDI-TOF mass spectrometry without fragmentation: Au25(SCH2CH2Ph)(18) and mixed monolayer Au-25(SCH2CH2Ph)(18-x)(L)(x). *J Am Chem Soc*, **130**, 5940-5946.

41. Vasil'ev, Y. V., Khvostenko, O. G., Streletskii, A. V., Boltalina, O. V., Kotsiris, S. G. and Drewello, T. (2006) Electron transfer reactivity in matrix-assisted laser desorption/ionization (MALDI): Ionization energy, electron affinity and performance of the DCTB matrix within the thermochemical framework. *J Phys Chem A*, **110**, 5967-5972.

42. Tracy, J. B., Kalyuzhny, G., Crowe, M. C., Balasubramanian, R., Choi, J. P. and Murray, R. W. (2007) Poly(ethylene glycol) ligands for high-resolution nanoparticle mass spectrometry. *J Am Chem Soc*, **129**, 6706-6707.

43. Negishi, Y., Chaki, N. K., Shichibu, Y., Whetten, R. L. and Tsukuda, T. (2007) Origin of Magic Stability of Thiolated Gold Clusters: A Case Study on Au25(SC6H13)18 *J Am Chem Soc*, **129**, 11322-11323.

44. Chaki, N. K., Negishi, Y., Tsunoyama, H., Shichibu, Y. and Tsukuda, T. (2008) Ubiquitous 8 and 29 kDa gold: Alkanethiolate cluster compounds: Mass-spectrometric determination of molecular formulas and structural implications. *J Am Chem Soc*, **130**, 8608-8610.

45. Marshall, A. G., Hendrickson, C. L. and Shi, S. D. H. (2002) Scaling MS plateaus with high-resolution FT-ICRMS. *Anal Chem*, **74**, 253a-259a.

46. Dass, A., Holt, K., Parker, J. F., Feldberg, S. W. and Murray, R. W. (2008) Mass Spectrometrically Detected Statistical Aspects of Ligand Populations in Mixed Monolayer Au25L18 Nanoparticles. *J Phys Chem C*, **112**, 20276-20283.

47.   Hostetler, M. J., Templeton, A. C. and Murray, R. W. (1999) Dynamics of place-exchange reactions on monolayer-protected gold cluster molecules. *Langmuir*, **15**, 3782-3789.

48.   Gies, A. P., Hercules, D. M., Gerdon, A. E. and Cliffel, D. E. (2007) Electrospray mass spectrometry study of tiopronin monolayer-protected gold nanoclusters. *J Am Chem Soc*, **129**, 1095-1104.

49.   Simpson, C. A., Farrow, C. L., Tian, P., Billinge, S. J. L., Huffman, B. J., Harkness, K. M. and Cliffel, D. E. (2010) Tiopronin Gold Nanoparticle Precursor Forms Aurophilic Ring Tetramer. *Inorg Chem*, **49**, 10858-10866.

50.   Harkness, K. M., Fenn, L. S., Cliffel, D. E. and McLean, J. A. (2010) Surface Fragmentation of Complexes from Thiolate Protected Gold Nanoparticles by Ion Mobility-Mass Spectrometry. *Anal Chem*, **82**, 3061-3066.

51.   Fields-Zinna, C. A., Sampson, J. S., Crowe, M. C., Tracy, J. B., Parker, J. F., deNey, A. M., Muddiman, D. C. and Murray, R. W. (2009) Tandem Mass Spectrometry of Thiolate-Protected Au Nanoparticles NaxAu25(SC2H4Ph)(18-y)(S(C2H4O)(5)CH3)(y). *J Am Chem Soc*, **131**, 13844-13851.

52.   Voznyy, O., Dubowski, J. J., Yates, J. T. and Maksymovych, P. (2009) The Role of Gold Adatoms and Stereochemistry in Self-Assembly of Methylthiolate on Au(111). *J Am Chem Soc*, **131**, 12989-12993.

53.   Häkkinen, H., Walter, M. and Gronbeck, H. (2006) Divide and Protect: Capping Gold Nanoclusters with Molecular Gold-Thiolate Rings. *J Phys Chem B*, **110**, 9927-9931.

54.   Grönbeck, H., Walter, M. and Häkkinen, H. (2006) Theoretical characterization of cyclic thiolated gold clusters. *J Am Chem Soc*, **128**, 10268-10275.

55.   Grönbeck, H., Häkkinen, H. and Whetten, R. L. (2008) Gold-Thiolate Complexes Form a Unique c(4 x 2) Structure on Au(111). *J Phys Chem C*, **112**, 15940-15942.

56.   Briñas, R. P., Hu, M. H., Qian, L. P., Lymar, E. S. and Hainfeld, J. F. (2008) Gold nanoparticle size controlled by polymeric Au(I) thiolate precursor size. *J Am Chem Soc*, **130**, 975-982.

57.   Zhu, M., Lanni, E., Garg, N., Bier, M. E. and Jin, R. (2008) Kinetically controlled, high-yield synthesis of Au-25 clusters. *J Am Chem Soc*, **130**, 1138-1139.

58.   Zhu, M. Z., Eckenhoff, W. T., Pintauer, T. and Jin, R. C. (2008) Conversion of anionic [Au-25(SCH2CH2Ph)(18)](-) cluster to charge neutral cluster via air oxidation. *J Phys Chem C*, **112**, 14221-14224.

59. Cliffel, D. E., Zamborini, F. P., Gross, S. M. and Murray, R. W. (2000) Mercaptoammonium-Monolayer-Protected, Water-Soluble Gold, Silver, and Palladium Clusters. *Langmuir*, **16**, 9699-9702.

60. Templeton, A. C., Chen, S., Gross, S. M. and Murray, R. W. (1999) Water-Soluble, Isolable Gold Clusters Protected by Tiopronin and Coenzyme A Monolayers. *Langmuir*, **15**, 66-76.

61. Walter, M., Akola, J., Lopez-Acevedo, O., Jadzinsky, P. D., Calero, G., Ackerson, C. J., Whetten, R. L., Gronbeck, H. and Hakkinen, H. (2008) A unified view of ligand-protected gold clusters as superatom complexes. *Proc Natl Acad Sci U S A*, **105**, 9157-9162.

62. Jiang, D. E. (2009) Au adatom-linked CH3S-Au-SCH3 complexes on Au(111). *Chem Phys Lett*, **477**, 90-94.

63. Singh, C., Ghorai, P. K., Horsch, M. A., Jackson, A. M., Larson, R. G., Stellacci, F. and Glotzer, S. C. (2007) Entropy-Mediated Patterning of Surfactant-Coated Nanoparticles and Surfaces. *Phys Rev Lett*, **99**, 226106.

64. Gentilini, C., Franchi, P., Mileo, E., Polizzi, S., Lucarini, M. and Pasquato, L. (2009) Formation of Patches on 3D SAMs Driven by Thiols with Immiscible Chains Observed by ESR Spectroscopy. *Angew Chem*, **121**, 3106-3110.

65. Pradhan, S., Xu, L. and Chen, S. (2007) Janus Nanoparticles by Interfacial Engineering. *Adv Funct Mater*, **17**, 2385-2392.

66. Akola, J., Walter, M., Whetten, R. L., Hakkinen, H. and Gronbeck, H. (2008) On the structure of thiolate-protected Au25. *J Am Chem Soc*, **130**, 3756-3757.

67. Lopez-Acevedo, O., Tsunoyama, H., Tsukuda, T., Hakkinen, H. and Aikens, C. M. (2010) Chirality and Electronic Structure of the Thiolate-Protected Au38 Nanocluster. *J Am Chem Soc*, **132**, 8210-8218.

68. Jiang, D. E. and Dai, S. (2009) Constructing Gold-Thiolate Oligomers and Polymers on Au(111) Based on the Linear S-Au-S Geometry. *J Phys Chem C*, **113**, 7838-7842.

69. Voznyy, O. and Dubowski, J. (2009) c (4× 2) Structures of Alkanethiol Monolayers on Au (111) Compatible with the Constraint of Dense Packing. *Langmuir*, **25**, 7353-7358.

70. Love, J. C., Estroff, L. A., Kriebel, J. K., Nuzzo, R. G. and Whitesides, G. M. (2005) Self-Assembled Monolayers of Thiolates on Metals as a Form of Nanotechnology. *Chem Rev (Washington, DC, U S)*, **105**, 1103-1170.

71. Carro, P., Corthey, G. n., Rubert, A. A., Benitez, G. A., Fonticelli, M. H. and Salvarezza, R. C. (2010) The Complex Thiol−Palladium Interface: A Theoretical and Experimental Study. *Langmuir*, **26**, 14655-14662.

72. Corthey, G. n., Rubert, A. A., Benitez, G. A., Fonticelli, M. H. and Salvarezza, R. C. (2009) Electrochemical and X-ray Photoelectron Spectroscopy Characterization of Alkanethiols Adsorbed on Palladium Surfaces. *J Phys Chem C*, **113**, 6735-6742.

73. Huang, T. and Murray, R. W. (2003) Luminescence of tiopronin monolayer-protected silver clusters changes to that of gold clusters upon galvanic core metal exchange. *J Phys Chem B*, **107**, 7434-7440.

74. Wu, Z., Lanni, E., Chen, W., Bier, M. E., Ly, D. and Jin, R. (2009) High Yield, Large Scale Synthesis of Thiolate-Protected Ag7 Clusters. *J Am Chem Soc*, **131**, 16672-16674.

75. Zamborini, F. P., Gross, S. M. and Murray, R. W. (2000) Synthesis, Characterization, Reactivity, and Electrochemistry of Palladium Monolayer Protected Clusters. *Langmuir*, **17**, 481-488.

76. Xiang, H., Wei, S.-H. and Gong, X. (2010) Structures of [Ag7(SR)4]− and [Ag7(DMSA)4]−. *J Am Chem Soc*, **132**, 7355-7360.

77. Knecht, M. and Pacardo, D. (2010) Employing high-resolution materials characterization to understand the effects of Pd nanoparticle structure on their activity as catalysts for olefin hydrogenation. *Anal Bioanal Chem*, **397**, 1137-1155.

78. Zhu, Y., Qian, H. and Jin, R. (2010) An Atomic-Level Strategy for Unraveling Gold Nanocatalysis from the Perspective of Aun(SR)m Nanoclusters. *Chem-Eur J*, **16**, 11455-11462.

79. Brauer, G. *Handbook of preparative inorganic chemistry*, Academic Press New York, 1965, 2, 1054.

80. Karas, M. and Hillenkamp, F. (1988) Laser Desorption Ionization of Proteins with Molecular Masses Exceeding 10000 Daltons. *Anal Chem*, **60**, 2299-2301.

81. Wu, Z., Gayathri, C., Gil, R. R. and Jin, R. (2009) Probing the Structure and Charge State of Glutathione-Capped Au25(SG)18 Clusters by NMR and Mass Spectrometry. *J Am Chem Soc*, **131**, 6535-6542.

82. Parker, J. F., Fields-Zinna, C. A. and Murray, R. W. (2010) The Story of a Monodisperse Gold Nanoparticle: Au25L18. *Acc Chem Res*.

83.   Dass, A., Dubay, G. R., Fields-Zinna, C. A. and Murray, R. W. (2008) FAB Mass Spectrometry of Au25(SR)18 Nanoparticles. *Anal Chem*, **80**, 6845–6849.

84.   McLean, J. A., Stumpo, K. A. and Russell, D. H. (2005) Size-Selected (2-10 nm) Gold Nanoparticles for Matrix Assisted Laser Desorption Ionization of Peptides. *J Am Chem Soc*, **127**, 5304-5305.

85.   Tsunoyama, R., Tsunoyama, H., Pannopard, P., Limtrakul, J. and Tsukuda, T. (2010) MALDI Mass Analysis of 11 kDa Gold Clusters Protected by Octadecanethiolate Ligands†. *J Phys Chem C*, **114**, 16004-16009.

86.   Goulet, P. J. G. and Lennox, R. B. (2010) New Insights into Brust−Schiffrin Metal Nanoparticle Synthesis. *J Am Chem Soc*, **132**, 9582-9584.

87.   Reilly, S. M., Krick, T. and Dass, A. (2010) Surfactant-free Synthesis of Ultrasmall Gold Nanoclusters. *J Phys Chem C*, **114**, 741-745.

88.   Tsipis, A. C. and Tsipis, C. A. (2005) Ligand-stabilized aromatic three-membered gold rings and their sandwichlike complexes. *J Am Chem Soc*, **127**, 10623-10638.

89.   Negishi, Y., Takasugi, Y., Sato, S., Yao, H., Kimura, K. and Tsukuda, T. (2004) Magic-numbered Au-n clusters protected by glutathione monolayers (n=18, 21, 25, 28, 32, 39): Isolation and spectroscopic characterization. *J Am Chem Soc*, **126**, 6518-6519.

90.   Tsai, D. H., Zangmeister, R. A., Pease, L. F., Tarlov, M. J. and Zachariah, M. R. (2008) Gas-phase ion-mobility characterization of SAM-functionalized Au nanoparticles. *Langmuir*, **24**, 8483-8490.

91.   Jarrold, M. F. and Bower, J. E. (1993) Mobilities of metal cluster ions aluminum (Aln+ and Aln2+): effect of charge on cluster geometry. *J Phys Chem*, **97**, 1746-1748.

92.   Jarrold, M. F. and Bower, J. E. (1993) Mobilities of metal cluster ions: Aluminum and the electronic shell model. *J Chem Phys*, **98**, 2399-2407.

93.   Gilb, S., Weis, P., Furche, F., Ahlrichs, R. and Kappes, M. M. (2002) Structures of small gold cluster cations (Au_n^+, n<14): Ion mobility measurements versus density functional calculations. *J Chem Phys*, **116**, 4094-4101.

94.   Furche, F., Ahlrichs, R., Weis, P., Jacob, C., Gilb, S., Bierweiler, T. and Kappes, M. M. (2002) The structures of small gold cluster anions as determined by a combination of ion mobility measurements and density functional calculations. *J Chem Phys*, **117**, 6982-6990.

95.   Fenn, L. S. and McLean, J. A. (2008) Biomolecular structural separations by ion mobility-mass spectrometry. *Anal Bioanal Chem*, **391**, 905-909.

96.   Giles, K., Pringle, S. D., Worthington, K. R., Little, D., Wildgoose, J. L. and Bateman, R. H. (2004) Applications of a travelling wave-based radio-frequency-only stacked ring ion guide. *Rapid Commun Mass Spectrom*, **18**, 2401-2414.

97.   Fenn, L. S. and McLean, J. A. (2008) Enhanced carbohydrate structural selectivity in ion mobility-mass spectrometry analyses by boronic acid derivatization. *Chem Commun (Cambridge, U K)*, 5505-5507.

98.   Gant-Branum, R. L., Kerr, T. J. and McLean, J. A. (2009) Labeling strategies in mass spectrometry-based protein quantitation. *Analyst*, **134**, 1525-1530.

99.   Bonasia, P. J., Gindelberger, D. E. and Arnold, J. (1993) Synthesis and characterization of gold(I) thiolates, selenolates, and tellurolates: x-ray crystal structures of Au4[TeC(SiMe3)3]4, Au4[SC(SiMe3)3]4, and Ph3PAu[TeC(SiMe3)3]. *Inorg Chem*, **32**, 5126-5131.

100.   Howard-Lock, H. E. (1999) Structures of Gold(I) and Silver(I) Thiolate Complexes of Medicinal Interest: A Review and Recent Results. *Met-Based Drugs*, **6**, 201-209.

101.   Templeton, A. C., Hostetler, M. J., Warmoth, E. K., Chen, S., Hartshorn, C. M., Krishnamurthy, V. M., Forbes, M. D. E. and Murray, R. W. (1998) Gateway Reactions to Diverse, Polyfunctional Monolayer-Protected Gold Clusters. *J Am Chem Soc*, **120**, 4845-4849.

102.   Fuente, J. M. d. l., Barrientos, A. G., Rojas, T. C., Rojo, J., Canada, J., Fernandez, A. and Penades, S. (2001) Gold Glyconanoparticles as Water-Soluble Polyvalent Models To Study Carbohydrate Interactions. *Angew Chem, Int Ed*, **40**, 2257-2261.

103.   Ackerson, C. J., Jadzinsky, P. D., Sexton, J. Z., Bushnell, D. A. and Kornberg, R. D. (2010) Synthesis and Bioconjugation of 2 and 3 nm-Diameter Gold Nanoparticles. *Bioconjugate Chem*, **21**, 214-218.

104.   Wuelfing, W. P., Gross, S. M., Miles, D. T. and Murray, R. W. (1998) Nanometer gold clusters protected by surface-bound monolayers of thiolated poly(ethylene glycol) polymer electrolyte. *J Am Chem Soc*, **120**, 12696-12697.

105.   Wuelfing, W. P. and Murray, R. W. (2002) Electron Hopping through Films of Arenethiolate Monolayer-Protected Gold Clusters. *J Phys Chem B*, **106**, 3139-3145.

106. DeVries, G. A., Brunnbauer, M., Hu, Y., Jackson, A. M., Long, B., Neltner, B. T., Uzun, O., Wunsch, B. H. and Stellacci, F. (2007) Divalent Metal Nanoparticles. *Science*, **315**, 358-361.

107. Song, Y., Huang, T. and Murray, R. W. (2003) Heterophase ligand exchange and metal transfer between monolayer protected clusters. *J Am Chem Soc*, **125**, 11694-11701.

108. Grainger, D. W. and Castner, D. G. (2008) Nanobiomaterials and Nanoanalysis: Opportunities for Improving the Science to Benefit Biomedical Technologies. *Adv Mater (Weinheim, Ger)*, **20**, 867-877.

109. Reyes, E., Madueno, R., Blazquez, M. and Pineda, T. (2010) Facile Exchange of Ligands on the 6-Mercaptopurine-Monolayer Protected Gold Clusters Surface. *J Phys Chem C*, **114**, 15955-15962.

110. Jimenez, V. L., Leopold, M. C., Mazzitelli, C., Jorgenson, J. W. and Murray, R. W. (2002) HPLC of Monolayer-Protected Gold Nanoclusters. *Anal Chem*, **75**, 199-206.

111. Templeton, A. C., Cliffel, D. E. and Murray, R. W. (1999) Redox and fluorophore functionalization of water-soluble, tiopronin-protected gold clusters. *J Am Chem Soc*, **121**, 7081-7089.

112. Badia, A., Singh, S., Demers, L., Cuccia, L., Brown, G. R. and Lennox, R. B. (1996) Self-assembled monolayers on gold nanoparticles. *Chemistry-a European Journal*, **2**, 359-363.

113. Song, Y., Harper, A. S. and Murray, R. W. (2005) Ligand Heterogeneity on Monolayer-Protected Gold Clusters. *Langmuir*, **21**, 5492-5500.

114. Zhu, Z.-J., Ghosh, P. S., Miranda, O. R., Vachet, R. W. and Rotello, V. M. (2008) Multiplexed Screening of Cellular Uptake of Gold Nanoparticles Using Laser Desorption/Ionization Mass Spectrometry. *J Am Chem Soc*, **130**, 14139-14143.

115. Zhu, Z.-J., Rotello, V. M. and Vachet, R. W. (2009) Engineered nanoparticle surfaces for improved mass spectrometric analyses. *Analyst*, **134**, 2183-2188.

116. Yan, B., Zhu, Z.-J., Miranda, O., Chompoosor, A., Rotello, V. and Vachet, R. (2010) Laser desorption/ionization mass spectrometry analysis of monolayer-protected gold nanoparticles. *Anal Bioanal Chem*, **396**, 1025-1035.

117. Tracy, J. B., Crowe, M. C., Parker, J. F., Hampe, O., Fields-Zinna, C. A., Dass, A. and Murray, R. W. (2007) Electrospray Ionization Mass Spectrometry of Uniform and Mixed Monolayer Nanoparticles: Au25[S(CH2)2Ph]18 and Au25[S(CH2)2Ph]18-x(SR)x *J Am Chem Soc*, **129**, 16209-16215.

118. Mrksich, M. (2008) Mass Spectrometry of Self-Assembled Monolayers: A New Tool for Molecular Surface Science. *ACS Nano*, **2**, 7-18.

119. Harkness, K. M., Cliffel, D. E. and McLean, J. A. (2010) Characterization of thiolate-protected gold nanoparticles by mass spectrometry. *Analyst*, **135**, 868-874.

120. Medzihradszky, K. F., Campbell, J. M., Baldwin, M. A., Falick, A. M., Juhasz, P., Vestal, M. L. and Burlingame, A. L. (2000) The Characteristics of Peptide Collision-Induced Dissociation Using a High-Performance MALDI-TOF/TOF Tandem Mass Spectrometer. *Anal Chem*, **72**, 552-558.

121. Tang, Z., Xu, B., Wu, B., Germann, M. W. and Wang, G. (2010) Synthesis and Structural Determination of Multidentate 2,3-Dithiol-Stabilized Au Clusters. *J Am Chem Soc*, **132**, 3367-3374.

122. Bland, J. M. and Altman, D. G. (1986) Statistical methods for assessing agreement between two methods of clinical measurement. *The Lancet*, **327**, 307-310.

123. Qian, X., Peng, X.-H., Ansari, D. O., Yin-Goen, Q., Chen, G. Z., Shin, D. M., Yang, L., Young, A. N., Wang, M. D. and Nie, S. (2008) In vivo tumor targeting and spectroscopic detection with surface-enhanced Raman nanoparticle tags. *Nat Biotechnol*, **26**, 83-90.

124. Simpson, C. A., Huffman, B. J., Gerdon, A. E. and Cliffel, D. E. (2010) Unexpected Toxicity of Monolayer Protected Gold Clusters Eliminated by PEG-Thiol Place Exchange Reactions. *Chem Res Toxicol*, **23**, 1608-1616.

125. Bresee, J., Maier, K. E., Melander, C. and Feldheim, D. L. (2010) Identification of antibiotics using small molecule variable ligand display on gold nanoparticles. *Chem Commun (Cambridge, U K)*, **46**, 7516-7518.

126. Centrone, A., Penzo, E., Sharma, M., Myerson, J. W., Jackson, A. M., Marzari, N. and Stellacci, F. (2008) The role of nanostructure in the wetting behavior of mixed-monolayer-protected metal nanoparticles. *Proc Natl Acad Sci U S A*, **105**, 9886-9891.

127. Verma, A. and Stellacci, F. (2010) Effect of Surface Properties on Nanoparticle–Cell Interactions. *Small*, **6**, 12-21.

128. Astier, Y., Uzun, O. and Stellacci, F. (2009) Electrophysiological Study of Single Gold Nanoparticle/α-Hemolysin Complex Formation: A Nanotool to Slow Down ssDNA Through the α-Hemolysin Nanopore. *Small*, **5**, 1273-1278.

129. Jackson, A. M., Hu, Y., Silva, P. J. and Stellacci, F. (2006) From Homoligand- to Mixed-Ligand- Monolayer-Protected Metal Nanoparticles: A Scanning Tunneling Microscopy Investigation. *J Am Chem Soc*, **128**, 11135-11149.

130. Centrone, A., Hu, Y., Jackson, Alicia M., Zerbi, G. and Stellacci, F. (2007) Phase Separation on Mixed-Monolayer-Protected Metal Nanoparticles: A Study by Infrared Spectroscopy and Scanning Tunneling Microscopy. *Small*, **3**, 814-817.

131. Harkness, K. M., Hixson, B. C., Fenn, L. S., Turner, B. N., Rape, A. C., Simpson, C. A., Huffman, B. J., Okoli, T. C., McLean, J. A. and Cliffel, D. E. (2010) A Structural Mass Spectrometry Strategy for the Relative Quantitation of Ligands on Mixed Monolayer-Protected Gold Nanoparticles. *Anal Chem*, **82**, 9268-9274.

132. Li, L., Golding, R. E. and Whittal, R. M. (1996) Analysis of Single Mammalian Cell Lysates by Mass Spectrometry. *J Am Chem Soc*, **118**, 11662-11663.

133. Carney, R. P., DeVries, G. A., Dubois, C., Kim, H., Kim, J. Y., Singh, C., Ghorai, P. K., Tracy, J. B., Stiles, R. L., Murray, R. W., Glotzer, S. C. and Stellacci, F. (2007) Size Limitations for the Formation of Ordered Striped Nanoparticles. *J Am Chem Soc*, **130**, 798-799.

134. Uzun, O., Hu, Y., Verma, A., Chen, S., Centrone, A. and Stellacci, F. (2008) Water-soluble amphiphilic gold nanoparticles with structured ligand shells. *Chem Commun (Cambridge, U K)*, 196-198.

135. DeVries, G. A., Talley, F. R., Carney, R. P. and Stellacci, F. (2008) Thermodynamic Study of the Reactivity of the Two Topological Point Defects Present in Mixed Self-Assembled Monolayers on Gold Nanoparticles. *Adv Mater (Weinheim, Ger)*, **20**, 4243-4247.

CURRICULUM VITAE

Kellen Harkness

  address: 722 Fox Ridge Dr, Brentwood, TN 37027

  phone: 434.851.2232

  email: kellen.harkness@gmail.com

Education:

  Vanderbilt University, Nashville, TN

- Ph.D Analytical Chemistry, defense scheduled March 25 2011

- Research: Structural Characterization of Monolayer-Protected Metal Nanoparticles by Ion Mobility-Mass Spectrometry

- Co-advisors: Profs. David E. Cliffel and John A. McLean

  Harding University, Searcy, AR

- B.S. Chemistry *magna cum laude*, May 2007

- Research: Ultraviolet Emissions Spectroscopy of Hybrid Rocket Motor Exhaust Plumes

Selected Awards and Fellowships

- Arkansas Governor's Distinguished Scholarship, 2003-2007

- Harding University Honors Scholar, 2003-2007

- Member, Omicron Delta Kappa (national leadership honors society)

- Mitchum Warren Fellowship, 2007-2009

- Vanderbilt Chemistry-Biology Trainee, 2008-2010

- Vanderbilt Institute for Nanoscale Science & Engineering Fellowship, 2011

Presentations

1. Harkness, K. M.; McLean, J. A.; Cliffel, D. E. Surface Characterization of Monolayer-Protected Gold Nanoparticles by Ion Mobility-Mass Spectrometry, PittCon Conference & Expo, Atlanta, GA, March 16, 2011. (*presider*)

2. Harkness, K. M.; McLean, J. A.; Cliffel, D. E. Analyzing Supramolecular Assemblies on Gold Surfaces, Vanderbilt Institute of Chemical Biology Symposium, Nashville, TN, August 12, 2010.

3. Harkness, K. M.; McLean, J. A.; Cliffel, D. E. Characterization of Ligands Conjugated to Gold Nanoparticles by Ion Mobility-Mass Spectrometry, Vanderbilt Institute of Chemical Biology Symposium, Nashville, TN, August 13, 2009.

4. Harkness, K. M.; McLean, J. A.; Cliffel, D. E. Ion Mobility-Mass Spectrometry: A Novel Approach to the Analysis of Gold Monolayer Protected Clusters, 57th ASMS Conference on Mass Spectrometry and Allied Topics, Philadelphia, PA, May 2, 2009.

5. Harkness, K.M.; Wilson, E.W. Emission spectroscopy of hydroxyl radicals in the 306 nm to 324 nm region of the electromagnetic spectrum, 232nd ACS National Meeting, San Francisco, CA, September 12, 2006.

Publications

1. Harkness, K. M.; Cliffel, D. E.; McLean, J. A., Characterization of thiolate-protected gold nanoparticles by mass spectrometry. *Analyst* **2010**, *135* (5), 868-874.

2. Harkness, K. M.; Fenn, L. S.; Cliffel, D. E.; McLean, J. A., Surface Fragmentation of Complexes from Thiolate Protected Gold Nanoparticles by Ion Mobility-Mass Spectrometry. *Anal. Chem.* **2010**, *82* (7), 3061-3066.

3. Harkness, K. M.; Hixson, B. C.; Fenn, L. S.; Turner, B. N.; Rape, A. C.; Simpson, C. A.; Huffman, B. J.; Okoli, T. C.; McLean, J. A.; Cliffel, D. E., A Structural Mass Spectrometry Strategy for the Relative Quantitation of Ligands on Mixed Monolayer-Protected Gold Nanoparticles. *Anal. Chem.* **2010**, *82* (22), 9268-9274.

4. Simpson, C. A.; Farrow, C. L.; Tian, P.; Billinge, S. J. L.; Huffman, B. J.; Harkness, K. M.; Cliffel, D. E., Tiopronin Gold Nanoparticle Precursor Forms Aurophilic Ring Tetramer. *Inorg. Chem.* **2010**, *49* (23), 10858-10866.

5. Simpson, C. A.; Agrawal, A. C.; Balinski, A.; Harkness, K. M.; Cliffel, D. E., Short-Chain PEG Mixed-Monolayer Protected Gold Clusters Increase Clearance and Red Blood Cell Counts. *ACS Nano* 2011, accepted.

Works in Progress

1. Harkness, K. M.; Balinski, A.; McLean, J. A.; Cliffel, D. E., Structural Investigation of Supramolecular Assemblies on Gold Nanoparticle Surfaces. *In preparation.*

2. Harkness, K. M.; Balinski, A.; Casey, M. C.; McLean, J. A.; Cliffel, D. E., Evidence of Protecting Metal-Thiolate Complexes on Silver, Platinum, and Palladium Nanoparticles. *In preparation.*

Research Experience

- Analytical instrumentation operation: mass spectrometers with and without ion mobility separation (Finnigan LCQ, Waters Synapt, Applied Biosystems

Voyager), UV-Vis, NMR, and FT-IR spectroscopy, transmission electron microscopy

- Data processing and spectral interpretation: developed first published methodology to separate and characterize unknown organometallic compounds by ion mobility-MS

- Computer software: developed automated program to process raw data files and assign molecular formulas for organometallic ions. Experience with MATLAB, Origin, and LabVIEW software.

- Interdisciplinary training: Chemistry-Biology Interface trainee and Vanderbilt Institute for Nanoscale Science & Engineering Fellow